DISSERTATION

DYNAMICS OF FLOW IN RIVER BENDS

Submitted by

Oladapo Aseperi

Department of Civil and Environmental Engineering

In partial fulfilment of the requirements

For the Degree of Doctor of Philosophy

Colorado State University

Fort Collins, Colorado

Fall 2018

Doctorial Committee:

Advisor: Subhas K. Venayagamoorthy

Pierre Y. Julien
Jorge A. Ramirez
Elizabeth Barnes

ABSTRACT

DYNAMICS OF FLOW IN RIVER BENDS

Water is indispensable to life and the means by which it is conveyed is equally important. Natural rivers and manmade channels play a critical role in this respect because they are vital for water supply, navigation, transport of sediments, pollutants and nutrients. Most natural rivers typically have meandering (curved) geometries which make a direct study of their flow dynamics cumbersome. In order to reduce this complexity, natural rivers are usually idealized as open channel bends with rigid boundaries in order to gain insights into the flow dynamics. As such, this research examines the dynamics of flow in open channel bends with rigid boundaries, using computational fluid dynamics (CFD). The particular computational fluid dynamics code used in this research, discretizes the equations of fluid motion (i.e. the Navier-Stokes equations) using a finite volume scheme while tracking the free surface with the volume of fluid method. Turbulence was incorporated into the solution of the equations using large eddy simulation techniques.

Even though the general aim is to improve current understanding of natural river bend physics, the specific aims of this research are threefold. These are: (1) to study the effects of radius of curvature on the flow physics of an idealized river bend; (2) to study in detail the effect of a variation in curvature length on the flow structure and dynamics of an open channel bend; and (3) examine in detail the effect of inertial forces on the flow dynamics of an idealized river bend by varying the inflow Froude number.

While some of the findings in this research confirm some of the results that has already appeared in literature, a significant amount of results highlight new insights into dynamic events in an open channel bend. As a concrete example on the effect of curvature on the flow structure, simulation results show that

the maximum bed and wall shear stress are exerted on the inner wall at the entrance to the curve regardless of curvature. However, further into the bend, the maximum shear stress shifts to the outer bend and wall region. Furthermore, the angular distance into the bend at which this occurs is found to depend on the curvature of the channel. Thus, for a mild channel, the maximum shear stress shifts to the outer bend and wall region a short angular distance from the entrance. This distance increases with a decrease in radius of curvature (i.e. as the channel gets tighter) with the maximum shear stress in the tightest channel (that was simulated in this study) always occurring on the inner side of the bend for the entire channel length.

Another key finding comes from an investigation of the effect of the variation of curvature length on the flow structure and dynamics of open channel bends. It was found that the flow circulation pattern depends on the curvature length. Simulation results showed that shorter channel bends reached fully developed vortical states faster than similar channels with longer lengths. Furthermore, new results from this study provide a clear explanation for the emergence of a three-cell circulation structure in tight channel bends that occurs as a result of the splitting of the main cell circulation due to the enhanced vorticity in tight bends.

Finally, the study on the effects of Froude number on flow structure clearly shows that an increase in the inertia of the fluid does not affect the radial pressure gradient force (a very important force that plays a critical role in shaping the bend channel dynamics) in a mild channel. Remarkably in the tight channels, there seems to be a positive correlation between the magnitudes of the fluid inertia (as measured by the velocity) and the radial pressure gradient force. This finding has important implications for the modeling of river bends since geometric factors are not sufficient to adequately parameterize the flow structure under certain circumstances in reduced order models.

These and more results not mentioned in this abstract are detailed in this dissertation. The overall aim of this research is to provide better insights into bend channel flow dynamics so as to enable engineers to carry out more accurate river modeling and training works.

ACKNOWLEDGMENTS

I sincerely would like to thank my academic advisor Professor Karan Venayagamoorthy for taking a chance on me. I am indeed grateful for his support, academic guidance and extreme patience during my doctoral studies. The enthusiasm with which he imparts new ideas, and his investments in my progress has made my time working with him memorable.

I wish to extend my deepest appreciation to members of my doctorial committee Professor Pierre Julien, Professor Jorge Ramirez, and Professor Elizabeth Barnes, for reviewing my work, offering helpful comments and providing mentorship at various stages of my doctorial work. I would also like to thank Professor Thomas Birner for previously serving on my dissertation committee.

Studying fluid mechanics at Colorado State University has been a fantastic journey, thanks in part to my laboratory colleagues Dr. Amrapalli Garanaik, Dr. Jian Zhou, Ajith Nithianantham, Jessica Baker (kind enough to help in editing this work), Sydney Turner, Mathew Klema, and Jeremy Carlston. I would especially like to thank Dr. Marie Rostello with whom I was fortunate to have engaging discussions in hydraulics that helped crystalize some of the new ideas that made it into this dissertation.

I would sincerely like to thank my family especially my parents Dr. and Mrs Taiwo Aseperi for their unfading psychological and moral support. Their motivational talks with me has helped get me through hard times during the course of my studies. I would like to acknowledge my sister and her contribution to this endeavor. I also want to thank Engineer Egwuatu for his fatherly advice and moral support.

Ultimately I thank the almighty God for bringing me thus far.

TABLE OF CONTENTS

LIST OF TABLES

LIST OF FIGURES

Chapter 1

Introduction

1.1 Background

Rivers are an essential feature of the planet surface conveying water, sediments, and nutrients from one place to another. In addition rivers can be a source for food, navigational routes, and many other recreational benefits. In order to maintain these benefits and avoid catastrophes such as flooding, engineers and scientists must understand the character of river systems. Excluding the effects of confluences and junctions, there are two main factors that make the study of the dynamics of rivers from a fluid mechanics perspective difficult. On one hand there is the extremely complex winding geometry of rivers which makes their direct study cumbersome, while on the other hand the presence of many forms of sediments complicates the dynamics of flow. In order to bring the complexity of the study of river mechanics down to a tractable level, simplifying assumptions must be made. These assumptions however must be carefully chosen so that results obtained still remain of practical value. In dealing with the issue of complex geometry a perusal of available literature seems to suggest that the acceptable compromise between simplicity and practical relevance is to idealize river systems as a single channel bend (see figure 1.1). As a first step, studies can then be carried out on the dynamics of bend to understand the character of river systems. In addition, single channel bends are assumed to have rigid boundaries without any sediments in order to further simplify the problem of understanding river dynamics.

(a)

(c)

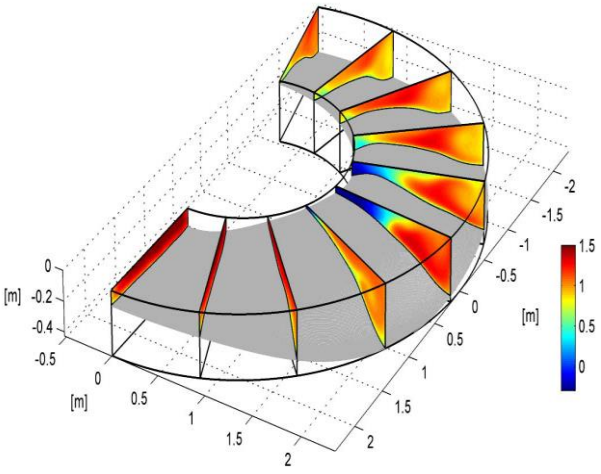

(b)

(d)

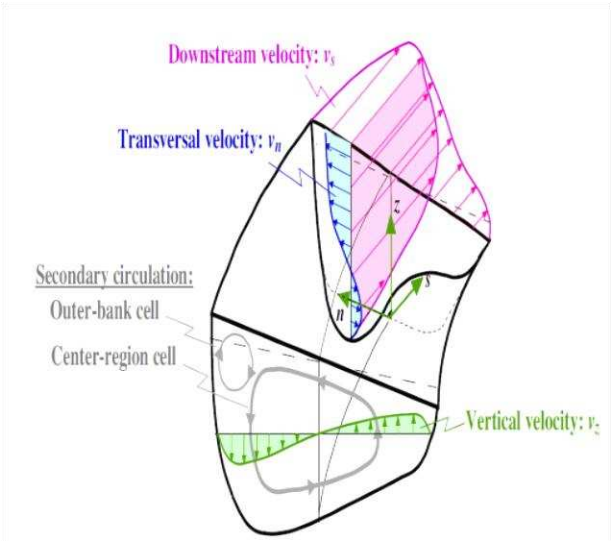

Figure 1.1: A couple of examples of natural rivers are shown in (a) and (b). Schematic of a simple bend (c) and a schematic of the typical circulation structure in a bend (d). Image Sources: *(a)*: University of Oregon. (b): Van Balen 2009. (c): Van Balen 2009. (d): Blanckaert and Graf 2010 (note the diagram d alone is laterally inverted).

There exists a vast body of work in literature using the approach outlined in the preceding paragraph (with the exception of field measurement campaigns where river parameters are measured directly). This approach then requires selection of the right tool for the study of the single channel bend. One tool

available to scientist and engineers is laboratory scale modeling, where miniature replicas of river bends are reproduced with the right boundary and flow conditions to imitate parts of the natural river flows. This tool, however, has certain limitations one of which is the prohibitive cost (in time and money) of building physical models (to great detail). While it is possible to vary parameters to study cause and effect with laboratory scale modeling, the time required can be enormous and in some cases could mean rebuilding models from scratch. Furthermore, ensuring geometric and dynamic similarity is rarely realizable in such modeling studies. This, coupled with the uncertainty in measurements obtained from scale models makes this a choice of last resort in many cases. Field measurements of river parameters is another option available for the study of the various aspects of river systems. However the complex nature of river systems (in terms of its geometry and dynamics) makes such an endeavor extremely expensive. This in addition to the lack of flexibility in varying parameters like with scale models makes field measurement campaign more suitable as tool for validation of other types of models. In recent decades, with the introduction of super-fast computers, the equations of fluid dynamics can now be solved for various idealized river geometries to gain more insight into the physics of fluid flow and sediment transport. This tool that includes solving the Navier Stokes equation (the equations of the dynamics of fluid) is called computational fluid dynamics (CFD). Similar to other tools available to engineers for the study of the physics of river systems, CFD has both strengths and weaknesses. Since the full Navier Stokes equations cannot be solved analytically, a numerical method must be chosen to obtain the flow field solution. These solution methods are prone to error depending on factors such as the type and size of mesh, the numerical scheme chosen to discretize the equations, and solution scheme in space and time. Furthermore, errors could be introduced in the post processing phase of analysis if care is not taken. However of the three tools enumerated above, CFD is the most flexible in studying cause and effect of various aspects of river system as it has the least cost, and various steps can be taken to minimize any

error in the solution schemes so that results obtained can be reasonably used to study the flow structure and dynamics of river systems.

It is for this reason that a combination of computational methods, dimensional analysis, and physical reasoning was chosen in this research to study the dynamics of flow in single river bends as a way to gain better insight into how river systems work. This combination aims to minimize the weaknesses which any one tool is prone to by combining the strengths outlined above. The specific objectives of this dissertation research are outlined in the next section.

1.2 Objectives

In the preceding section reference was made to the vast body of work available in literature on river bend dynamics, some of these include Barthust et al (1977), Thorne (1985), De Vriend (1981), Odgaard & Bergs (1988), Whiting and Dietrich (1993a & b), Blanckaert & Graf (2001), Booij (2003), Blanckaert & De Vriend (2004), Blanckaert and Graf (2004), Blanckaert (2009). While these published works have provided good insight on the general patterns of flow behavior in a single bend, there are still some intricate details that are missing in current knowledge. For example, there has been no systematic study of the effect of curvature length on the evolution of flow structure and dynamics in a river bend. This and a couple of other unknown mechanisms that characterizes the physics of bend flow leaves a knowledge gap that this research partly hopes to fill. Thus the objectives of this research are:

1. It is known that an important factor that determines the distribution of various flow parameters in a bend is the curvature (defined as the ratio of the radius of curvature to the top width). This research aims to investigate the effect of varying the curvature on the evolution of the flow structure and dynamics of a single channel bend.
2. This research also seeks to study the effect of the variation of curvature length in determining the flow structure and physics of bend channel flow.

3. Finally this research investigates the effect of varying the Froude number (the ratio of the inertia to gravitational forces) on the evolution of the behavior of flow in a channel bend.

The three objectives outlined above would be achieved by using computational fluid dynamics to solve for the flow field in order to analyze fluid behavior under the various conditions consistent with the objectives of this research. It is hoped that this research would produce a better understanding of the details of bend channel flow than is currently available.

1.3 Thesis Outline

This thesis has six more chapters. In the next chapter, existing literature in the field of river bend dynamics is reviewed. Chapter 3 deals with the numerical methodology used in this research with a thorough validation of the computational fluid dynamics code chosen. After confidence has been established in the set of tools chosen, Chapter 4 proceeds to study the effect of the variation of curvature on the dynamics and flow structure of a river bend. Chapter 5 discusses the effect of variation in curvature length on the physics of fluid flow in an open channel bend while Chapter 6 studies the effect of changing Froude number on the dynamics of flow in a river bend. Chapter 7 concludes with a summary of the main findings and contribution to knowledge. Each chapter in this thesis (except chapter one) would begin with a preamble (like an abstract) summarizing in more detail what that chapter hopes to achieve.

1.4 Summary

In summary, this work seeks to re-examine the physics and flow structure in open channel bends using a combination of dimensional analysis, physical reasoning, and three dimensional computational fluid dynamics simulations. This combination of tools represents a holistic approach to deciphering the flow structure and dynamics in an open channel bend under various conditions. It is hoped that the findings in this research would provide better insights into the physics of bend flow and ultimately the workings of natural river systems.

Chapter 2

Literature Review

2.1 Preamble

This chapter reviews literature tracing the beginnings and the evolution of river dynamics research to the present day. The chapter reviews literature in four sections. Section 2.2 examines the contribution of field measurement campaigns to our current understanding of the physics of river bend flows, while section 2.3 goes on to analyze knowledge derived from laboratory scale experiments and how they improved knowledge of river flow dynamics. In section 2.4 the history and application of mathematical models to river dynamics research is examined with a particular emphasis on three-dimensional computational fluid dynamics simulations where the equations of fluid motions are solved numerically to analyze fluid behavior. Section 2.5 explains the current scientific consensus concerning the dynamics of bend channel flows. Finally, this chapter closes with a summary of all the major points in section 2.6.

2.2 Contribution of field measurement to current knowledge

Some of the earliest attempts at understanding the mechanics of river flows have been by means of field measurement campaigns (where flow parameters were obtained by means of direct collection of data). Researchers like Rozovkii reported natural channel measurements of two dimensional velocity components as early as 1957, while others like Barthust et al., (1977) and Thorne (1985), Dietrich and Smith (1983), Nelson and Smith (1989) reported measurements on various other aspects of natural river flows. Unfortunately, due to the crudeness of the flow measurement devices available at the time, insight into natural bend flow physics of rivers was hampered. For instance, the most common devices for field measurements at the time was the electromagnetic flow meter (Barthust et al (1977), Thorne (1985)) which could only measure the velocity in two mutually perpendicular directions and could not resolve the turbulent stresses. Since the flow in a natural river is three dimensional, the two dimensional

measurements offered by such instruments could not adequately reproduce the hydrodynamics of river flows. Some researchers (McLelland et al., 1996, DeSerres et al., 1999) tried to remedy this situation in two ways. One was combining more flow measuring instruments (with rather large sampling volumes) at the same point with axes mutually perpendicular to measure flow in its full dimensionality. While the other was taking measurements at the same point but changing the orientation of the instrument at different times. Neither of these methods were able to reproduce the true three dimensionality of the flow and the small scales as evidenced by the attribution of all phenomena observed to large scale parameters with little or no mention of the role of turbulent stresses in shaping river flow dynamics. As flow measurement devices improved such that flow measuring instruments could measure the three components of velocity and resolve some part of the turbulent stresses, it became clear that these stresses play a key role in the dynamics of river bend flows. Lane et al., (1998) seems to have been the first to measure rivers flow in its full 3 dimensions, while Sukhodolov et al., (2001) seems to be the first to include the measurement of turbulent stress in addition. Other detailed field campaigns were conducted by Frottingham and Rhode (2003) and Blanckaert et al., (2009).

While the crudeness of the flow measuring instruments in the early days of river dynamics research has been acknowledged, the insights gained from these early studies are remarkable given their limitation. As an example, a perusal of literature would reveal that as early as 1957 (Rozovkii 1957) the two cell circulation structure had already been observed with Barthust and Thorne (1985) showing similar results as seen in Figure 2.1 (Please note that this figure is laterally inverted and the outer bank is on the left side). While both authors attributed this phenomenon to the interaction between the mainstream velocity and the centrifugal acceleration, a fact that would change with improvements in measurements, the basic theory of the two cell circulation which they observed has stood relevant till the present day.

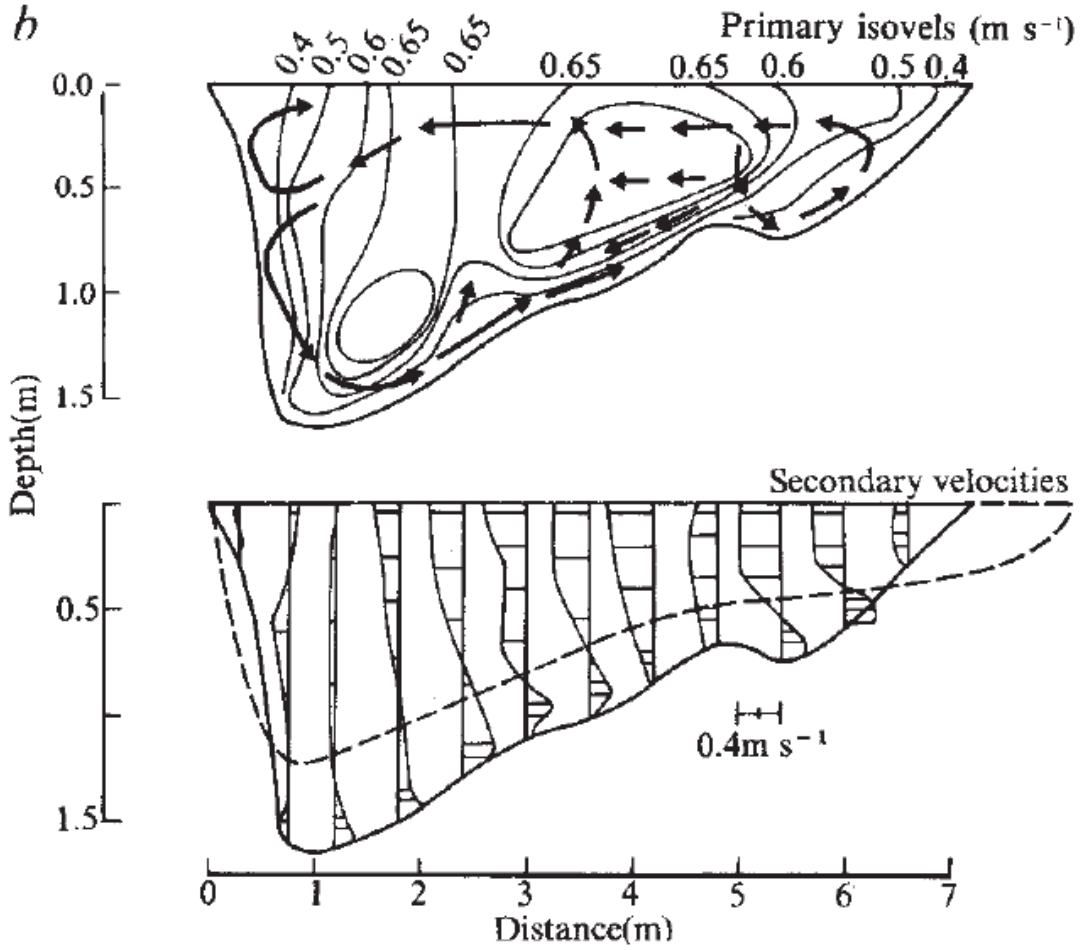

Figure 2.1: The two cell circulation structure in a river bend from Thorne et al., in 1985. The top diagram shows the mainstream isovels. The bottom diagram shows the depth profiles of the secondary velocities (Source Thorne et al 1985).

Even though field measurement campaigns have contributed greatly to knowledge of river bend flows (providing evidence of the three dimensional helical circulation), they are still plagued with various problems from the stand point of river mechanics research. Among the many problems is the fact that by virtue of its nature (especially its geometry) river parameters cannot be varied to ascertain cause and effect which is a very important point when the goal is a fundamental understanding of a field that is still largely plagued by high uncertainties. These uncertainties become even more problematic when we consider the complexity of the bed topography of a typical river. Because most rivers with sediments are shallow on the inner bank because of the formation of accumulated sediment (this structure is usually

called a point bar) and deep on the outside (usually referred to as a pool) the extra phenomena of topographic stirring sets in. This coupled with the sometimes random nature of the hydrodynamic behavior of sediment in suspension or as bed load makes the data obtained of less use than it would have been in a more deterministic system. There is also the issue of huge costs in time and finances which explains the relative scarcity of field measurement data compared to laboratory experimental data and computational data. Clearly there is the need for better methods to study river bend dynamics that avoids the problems enumerated above and that gives deeper insight into the fluid mechanics at all possible scales.

2.3 Contribution of experiments to current knowledge

As explained in the previous chapter, the complexities of the problem of river dynamics compels scientists and engineers to make difficult choices. This means simplifying the usually complex meandering geometry of a typical river down to a single channel bend with or without rigid boundaries. Since this geometry is seen as an idealized river bend, the single channel bend can be studied experimentally to gain insight into the physics of river flows. Experimental works of this kind has been performed by De Vriend (1981), Odgaard & Bergs (1988), Whiting and Dietrich (1993), Blanckaert & Graf (2001), Booij (2003), Blanckaert & De Vriend (2004), Blanckaert (2009). While this list is not exhaustive, Table, 2.1 reproduced from Blanckaert & Graf (2001) gives more details of some of the experimental works that have been carried out in open channel bend flow. Essentially the contribution of laboratory scale studies to current knowledge improved with the evolution of instrumentation technology and analysis techniques as can be seen from literature. As a concrete example, Ippen and Drinker in 1962 focused experimental effort on the shear stress distribution in open channel bends with a trapezoidal cross section. However, at the time of this study the equipment used in collecting boundary shear stress and velocity data was the Preston tube (also known as the Pitot static tube). While it gave reasonable accuracy in measurement, the Preston tube had to be calibrated, thus the quality of data produced was only as good as the quality of data used

in its calibration. Some years later with improved instrumentation and technology, Odgaar and Bergs (1988) performed studies of open channel bend flow with erodible bed material. In obtaining the velocity measurements they used an electromagnetic flow meter which was less intrusive than the Preston tube but could only measure velocity in two mutually perpendicular directions without resolving the turbulence. Other instruments like the depth sonic sounder for bathymetry and flow depth measurement (as opposed to the use of the sometimes intrusive point gauge) helped produce better data that improved understanding of erodible bend dynamics. The introduction of more sophisticated laboratory data collection techniques like the Acoustics Doppler Velocimetry (ADV) and the Laser Doppler Velocimetry (LDV) brought a profound increase in insight for the physics of bend channel flows. This is due in part to the fact that velocity in 3 components as well as the turbulent components could be collected on a fine grid. While modern field campaigns using some of these data collection techniques indicated that turbulence played a general role in the formation of flow structures (as older field studies also showed) the particular details of the role of turbulence was not clearly known. This is because the cost of conducting field campaigns that measure river sections on a fine enough grid to ascertain events at the small scale is prohibitive. This cost however is reduced in a laboratory reproduction of river flows. Hence, it is not surprising that scientists and engineers only began to understand the role of turbulence structure with improvements in laboratory scale experiment. One of the facts that makes this obvious is that field data had shown the existence of the two cell circulation structure and even hinted that turbulence played a role. However only with detailed laboratory measurements and analysis by researchers like Blanckaert & De Vriend (2004), Blanckaert & Graf (2001), Booij (2003) did the understanding begin to emerge that the turbulent stresses play a very limited role in the formation of the main cell circulation (also known as the center cell circulation), but are a major factor in the formation of the counter rotating cell often observed close to the outer bend of a river. Furthermore prior to the detailed experimental analysis of Blanckaert & De Vriend (2004), the role of the Reynolds stresses in maintaining the stability of outer river

banks was underestimated. It is now clear after several experimental studies in literature that the turbulent stresses play a major role in the formation of the counter-rotating outer cell which in turn reduces the turbulence shear exerted on the outer wall. This means less shear stress is exerted on the outer wall of a bend compared to a straight channel of equivalent dynamics (Van Balen 2009). The relative stability of the outer bank of a river bend is thus dependent on the turbulence structure in the bend. Such a detailed understanding could not have come from field measurements alone for reasons already explained above.

Table 2.1: showing some of the experimental works on bend channel dynamics (Source Blankert and Graf 2001)

Literature	Cross section and channel bed	Planform	Flow regime	Size of measuring grid (approximately)	Number of vertical profiles in outer-bank region	Flow and turbulence measurements
Rozovskii (1957)	Rectangular: smooth bed rough bed Triangular	Single bend, 180°	Transition Rough turbulent Transition	$H/7 \times B/8$ $H/7 \times B/8$ $H/7 \times B/4$	2 2 1	v_s, v_n
Götz (1975)	Rectangular smooth bed	Single bend, 180°	Transition	$H/5 \times B/10$ (denser near banks and bottom)	2, 3, 4, 5 (for aspect ratios of 20, 10, 4.6, 2.9)	v_s, v_n
de Vriend (1979)	Rectangular smooth bed	Single bend, 180°	Transition	$H/10 \times B/10$	3	v_s, v_n
de Vriend (1981)	Rectangular rough bed	Single bend, 180°	Rough turbulent	$H/10 \times B/10$	3	v_s, v_n
Siebert (1982)	Rectangular smooth bed	Single bend, 180°	Transition	$H/5 \times B/4$ $z/H = 0.09, 0.66 \times B/3$	3 2	v_s, v_n v_s, $\overline{v_j' v_k'}$
Dietrich and Smith (1983)	Natural topography; sand bottom	Meander, field study	Rough turbulent	$H/6 \times B/13$	<10	v_s, v_n
Steffler (1984)	Rectangular smooth bed	Single bend, 270°	Transition	$H/10 \times B10$ (denser near bottom)	2	v_s, v_n, $\overline{v_s'^2}$, $\overline{v_n'^2}$
Anwar (1986)	Natural topography; sand bottom	Single bend, 35°; field study	Rough turbulent	$H/4 \times B/15$	<7	v_j, $\overline{v_j'^2}$ $\overline{v_s' v_n'}$, $\overline{v_s' v_z'}$
Odgaard and Bergs (1988)	Natural bed topography, fixed inclined banks; sand bottom	Single bend, 180°	Transition	$H/10 \times B/8$	1	v_s, v_n
Muto (1997)	Rectangular smooth bed	Meander	Transition	$H/10 \times B/10$	5	v_j, $\overline{v_j' v_k'}$
Tominaga et al. (1999)	Rectangular smooth bed + different configuration with vegetation	Single bend, 60°	Transition	$H/10 \times B/18$ (bend outlet section) $H/5 \times B/18$ (other sections)	6	v_s, v_n, v_z
Present study	Natural bed topography, fixed vertical banks; sand bottom	Single bend, 120°	Rough turbulent	$H/22 \times B/33$	65	v_j, $\overline{v_j' v_k'}$

Note: H = averaged water depth; B = channel width; z = distance above bed; outer-bank region = region extending $2H$ from outer bank; v_j ($j = s, n, z$): mean velocities; $\overline{v_j' v_k'}$ ($j, k = s, n, z$): turbulent correlations.

Profound as the contributions of laboratory scale experiments are to the understanding of bend channel dynamics, it is not in itself sufficient (as is every other tool in river dynamics research). While it is true that the relative cost of laboratory experiments compared to field measurements is less, conducting such experiments is still expensive. Also variation of parameters in order to determine cause and effect is

sometimes not easy in a laboratory setting. This is especially true with regards to varying geometric parameters where changing a parameter like the bend curvature could mean completely rebuilding the laboratory model several times. Modern measuring equipment has made measuring fluid data on a fine grid possible, however there are still limits to how fine such a grid can be. It is therefore clear that laboratory scale experiments alone cannot form the basis of a detailed study of river bend dynamics and as such there is the need for either a better study method or one that compliments experimental methods to produce better insight. Such a method is explored in the next section.

2.4 Contribution of mathematical simulations to current knowledge

Another alternative to laboratory experiments and field measurements is the use of mathematical models in river dynamics research. This tool involves describing the dynamics of bend channel flows with mathematical equations (usually partial differential equations with the appropriate boundary and initial conditions imposed) which can then be solved (usually numerically) to better understand the dynamics of river bends. Mathematical model studies of river bend dynamics have been carried out by Booij (2003) and Stoesser *et al.* (2008), among others. These models have served as a complimentary tool to laboratory experiments and field studies. A perusal of literature reveals that mathematical models of river bends can be classified in terms of dimensionality. As such, there exist reduced order models like one- and two-dimensional bend models as well as full three-dimensional models. Reduced order models are so called because they use approximations of certain aspects of three dimensional flows in bends. For example, the two-dimensional model by Lien et al., (1999) approximates the vertical flow structure by averaging the velocity over the depth. Many one-dimensional river models are in existence today and can be categorized into linear models (Engelund, 1974, De Vriend 1977, Odgaard 1986), where the velocity strength is a linear function of the depth to radius ratio, and nonlinear models, where the velocity strength is a nonlinear function of the depth to radius ratio (Jin and Steffler 1993, Yeh and Kennedy 1993, Blanckaert and De Vriend 2004). In literature, the linear bend flow models give reasonably good results only in mild bend

channel since they fail to reproduce essential flow structures in even moderately tight bends. On the other hand, nonlinear river bend models reasonably reproduce essential flow features even in tight bends because they incorporate the feedback process between terms that models the dispersive forcing and the mainstream forcing. Despite these short comings, the linear models are still widely used in river management because of their reduced computational cost compared to nonlinear models.

The full three-dimensional bend flow models provide the closest approximation to reality. Since most natural river flows are turbulent with Reynolds numbers usually far exceeding 4000, solutions to these three dimensional river bend models must properly incorporate turbulence if they are to be of practical relevance. Based on turbulence resolution, mathematical river bend models can average the equations of fluid motion (known as the Navier-Stokes Equations) and model all of the turbulence. This approach is called Reynolds Averaging and it simulates the flow by solving for the average velocities while approximating the turbulent fluctuations via a model. A particularly popular turbulence model is the $k-\varepsilon$ model (despite its short coming in river bend simulations, Booij 2003) where transport equations for the production of turbulent kinetic energy (k) and its dissipation rate (ε) are solved. The solution to these are then used to calculate an eddy viscosity which can be used to compute the turbulent stresses. Other approaches to turbulence modelling in the Reynolds averaged framework include $k-\omega$ and the Reynolds Stress Models (RSM) where six separate equations are solved (assuming symmetry of the Reynolds Stress Tensor) to get each of the six Reynolds stress terms. The Reynolds Averaged Navier Stokes (RANS) simulations are used widely in engineering design and planning because of their extremely low computational cost when compared to other approaches at incorporating turbulence into river bend models.

In situations where more flow details are required, river bend models can incorporate turbulence by resolving the eddy motions on the larger scales while modeling the smaller scale turbulence. This method is based on the philosophy that the large scales depend on the boundary conditions of flow and exhibit

anisotropy in turbulence behavior while the really small (dissipative) scales of turbulence are isotropic with little dependence on the large scale flow conditions. Such turbulence simulation techniques are referred to by the name Large Eddy Simulation (LES). LES provides a better picture of flow events in river bends but is computationally more expensive than the RANS approach described earlier. However because of recent advances in computer technology and speed, such that super-fast server computers are now cheaper, LES has become the preferred choice for research, with researchers like Booij (2003), Van Balen (2009) and Blanckaert (2009) carrying out extensive LES studies of bend channel dynamics. When even more detail than what a LES can provide is required, the Navier-Stokes equation can be solved by resolving the turbulence completely to the smallest scales called the Kolmogorov scales. This method is referred to as Direct Numerical Simulation (DNS) and is only possible in flows in simple geometries and limited Reynolds Numbers. For practical problems, the computational cost is extremely high and is thus almost never used in river mechanics. A review of literature shows that various mathematical modeling studies of all the types described so far has been carried out with varying degrees of success. Table 2.2 reproduced from Shin (2014) summarizes some of the works in literature.

2.5 Current scientific consensus concerning the dynamics of river bend flows

The progress made in understanding river bend dynamics has been remarkable, and culminates in what is today believed to be the scientific explanation of the various flow patterns observed in river bend flows. This explanation is summed up as follows. When a flowing fluid encounters a single channel bend it is subject to a centrifugal acceleration ($\frac{v^2}{r}$). Since naturally the depth velocity profile for an open channel is such that velocity close to the surface is “free slip” (meaning that they are free to move and are hardly subject to boundary restraints) while those at the bed are “no slip “(meaning they are restrained by the presence of the boundary) the centrifugal acceleration has a variable effect on the depth profile of velocity. Thus the centrifugal acceleration pushes fluid close to the surface towards the outer bend while pushing fluid close to the bed towards the inner bend (Van Balen 2009). The fluid pushed outward

increases the flow depth towards the outer bend setting up the super-elevation of the free surface and introducing another factor: the radial pressure gradient.

Table 2.2: showing some of the numerical simulation studies in bend channel dynamics (Source Shin 2014).

Researcher	Dimensions of the Model	Model Selection	Simulated Variables	Validation with Field or Laboratory Data
Odgaard (1989)	2D	Numerical	Transverse bed slope	Yes
Jin et al. (1993)	2D	Depth-averaged	Depth-averaged velocity	Yes
Hodskinson and Ferguson (1998)	3D	RNG k-ε model	Flow velocity	Yes
Lien et al. (1999)	2D	Depth-averaged	Velocity ratio across dimensionless channel Width	Yes
Wilson et al. (2003)	3D	Standard k-ε model	Flow velocity	Yes
Rameshwaran et al. (2005)	3D	Standard k-ε model	Transverse free surface profile, bed shear stresses, streamwise velocity and transverse velocity	Yes
Khosronejad et al. (2007)	3D	Low-Reynolds number k-ω model and standard k-ε model	Longitudinal flow velocity, transverse flow velocity, and bathymetry change	Yes
Blanckaert et al. (2009)	3D	LES and RANS Model	Flow velocity, secondary Flow,	Yes
van Balen (2010)	3D	LES	Flow velocity, secondary flow,	Yes
Zeng et al. (2010)	3D	RANS model	Flow velocity, flow depth, change of the bathymetry, bed shear stress	Yes
Son et al. (2011)	2D and 3D	RNG k-ε model	Flow velocity, free surface elevation and shear stress	Yes

This interaction between the centrifugal acceleration and the radial pressure gradient sets up a force distribution (see figure 2.2) such that there is a main circulation cell in the plane perpendicular to the main stream direction of flow. This interacts dynamically with the mainstream flow to produce the three dimensional helical motion that has been observed in literature. Also observed in literature is the presence of a second counter rotating cell close to the top outer bank corner which cannot be explained by the interaction between the centrifugal acceleration and the radial pressure gradient alone. It has been shown in literature (Van Balen 2009, Blankert 2009) that this counter rotating cell (also known as the turbulence induced secondary cell) exists as a result of the complex interaction between the centrifugal acceleration and the turbulent stresses. It is therefore the consensus in the scientific community that bend channel dynamics can be described adequately by a main stream flow perpendicular to a plane with a two cell circulation structure where the bigger circulation is clockwise and the smaller cell at the top outer corner is counter-clockwise (see figure 2.3 for a schematic of the physics of an open bend channel flow). This creates the distribution of velocities and boundary shear stresses that has been observed extensively in literature. While this theory of bend channel flow has held for over 70 years and has so far allowed reasonably accurate modelling of river processes, can it really be true that all river bends with all the diverse boundary and flow conditions that can exist follow this simple three-dimensional helical flow model with a two cell planer circulation structure ? This overarching question forms the basis of the research presented in this dissertation.

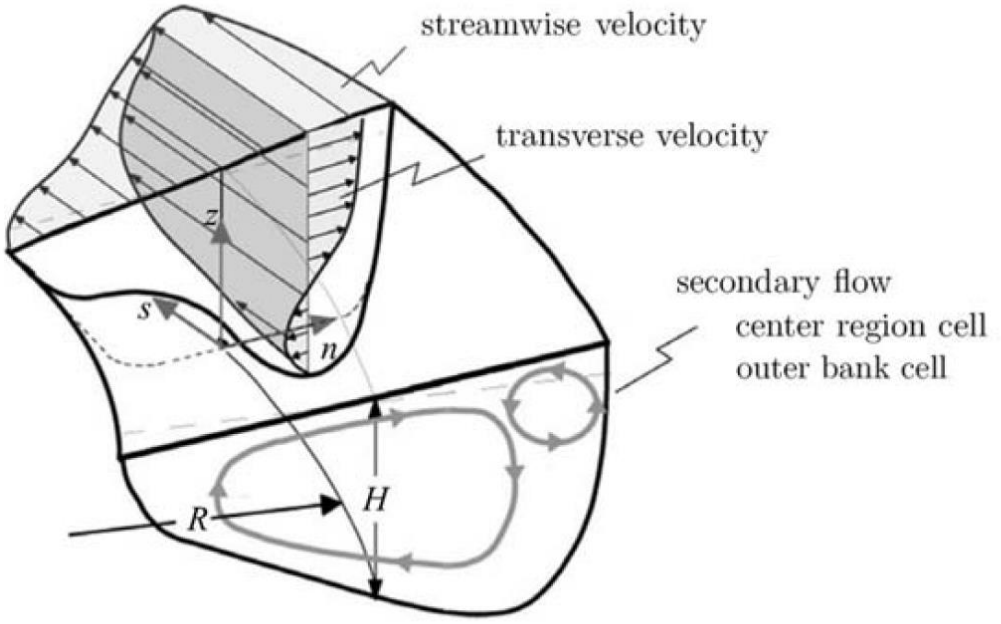

Figure 2.2: Schematic of the two cell circulation structure of flow in a bend (source Van Balen 2009).

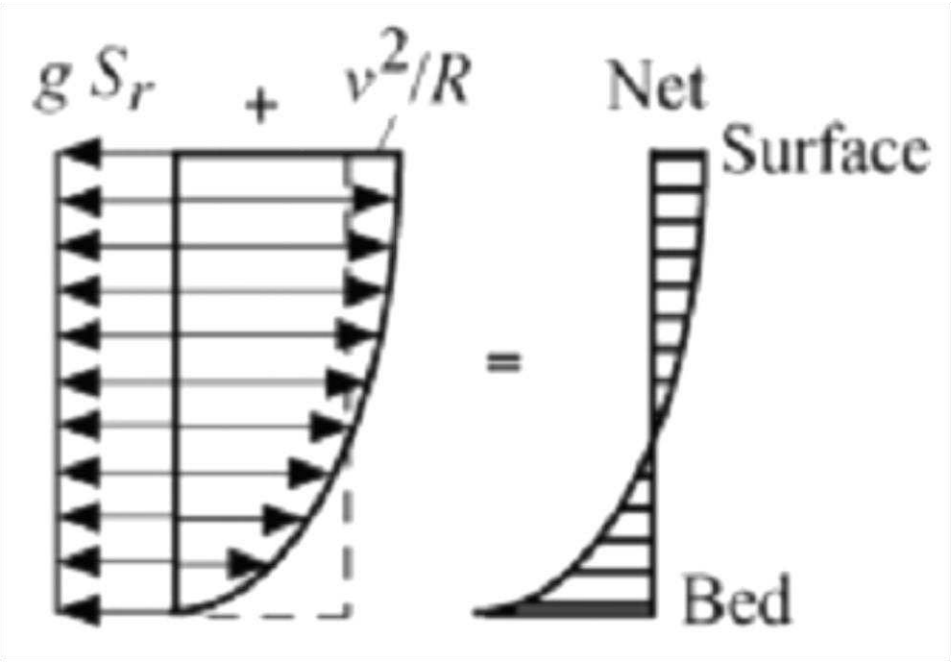

Figure 2.3: A schematic depicting the force distribution in a typical plain of a curved channel (source Julien 2002).

2.6 Summary

This chapter reviewed the literature in river bend dynamics from a historical perspective. Some of the earliest results in river dynamics were due to direct data collection. In the earlier sections of this chapter, the deficiencies of the various techniques used were detailed. Those sections also emphasized the contribution of field measurement campaigns to our current understanding of river bend flows. The chapter then goes on to detail the contribution of laboratory scale experiments to current knowledge. It is clear from a perusal of literature that significant contributions came because of improvements in laboratory instrumentation and data analysis techniques. The third section of this chapter detailed some of its short comings. Complementing laboratory scale experiments are mathematical models and the fourth section of this chapter discussed the details of such models with an emphasis on three-dimensional Computational Fluid Dynamics (including its deficiencies and advantages). Essentially Computational Fluid Dynamics (CFD) has become a viable tool in river dynamics research because of its flexibility, low cost and the availability today of affordable super-fast computers. The closing section of this chapter detailed the current scientific consensus concerning the physics of bend channel flows. The consensus is that any plain perpendicular to the mainstream flow in a curved channel has a two cell circulation structure with the bigger clock wise cell resulting from the interaction between the centrifugal acceleration and the radial pressure gradient while the smaller counter-rotating cell is a result of the complex interaction between the centrifugal acceleration and the Reynolds stresses. This combined with the mainstream flow forms the three-dimensional helical structure which has been observed extensively in literature. In the next chapter, the numerical framework employed for this research is explained and its validation is presented.

Chapter 3

Numerical Methodology

3.1 Preamble

This chapter introduces Computational Fluid Dynamics (CFD) as a tool and details the inner working of the particular CFD tools chosen for this research. Due to the relative scarcity of experimental data and the number of simulations carried out in this research, this chapter attempts to examine and validate the CFD tool chosen for this research once and for all. The essence is to prove that the code used is robust and accurate enough to capture the physics of fluid flow in a wide variety of river bends that this research would eventually examine. Thus after the validation in this chapter, results obtained from simulations in the coming chapters can be treated with some measure of confidence. The next section of this chapter explains the mathematics of the Navier-Stokes equations which is the model used to simulate fluid flow. The discussion also includes the initial and boundary conditions (subsection 3.21), the turbulence modeling (subsection 3.22), and how the free surface is handled (subsection 3.23). In section 3.3 the computational code used is first validated by an examination of the hydraulics of the straight inlet (subsection 3.31), after which in subsection 3.32 the results of a simulation are compared with experimental data. A very important test of accuracy and robustness of any numerical tool (i.e. numerical tools that use meshing for discretization) is the invariance of results obtained with a change in mesh size. Therefore section 3.4 of this chapter presents findings from a grid sensitivity of the CFD tool used in this research and shows that the tool is accurate enough to reproduce the flow physics relevant to this research.

3.2 Background

The choice of Computational fluid dynamics as the primary tool for this research (in conjunction with physical reasoning and dimensional analysis) has been justified previously. Computational fluid dynamics as a tool includes all steps taken to solve the equations of fluid motion in order to obtain a result. The equations of fluid motions are derived from Newton's second law of motion which states that the rate of change of momentum of a moving body is proportional to the resultant of all the external forces acting on the body. However, because the law was formulated in a Lagrangian frame of reference (an inconvenient paradigm when dealing with many particles like is common in fluid dynamics), the equations are reformulated in an Eulerian framework. These equations together with the continuity equation are given in equations 3.1 to 3.4.

$$\frac{1}{r}\frac{\partial}{\partial r}(ru_r) + \frac{1}{r}\frac{\partial u_\theta}{\partial \theta} + \frac{\partial w}{\partial z} = 0 \ldots\ldots\ldots\ldots\ldots\ldots\ldots\ldots (3.1),$$

$$\frac{\partial u_r}{\partial t} + u_r\frac{\partial u_r}{\partial r} + \frac{u_\theta}{r}\frac{\partial u_r}{\partial \theta} + w\frac{\partial u_r}{\partial z} - \frac{u_\theta^2}{r} = -\frac{1}{\rho}\frac{\partial p}{\partial r} + \vartheta\left(\frac{\partial^2 u_r}{\partial r^2} + \frac{1}{r^2}\frac{\partial^2 u_r}{\partial \theta^2} + \frac{\partial^2 u_r}{\partial z^2} + \frac{1}{r}\frac{\partial u_r}{\partial r} - \frac{2}{r^2}\frac{\partial u_\theta}{\partial \theta} - \frac{u_r}{r^2}\right) \ldots (3.2),$$

$$\frac{\partial u_\theta}{\partial t} + u_r\frac{\partial u_\theta}{\partial r} + \frac{u_\theta}{r}\frac{\partial u_\theta}{\partial \theta} + w\frac{\partial u_\theta}{\partial z} + \frac{u_r u_\theta}{r} = -\frac{1}{\rho r}\frac{\partial p}{\partial \theta} + \vartheta\left(\frac{\partial^2 u_\theta}{\partial r^2} + \frac{1}{r^2}\frac{\partial^2 u_\theta}{\partial \theta^2} + \frac{\partial^2 u_\theta}{\partial z^2} + \frac{1}{r}\frac{\partial u_\theta}{\partial r} + \frac{2}{r^2}\frac{\partial u_r}{\partial \theta} - \frac{u_\theta}{r^2}\right) \ldots (3.3),$$

$$\frac{\partial w}{\partial t} + u_r\frac{\partial w}{\partial r} + \frac{u_\theta}{r}\frac{\partial w}{\partial \theta} + w\frac{\partial w}{\partial z} = -\frac{1}{\rho}\frac{\partial p}{\partial z} + \vartheta\left(\frac{\partial^2 w}{\partial r^2} + \frac{1}{r^2}\frac{\partial^2 w}{\partial \theta^2} + \frac{\partial^2 w}{\partial z^2} + \frac{1}{r}\frac{\partial w}{\partial r}\right) - g \ldots\ldots\ldots\ldots\ldots\ldots\ldots (3.4),$$

where u_r is the velocity in the main stream direction.

u_θ is the velocity in the cross stream direction,

w is the velocity in the depth direction,

ρ is the density of the fluid,

g is the acceleration due to gravity,

p is the pressure.

These equations of motion known as the Navier Stokes equations (equation 3.2 to 3.4) are a complex mix of elliptical (the pressure term), parabolic (the viscous term) and hyperbolic (the nonlinear advection term and the local acceleration) terms. These terms are physically significant as they model the various aspects of fluid motion subject to the boundary conditions. Thus the advection term models the change in momentum, in the Eulerian frame this term consists of the local acceleration (the rate of change of velocity with time), and the convective acceleration (the rate of change of spatial components of velocity with the three spatial dimensions). This change in momentum must be balanced (according to Newton's second law) by the resultant of all the external forces acting on a *control volume*. The external forces can be broadly categorized into contact forces (which requires some form of contact to exert influence like the viscous force and pressure force), and the body forces which act throughout the control volume without a specific point of contact (like the gravitational force). These explains the structure of equations 3.2 to 3.4.

In general, in order that the system of equations be determinate (having an equal number of equations and unknowns) the Navier Stokes equations are solved in conjunction with the continuity equation (equation 3.1). This equation (3.1) is derived from the principle that mass cannot be created or vanish during the flow process. The complexity in character of the Navier Stokes equations among other factors makes a closed form (analytical) solution impossible to find and hence, necessitate the use of a numerical approach. The numerical approach generally entails replacing a differential equation on a continuous domain with a set of algebraic equations on a discrete domain. This discrete domain is usually formed by (although there are other ways.) the intersection of lines at overlapping regular interval to

create a mesh. Meshes that are formed this way are called block or regular meshes and have the advantage of being easy to implement in a computer program. Then on these meshes, discrete equations approximating the nonlinear partial differential equations of motion are used to reformulate the problem in discrete space, this process is known as discretization.

There are several numerical solution schemes available but for this research the finite volume approach is used because of its wide use and its demonstrated ability to reasonably reproduce fluid physics under a wide range of conditions. Looking at the specific details, in the tool used in this thesis the equations of fluid motion are discretized with a first order forward in space finite volume scheme. The solution is formulated on a regular block mesh in such a way that the pressure coupling is implicit and is solved using the Generalized Minimal Residual Algorithm (GRMES) of Saad (1986). The solution is marched forward in time using an explicit first order scheme subject to the appropriate stability criterion. Since our scheme is first order accurate in time and space, extreme care has been taken to limit the size of the cells ensuring that the mesh used in every scenario is fine enough to produce reasonably accurate results. Also because of certain difficulties that may arise with the wide array of velocity and pressure distributions this research intends to examine, the dependent variable in the discrete equations are not all evaluated at the same set of discrete points, hence in the tool used the pressure is evaluated at the center of the respective control volumes while the velocities are evaluated at the faces of the control volumes. This formulation is called a staggered grid and has been found to be more robust in handling several types of velocity and pressure distributions.

3.21 Boundary and Initial Conditions.

Boundary and initial conditions are an important part of the specification of the equations solved to obtain flow results. In this research a large number of simulations were carried out all with the same initial and boundary conditions. This was done so that cause and effect could be more easily isolated as different geometric and flow parameters are varied one at a time with every simulation. Thus at the inlet to the

various curved channels simulated, a volumetric flow rate is always imposed at the straight entrance, while the free surface and the outlet have atmospheric pressure boundary conditions imposed. All walls (including the bed) are hydraulically smooth so a no slip boundary condition without a roughness component was imposed. All channels are initialized with a stationary fluid at start time and allowed to run until steady state conditions are reached before results are extracted and processed.

3.22 On the choice of LES

Most fluid flows of practical interest are turbulent, hence the process of incorporation of this phenomenon into the solution of the Navier Stokes equation is extremely important. Of all the choices available, the statistical averaging technique has been used extensively to study flow in curved channels by many researchers including Demureen and Rodi (1986), Lenchester and Rodi (1979) and Shin (2014) to name a few. This method of representing the effect of turbulence (known as Reynolds Averaging) however suffers from a major short coming. Since Reynolds averaging is a type of statistical average, it is important to note that important detailed information such as the fluctuating turbulence is lost in the process and hence the turbulence has to be modeled. Thus, key information including fluctuating velocity patterns, vorticity and even intermittent turbulent burst structures that would have been useful in providing the much needed insight are lost. For this reason, other turbulence modeling techniques that provide more detailed information of the flow field would better serve the purpose of this research. Thus the large eddy simulation (LES) technique is adopted where the Navier-Stokes equations are solved directly on a computational grid. Scales that are smaller than the mesh resolution are modeled using a subgrid-scale (SGS) turbulence model. While modeling the subgrid scales might seem to defeat the aim of choosing LES over Reynolds Averaged Navier Stokes (RANS) simulations, it is worthy to note that this approach is better because the large scales are explicitly resolved, hence the flow can be simulated in much greater detail than with the RANS approach. Resolving the flow to the smallest possible scale (called the Kolmogorov scale) while appealing and definitely provides greater detail than LES, comes with the problem of extreme

computational cost. The number of grid points N required for a direct numerical simulation (DNS) which also resolves the wall bounded areas in relation to the Reynolds number of the flow, scales as $N\alpha Re^{9/4}$ (Pope 2000). For a typical value of Reynolds number of about 10,000 which would be a common estimate for this study, more than 3 billion grid points would be required for a moderate sized domain at each time step. It is thus not feasible with the computational resources available today to perform a DNS for the problem at hand. Even though the computational cost reduces considerably for the LES study with grid point numbers that are about 2 orders of magnitude less than that required for DNS, the computational cost for LES that resolves the wall bounded regions is still prohibitively high. A more realistic computational cost is realized if instead flow close to the wall is modelled. In the specific tool used in this research the wall region is modelled using the standard law of the wall (equation 3.5).

$$u = u^* \left[\frac{1}{k} ln\left(\frac{\rho u_* d}{\mu}\right) + 5.0\right] \ldots\ldots\ldots\ldots\ldots\ldots\ldots\ldots (3.5),$$

where u is the parallel component of velocity computed adjacent to the wall.

u^* is the shear velocity,

ρ is the density of the fluid,

μ is the coefficient of dynamics viscosity of the fluid,

k is the Von Karman's constant,

d is the normal distance from the wall.

This implies that the treatment of turbulence eventually becomes a hybrid where the bulk of the flow is resolved using LES and the wall bounded region is treated using a RANS model of the k- ε flavor (Note that in this turbulence model k is the turbulent kinetic energy while ε is its dissipation rate). The usual way this is done is to assume local equilibrium between turbulent shear production and decay while k and ε are determined from equations (3.6a) and (3.6b). The reader is referred to Rodi (1980) and Demuren & Rodi (1986) for full details.

$$k_T = \frac{u_*^2}{\sqrt{C_\mu}}, \qquad (3.6a)$$

$$\varepsilon_T = \frac{u_*^3}{kd} \ldots\ldots\ldots\ldots\ldots (3.6b),$$

where k_T is the production of turbulent kinetic energy,

ε_T is the dissipation,

C_μ is a model constant. All other terms have previously been defined.

Concerning how the sub grid viscosity is handled, the tool used in this research uses the static sub gird model of Smagorinsky (1963) (equation (3.7)).

$$\vartheta_{sgs} = C_s^2 \Delta^2 \left|\widetilde{S_{ij}}\right| \ldots\ldots\ldots\ldots\ldots\ldots\ldots\ldots (3.7),$$

where ϑ_{sgs} is the sub grid viscosity,

C_s Is the Smagorinsky's constant,

Δ Is the filter length given by $\Delta = (\Delta x \Delta y \Delta z)^{1/3}$,

S_{ij} Is the mean strain rate.

3.23 The free surface

The free surface physics is an important part of the dynamics of open channel bend flow. However, simulating the free surface is not an easy task. In the past the vast majority of researchers including Van Balen (2009) and Shin (2014) have tried to circumvent this difficulty by assuming that the free surface behaves like a lid (or a slab) flowing passively with the fluid. This is called the rigid lid assumption. It has been argued in literature that even though this assumption introduces error into the simulation of open channel fluid flows, such errors are reasonably small as long as the Froude number is less than 0.5 (Kashyap et al., 2012). However, such an approach to simulating the free surface would not serve this research well considering the wide array of flow regimes that would be explored. It is for this reason that the free surface solver known as the Volume of Fluid method is used in this research. The Volume of Fluid

algorithm consists of three steps: (1) Definition of a volume of fluid function that delineates the position of the fluid surface at some initial time (of course this function would change as the solution marches forward in time). (2) A method to solve the Volume of Fluid transport equation (equation 3.8).

$$\frac{\partial F}{\partial t} + \frac{1}{V_F}\left[\frac{\partial u}{\partial x}(FA_x u) + \frac{\partial u}{\partial x}\left(FA_y v\right) + \frac{\partial u}{\partial x}(FA_z w)\right] = 0 \ldots\ldots\ldots\ldots\ldots\ldots\ldots\ldots (3.8),$$

where F is the function that represents the free surface profile,

V_F is the fluid volume fraction (fractional volume open to flow),

A_x is the fractional area open to flow in the x direction,

A_y is the fractional area open to flow in the y direction,

A_z is the fractional area open to flow in the z direction.

All other terms have been previously defined.

This equation is formulated using the area and porosity function paradigm in a method known as F.A.V.O.R (Fractional Area/Volume Obstacle Representation Method) (Hirts and Sicilian 1985) which is especially suitable for the representation of complex geometry. It represents the volume of fluid per total unit volume. (3) Setting the boundary conditions at the free surface, since the density of the gas above the fluid is negligibly small compared to the density of the fluid, a uniform pressure is exerted at the surface boundary (see Hirts 1981 for full details of the Volume of Fluid free surface solver).

All the procedures described above are encapsulated in Flow 3D a commercial computational fluid dynamics code developed by Flow Science Inc. This is the CFD code that was used to perform all the simulations in this research.

3.3 Validation

Computational fluid dynamics (CFD) is a tool, and like every other tool it has its strengths and weaknesses. Despite these weaknesses (which have extensively been discussed in previous sections), CFD as a tool comes with enormous advantages (which have also been extensively been discussed in previous

sections) which makes it indispensable in fluid mechanics research. The author of this thesis believes that the best way to use CFD is to minimize these weaknesses and build on its strengths. In building on the strengths of CFD, it must be shown that the particular code used can reasonably reproduce the relevant physics while minimizing error. This section is devoted to proving the validity of the CFD tool used in this research. First in validating the code, we examine the hydraulics of the straight portion of the channel. Because the fluid dynamics of straight channel flow is well established in literature and the goal is to isolate events in the bend, it must be shown that the fluid in the straight portion of the bend satisfies certain conditions given its length. This is done in the next section (section 3.31). The ultimate validation of a numerical code is perceived to be the ability of simulation results to reproduce and match experimental data. Hence section 3.32 provides results of a reproduction of experiments carried out on a bend section. The final section provides results from a grid sensitivity analysis of the CFD tool. Results from that analysis shows that the flow field solution is invariant with a change in mesh size. Essentially the aim of this section is to show once and for all that results produced by the CFD tool used in this research is reasonably accurate so that confidence can be established in its ability to reasonably describe the correct physics of what goes on in a bend.

3.31 Hydraulics of the straight inlet

It is known from basic fluid mechanics that when a fluid enters a straight channel there is a region when the boundary layer is developing and hence the velocity profile is changing usually in the main stream direction. If the channel is long enough, then after some distance, the velocity profile should stabilize and become invariant with respect to spatial distance. In order to test the hydraulics of the straight inlet, two channels were selected ($R/T_w = 8.2$ and $R/T_w = 0.75$) that represent both extremes of curvature. The straight inlet of both channels is 11 meters which is long enough to expect the velocity profile to be fully developed before encountering the bend. If our CFD code is indeed capturing the physics of the flow reasonably well, then at some point in the straight inlet the velocity profile must attain fully

developed status. Anything short of this would mean there is an undue mixing of changing velocity physics in the straight inlet with what should be non-uniform flow in the channel bend. This would make isolating events due to the curve difficult and would mean a violation of what we know from basics fluid dynamics of straight open channel flow. Shown in Figures 3.1 and 3.2 are the streamwise velocity profiles for the two selected channels in the fully developed region. The velocity profiles are taken from 5 equidistant points in the traverse direction 0.05m from either side wall. Vertical velocity profiles along 10 longitudinal positions where taken. Figures 3.1 and 3.2 show that the flow gets fully developed as expected before the fluid enters the bend. This provides a measure of confidence that the tool can reasonably capture the complex flow physics in the channel.

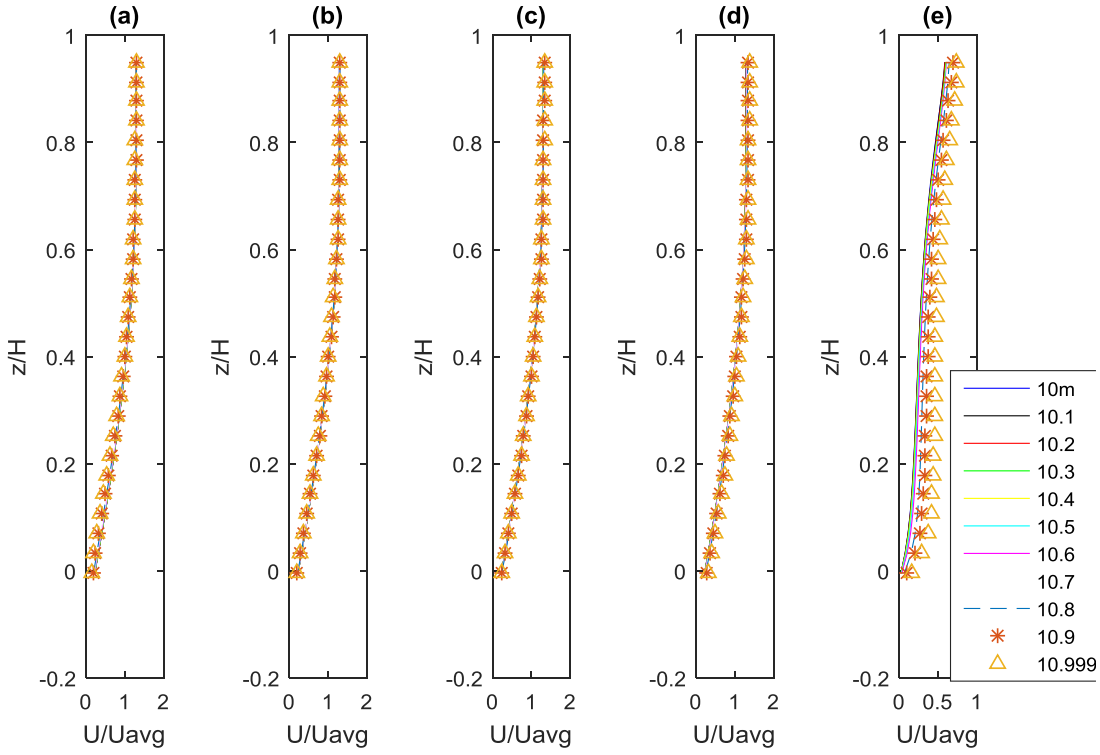

Figure 3.1: Fully developed stream wise velocity profiles in the straight inlet portion for the mild curve ($R/T_w = 8.2$). (a) The velocity profile 0.05m from the left wall, (b) velocity profile 0.15m from the left wall, (c) velocity profile 0.25m from the left wall, (d) velocity profile 0.35m from the left wall (e) velocity profile 0.05m from the right wall.

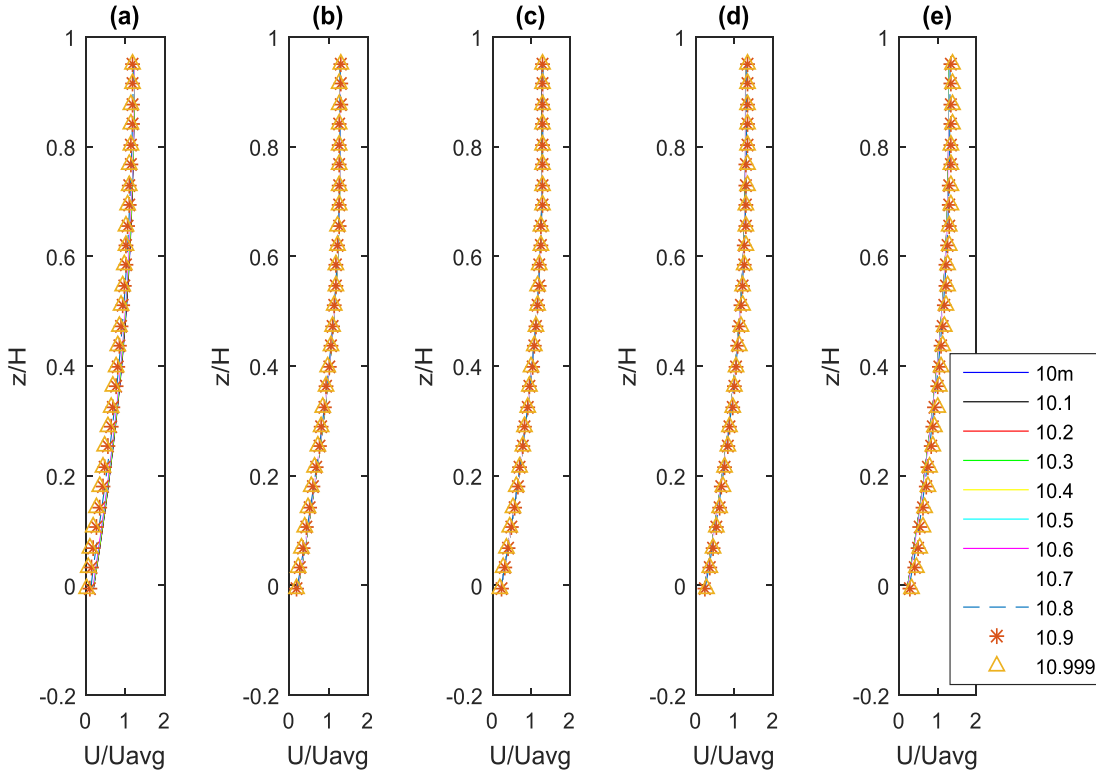

Figure 3.2: Fully developed stream wise velocity profiles in the straight inlet portion for the tight curve ($R/T_w = 0.75$). (a) The velocity profile 0.05m from the left wall, (b) velocity profile 0.15m from the left wall, (c) velocity profile 0.25m from the left wall, (d) velocity profile 0.35m from the left wall (e) velocity profile 0.05m from the right wall.

3.3.2 Experimental validation

The most common form of CFD code validation in literature is to compare experimental data with simulation results. If the results of the simulation are reasonably close to that of the experiment, then the code is said to have been validated and a reasonable measure of confidence is established in the ability of the code to reproduce accurate results.

Our computational fluid dynamics code was validated using the experimental data of Booij (2003). A schematic of the experimental channel is shown in Figure 3.4. The experimental apparatus has an 11m straight inlet, to ensure that the flow was fully developed before encountering the bend (this was already validated in section 3.3.1), a 180 degree curve with a radius of 4.1 m and an outlet of 6.7 m. The channel

width is 0.5 m with hydraulically smooth walls and at uniform flow depth upstream maintained (for the initial condition only) at 0.052 m. All measurements were taken at steady state from 9 equidistant locations between two points 0.05 m from the side walls at the 135 degrees plane (see Figure 3.4). This experiment was repeated using CFD with a simulation time of 600 seconds which was more than enough time for the flow to be steady. While hydraulic details of the simulation are shown in Table 3.1, the validation results are shown in Figure 3.5 with panels 1, 2, and 3 showing the non-dimensional main stream, cross stream, and depth velocities respectively. It is clear from the results that there is excellent agreement between the mainstream velocities in the experiment and the simulation. This agreement is important as it shows that the simulation is capable of capturing enough of the relevant physics to establish confidence in results of other simulations. The velocity distribution across the width also shows good agreement. For much of the channel cross-section, especially in the central sections and the inner bank, the depth velocities show good agreement. However, at the outer banks, the depth velocities show big differences between experimental results and simulation. This discrepancy can be explained as by Booij (2003):

''The *LDV beam configuration used for measuring through the bottom yields the largest error in the already small measured value of the vertical velocity component W. Hence the reliability of the obtained depth velocity is relatively poor*. ''

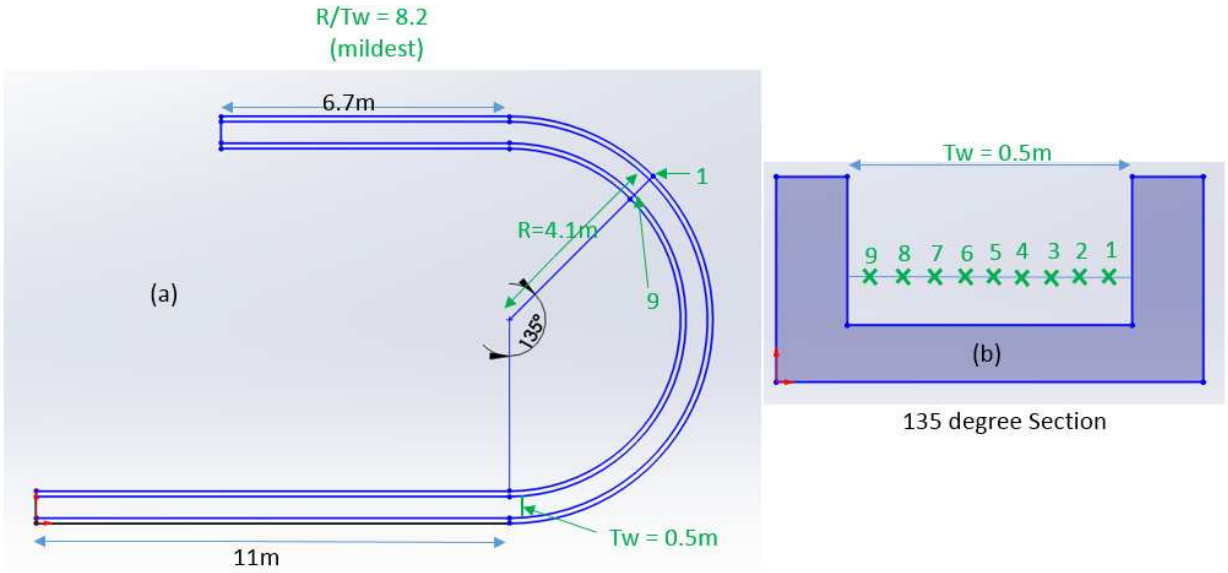

Figure 3.3: (a) Schematic of the curved open channel used to validate the CFD tool used in this research. Note all length measurements in the diagram are in meters. (b) The 135° section note the parts labelled 1 and 9 show the progression of point where the velocity measurement are taken.

Another important aspect of the validation is the correct reproduction of the large scale vortical structures in the flow. Figure 3.6 shows the vortex structure at the 135 degree plain in the experiment performed by Booij (2003) while Figure 3.7 shows a reproduction of the results using the our CFD code. The correct reproduction of the vortex structure by our CFD code has two significant implications for the validity of our tool in this research. First concerning the correct reproduction of the main body cell, it has been stated in literature that the main body circulation is due to the interaction between the centrifugal forces and radial pressure gradient (both are large scale external forces). This means that the CFD tool chosen for this research is capable of reproducing the large scale physics of fluid flow correctly. Secondly concerning the correct reproduction of the counter rotating circulation cell close to the outer bend, literature attributes this phenomenon to the complex interaction between the anisotropy of the turbulent stresses and the centrifugal force (Van Balen 2009). Booij (2003) showed that computational models that do not reproduce the anisotropy of the turbulent stresses fail to produce the counter rotating cell in their results (compare Figure 3.8 (a) and (b)). Therefore, since our model reproduced the counter rotating cell,

the approach taken to the representation of turbulence (Large Eddy Simulation) is adequately capable of reproducing the small scales and adding this effects to the large scale physics.

Table 3.1: Hydraulic details for the validation of experiment performed by Booij 2003.

R(m)	B(m)	H(m)	Q(m^3/s)	U_{avg}(m/s)	Re	Fr	R/B	R/H
4.1	0.5	0.052	0.0052	0.2	10400	0.28	8.2	78.8

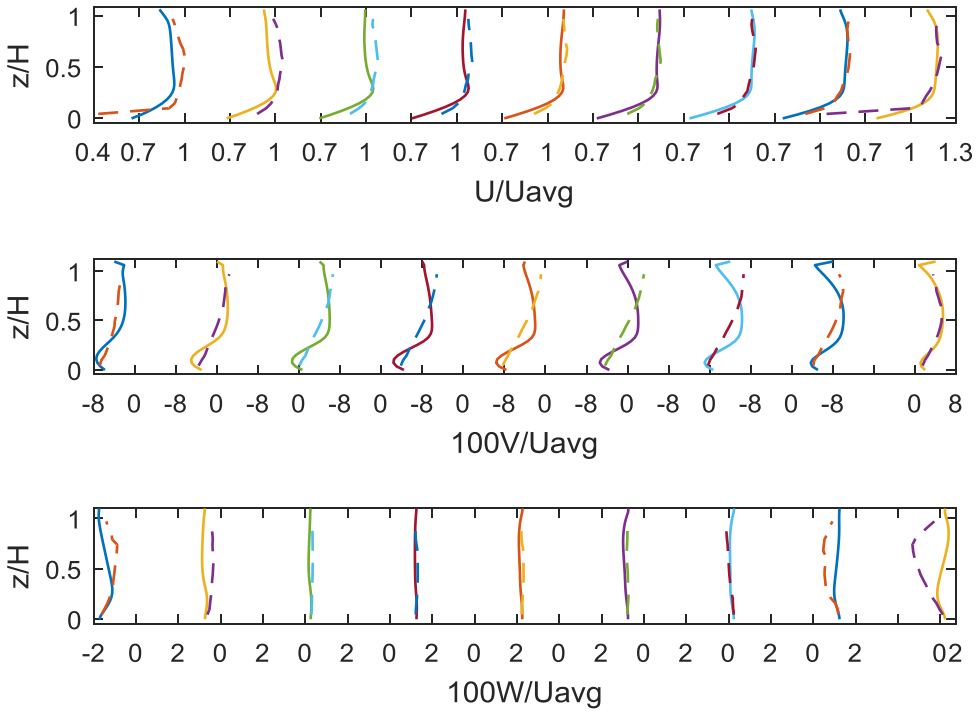

Figure 3.4: Validation plot for the experiment carried by Booij 2003 the solid lines are the LES simulation while the dashed lines (--) are the experimental results. Top panel shows the non-dimensional mainstream velocity, second panel shows the non-dimensional traverse velocity, and the bottom panel shows the non-dimensional depth velocity. All velocities are non-dimensionalized with the average velocity.

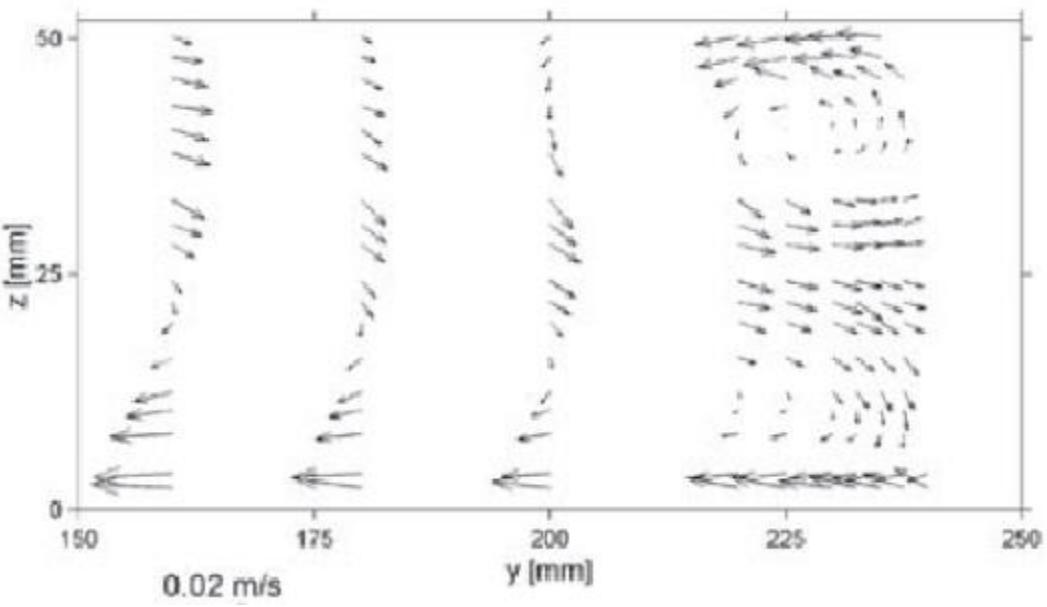

Figure 3.5: Results for the transverse velocity in the 135^{o} cross section for the experiment by Booij 2003.

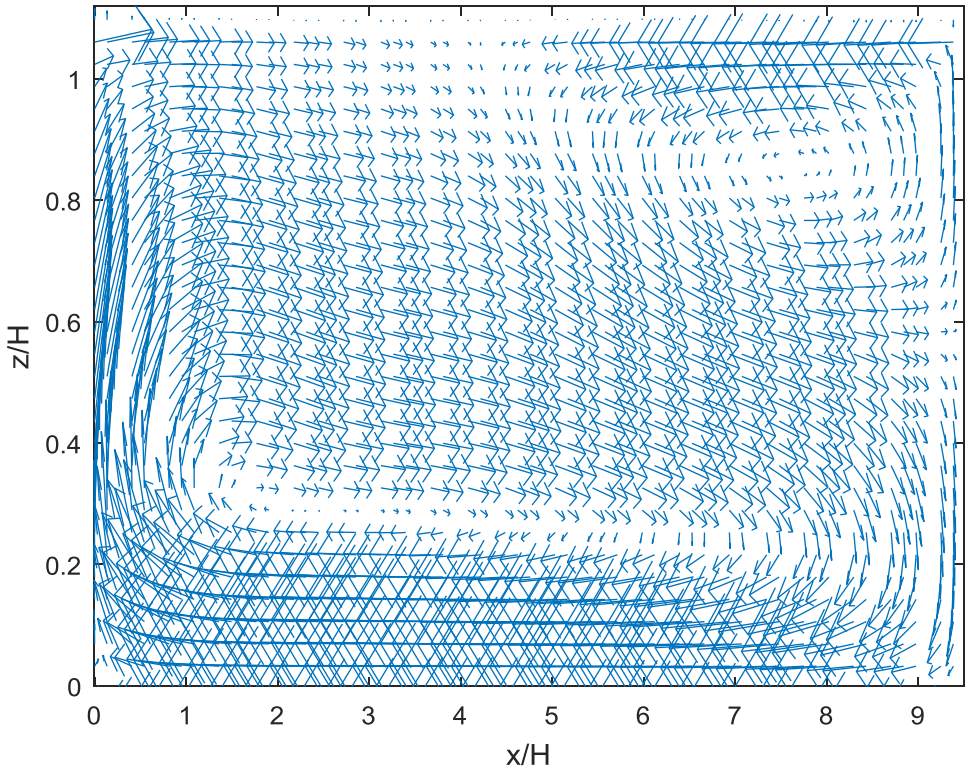

Figure 3.6: A Computational Fluid Dynamics reproduction of the experiment shown in figure 3.5.

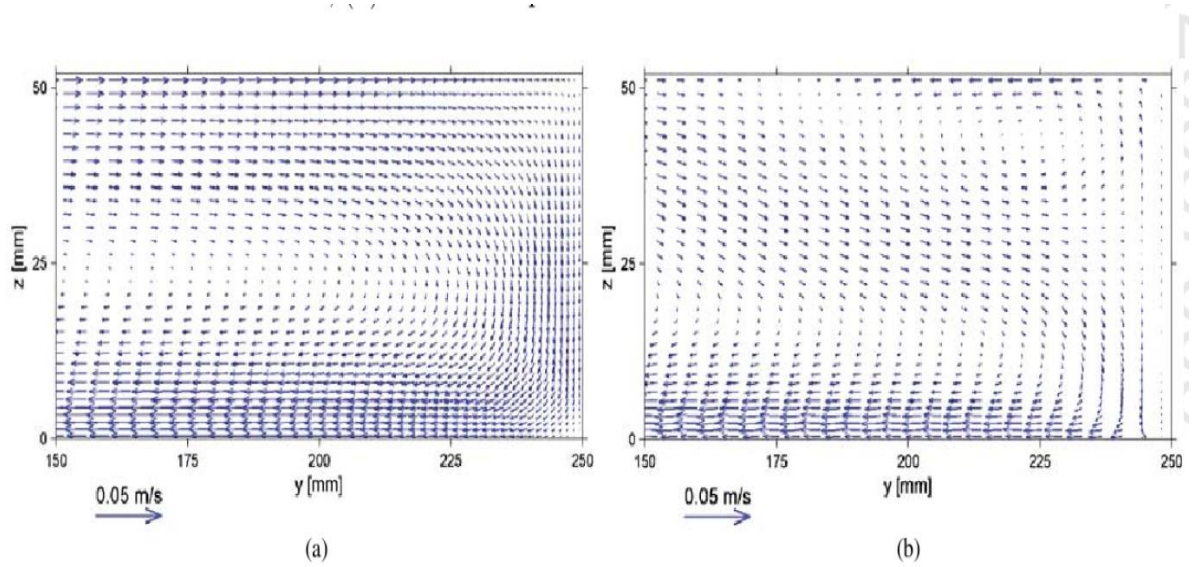

Figure 3.7: (a). The transverse velocity of a CFD simulation of the experiment by Booij using the k-ε turbulence model. (b). the same transverse velocity using a large eddy simulation model.

3.4 Grid sensitivity analysis

In validating a computational code an important test of the robustness and accuracy is the invariance of simulation results with a change in mesh size. A drastic change in results due to mesh size variation could be an indication of error accumulation or some other deficiency with the tool and results obtained from such a tool should be treated with some suspicion. In this research a grid sensitivity analysis was performed. The open channel bend of Booij (2003) (used to validate the code in section 3.32) was chosen with grid sizes (in the horizontal plain) of 0.005m, 0.01m and 0.02m in an attempt to test variation of the results. Figure 3.8 shows the velocity plot at 9 equidistant positions at the 135 ^{o} plane taken at steady state. The plot shows that the results at various grid sizes are almost identical indicating that it is insensitive to variation in grid size. However, there is a large variation with grid size at the outer bank for the cell size 0.02 m as seen in Figure 3.8 for the main stream and traverse velocities. The reason for this large variation is that at such a low resolution (compared to the other simulations) the wall bounded region in the horizontal plain is poorly resolved leading to results with higher error. The vertical velocities

in all three panels remain identical because the grid size for all three simulations in the vertical dimension was maintained at the same value.

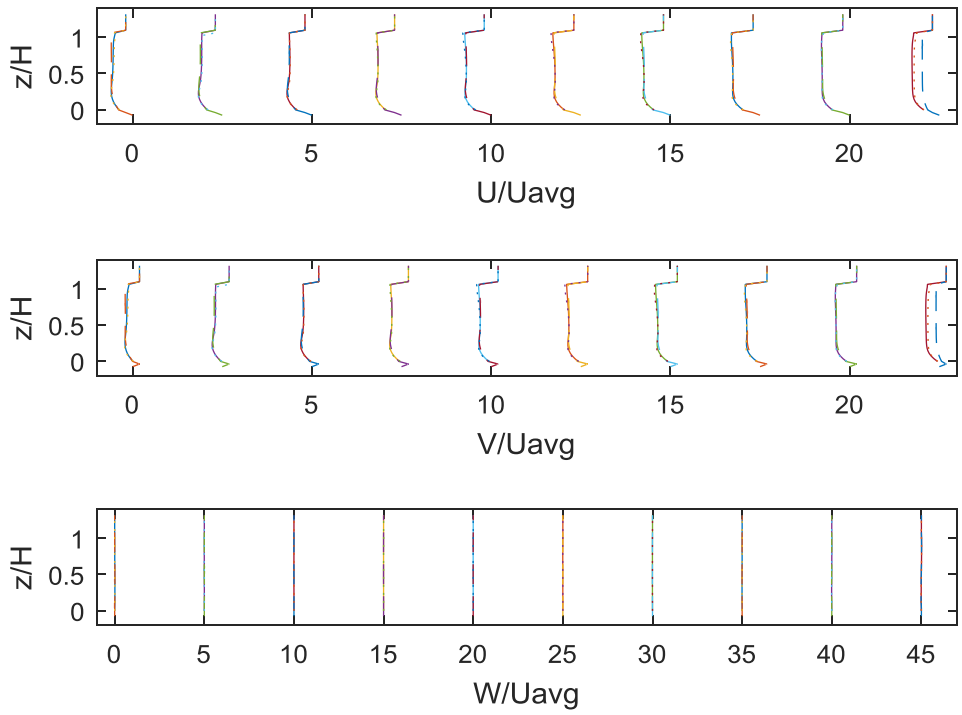

Figure 3.8: Grid Sensitivity plot. Note the velocities in this figure was taken from the 135 ^{o} plain. The solid lines (-) are for the cell size 0.01 m, the dashed line (--) are for the cell size 0.02 m and the dotted lines (..) are for the cell size 0.005 m. Top panel shows the mainstream velocity, second panel shows the traverse velocity, and the bottom panel shows the depth velocity.

3.5 Research framework

This section is used to set the context for the next three chapters of this dissertation (chapters 4, 5 and 6) and a conclusion provides results that detail the contributions of this research to current scientific knowledge in open channel bend flows. These contributions come from a total of 22 computational fluid dynamics simulations studying various aspects of river bend flows. However, much like other scientific works, this thesis builds on previous attempts at understanding the physics of bend channel flow especially the work of Shin (2014). His research established the basic framework encapsulated in equation

(3.9) which form the foundation of our study. Nevertheless, there are big distinctions between this research work and that of Shin (2014).

$$\frac{\tau}{\rho U^2} = f\left(\frac{L_c}{D}, \frac{R_c}{D}, F_r, Re, S_o, \frac{\varepsilon}{D}\right) \ldots\ldots\ldots\ldots\ldots\ldots\ldots\ldots (3.9),$$

where τ is the shear stress,

ρ is the fluid density,

U is the fluid velocity,

L_c is the length of the curve,

F_r is the Froude Number,

R_c is the Radius of curvature,

Re is the Reynolds Number,

S_o is the slope of the channel,

ε is the roughness height of the channel,

D is the flow depth.

One big distinction is that Shin (2014) was mainly interested in the distribution of boundary shear stresses (which is important for engineering design purposes) in an open channel bend with a view to parameterizing it in terms of a parameter called K_b (the ratio of the shear stress in the bend to the shear stress in the straight upstream channel) while this research focuses on examining the three-dimensional flow structure and dynamics of an open channel bend with a view to gaining better understanding of its physics. Moreover, equation (3.9) contains too many dimensionless groups and would greatly increase the time required for this study, therefore it would be desirable to make some more simplifying assumptions to reduce the number of dimensionless groups. In order to achieve this aim, it is assumed that the flow parameters are invariant with Reynolds number as long as the flow is turbulent. This is a reasonable assumption because in a turbulent flow the inertial forces are several orders larger than the viscous forces such that the counterbalancing effect of viscosity is virtually nonexistent. Another assumption is that the effects of changing the channel slope is negligible hence that dimensionless group

can be dropped from equation (3.9). While the slope plays an important role in natural rivers dynamics, the above assumption helps simplify our analysis while still maintaining the practical usability of our results since a slope typically just increases the inertia of the fluid. While roughness exists in natural rivers this research considers only smooth rigid boundaries with zero roughness. It is believed that future researchers can pick up from where this research stops and extend the results to boundaries with roughness. Applying the assumptions outlined above equation (3.9) becomes

$$\frac{\tau}{\rho U^2} = f\left(\frac{R}{T_w}, \frac{L}{T_w}, F_r\right) \ldots\ldots\ldots\ldots\ldots\ldots\ldots\ldots (3.10)$$

which defines the general framework this research would take (Note that the flow depth D has been replaced by the top width T_w). Thus, Chapter 4 would study the effect of curvature variation on the three dimensional flow structure of an open channel bend. Chapter 5 would examine the effects of changing the curvature length on open channel bend flow physics, while Chapter 6 would study the effect of the variation of Froude's number on the fluid dynamics of bend flows.

The bend geometries used in this numerical research are at a size scale of a laboratory replica of a natural river system. Nevertheless, this research is still applicable to river systems research for several reasons. One such reason is that even though natural rivers have larger flow depths than all of the numerical simulations carried out, the ratio in natural rivers of the main stream flow dimension to the depth is such that the general paradigm of the shallow water assumption still hold. This make our research relevant since the small flow depth used in our simulation is based on a shallow water assumption. Another reason why this research would be relevant is that despite the small Reynolds numbers of all our numerical models compared to natural river the basic assumption of turbulent flow is still realized.

To facilitate easier explanation in future chapters, this section of this thesis would be referred to as the Research framework section.

3.6 Summary

This chapter discussed in general, computational fluid dynamics as a tool and in detail, the particular tool that would be used in this research. The numerical tool solves the three-dimensional Navier-Stokes equations on a regular grid using the finite volume approach. This tool which represents the dependent variables on a staggered grid resolves the free surface of the fluid by solving a transport equation for the fluid surface in a method known as the Volume of Fluid method (V.O.F). Turbulence is incorporated into the model by Large Eddy Simulation technique. Because of the high computational cost of resolving fully the near wall turbulence a wall function is used. This essentially means that the model is an LES-RANS hybrid where the main body turbulence is resolved with LES and the near wall turbulence is resolved using a RANS model of the k- ε flavor. Several rigorous tests including an examination of the hydraulics of the straight inlet and comparison with results of available experiments have been used to show that the code adopted can reproduce a wide range of flow physics anticipated in this research. Hence the conclusion is that the CFD code chosen in conjunction with physical reasoning and dimensional analysis constitute an adequate collection of tools with which better insight into the physics of river bend flows can be gained.

Chapter 4

The effect of curvature on flow structure and dynamics of open channel bends

4.1 Preamble

This chapter studies the effect of a change in curvature (defined as the ratio of the radius of curvature to the top width) on the three dimensional flow structure and dynamics of open channel bend flows. In order to study these effects, a large eddy simulation tool is utilized which incorporates the volume of fluid free surface solver (already detailed in Chapter 3) to obtain results for analysis. The results concerning the effects of curvature on the distribution of shear stress in open channel bend flows are analyzed in section 4.3 after which section 4.4 looks at the evolution of velocity distribution with changes in channel curvature. Because of the importance of flow separation in fluid flows, section 4.5 examines in detail the boundary layer separation patterns in channels of different curvatures. In addition, since the rotational component of flow is crucial to a complete understanding of the flow physics in a bend, section 4.6 studies in detail the vorticity distribution and its evolution with channel curvature.

4.2 Background

In the Research framework section of this dissertation (see Section 3.5) a framework for the study of curved open channel flow was established (equation (3.10)). In this section the first dimensionless group on the right hand side of equation (3.10) is studied. Specifically, the effects of a change in curvature (defined as the ratio of the radius of curvature R to the top width T_w) on the three dimensional flow structure of an open channel bend. As has already been detailed in Chapter 2, several studies have been carried out on general bend channel flow dynamics by De Vriend (1981), Odgaard & Bergs (1988), Whiting and Dietrich (1993), Blanckaert & Graf (2001), Booij (2003), Blanckaert and De Vriend (2004), and Blanckaert (2009). In fact, there has been a couple of specific studies on the effects of curvature variation on bend channel flows (Kashyap 2012, Ottevanger 2011). Nevertheless, there are still a couple of factors

that leave room for improvements in the current understanding of the evolution of flow structure with changes in curvature. One such factor is the fact that the overwhelming majority of numerical studies carried out in this regard have used tools based on the Reynolds averaged Navier Stokes equations (see chapter 2). As has already been explained by Booij (2003), Van Balen (2009), and Blanckaert (2009), the Reynolds averaged equations with a turbulence model is incapable of reproducing some of the critical flow structures, hence a study of bend channel flows based on such an equation may not be the most appropriate in the present context. Even in bend channel studies that use LES, all the studies that have appeared in literature (to our knowledge) do not vary the geometry. While these studies provide valuable insight, it is known that a key parameter that affects the flow structure of a fluid in a bend is its curvature. Therefore, a proper understanding of the bend flow physics needs to include a component that studies the evolution of velocity distribution, vorticity structure, and shear stress distribution in a bend as the curvature changes.

Furthermore, choices of methods for resolving the free surface can introduce uncertainty. This is exemplified from the most popular method for resolving the free surface which assumes that the free surface is a rigid lid that flows with the fluid (Van Balen 2009). It has been argued in literature that as long as the longitudinal and traverse free surface slopes are small the errors introduced by this are not significant. Some studies have put the limit for the applicability of the rigid lid assumption at Froude Number <0.5 (Kashyap 2012) above which the errors can be expected to grow beyond acceptability. It should be noted however that while this limit was determined based on a sampling of curved channels of various curvatures, studies have shown (Ramamurthy et al., 2013) that there can be several instances where Froude's number stays below this limit but numerical tools based on this assumption fail to capture the relevant free surface dynamics correctly. This is especially true in sharp curved open channels where large regions of extreme free surface gradients exist. Despite this, and the fact that majority of eddy resolving flow studies use the rigid lid assumptions, results from such studies have provided valuable

insight such that some understanding of the physics of open channel bend flows is known today. However, since this research strives for more than just a general understanding, especially in a field like river dynamics that is still plagued by uncomfortable uncertainties, this study eliminates the possibility of such free surface errors occurring by using the volume of fluid method (Hirts 1981). It is for these reasons that this chapter investigates the effect of curvature variation on the flow structure and dynamics using large eddy simulation.

In studying the effects of curvature, four simulations with 180 degree curved channels were performed. The inlet to each of the channel is 11m long to allow for the flow to become fully developed before encountering the bend, while the outlet is 6.7m long. This study varies the geometry of the curve by examining flow in four curvatures ranging from mild at $\frac{R}{T_w} = 8.2$ to tight at $\frac{R}{T_w} = 0.75$ (see Tables 4.1 and 4.2 for details), Note that channels with curvature $\frac{R}{T_w} < 3$ are considered tight. This effectively means that the radius of curvature is varied since the top width remains constant for all channels. In order to enhance the isolation of the relevant physics the same initial and boundary conditions were imposed on all four simulations. At the upstream inlet a volume flow rate of 0.0052m^3/s was imposed while the wall being hydraulically smooth has the no slip boundary condition. An atmospheric boundary condition was imposed on the outlet and the free surface. The fluid was initialized as stationary with a flow depth of 0.052m and allowed to run up to steady state at which point all measurements in this chapter were collected. The hydraulic details are shown in Table 4.1 while the discretization details are shown in Table 4.2.

Table 4.1: Hydraulic details for the four simulations conducted.

	R(m)	R/Tw	R/H
Simulation 1	4.1	8.2	78.80
Simulation 2	2.0	4.0	38.46
Simulation 3	1.0	2.0	19.23
Simulation 4	0.375	0.75	7.212

* Note that the width B(m), uniform depth upstream H(m), volume flow rate Q(m^3/s), average velocity U_{avg}, Reynolds number Re and Froude's number Fr remained constant at values given in table 1 above for all 4 simulations.

Table 4.2: Meshing details for the four simulations conducted.

	Mesh Numbers	Total Number Cells
Simulation 1	3088 x 50 x 27	4168800
Simulation 2	2428 x 50 x 27	3277800
Simulation 3	2114 x 50 x 27	2853900
Simulation 4	1918 x 50 x 27	2589300

In order to facilitate better understanding, each of the four simulations used in this chapter are given aliases. These would be denoted in capital letters with quotes to distinguish them from single letters in a sentence. All reference to simulation number should be cross checked with Tables 4.1 and 4.2 for details. The mildest curve with a curvature $\frac{R}{T_w} = 8.2$ associated with simulation 1 in the relevant tables is denoted as $'EM'$ which stands for extremely mild. The second channel with the curvature $\frac{R}{T_w} = 4$ associated with simulation 2 is denoted as $'M'$ for mild. The channel with curvature $\frac{R}{T_w} = 2$ associated with simulation 3 is denoted as $'T'$ for tight. Finally the channel with curvature $\frac{R}{T_w} = 0.75$ associated with simulation 4 is

denoted as $'ET'$ for extremely tight. These aliases would be used inter-changeably with the details of the various simulation runs for the remainder of this chapter.

4.3 Shear stress distribution.

The distribution of the boundary shear stress reveals part of the dynamics of bend flows and is important from an engineering design perspective. This is because when designing curved channels or preparing a river training program, engineers need to know the distribution of forces exerted over the boundary area so that erosion, sediment movement, and other processes can be accounted for. A general exploration of the four channel runs in this study immediately reveal three distinct shear stress distributions. In the mild bends 'EM' and 'M', the maximum bed shear stress as the fluid moves into the curve is situated close to the outer wall and remains so till the exit (Figures 4.3 and 4.4). However in the tighter curves $'T'$ and $'ET'$ there seems to be two different bed shear stress distributions. The tightest curve $'ET'$ shows a shear stress distribution that never has its maximum close to the outer bend for the entirety of the bend length (Figure 4.1). The curve $'T'$ has a complex bed shear distribution such that initially the maximum bed shear is located close to the inner wall for more than three quarters of the curve length (this is different from the distribution in the mild channel were the maximum initially close to the inner bed at the inlet quickly shifts close to the outer bend a short angular distance from the inlet to the curve) after which the maximum moves close to the outer bend for the reminder of the curve length (see Figure 4.2).

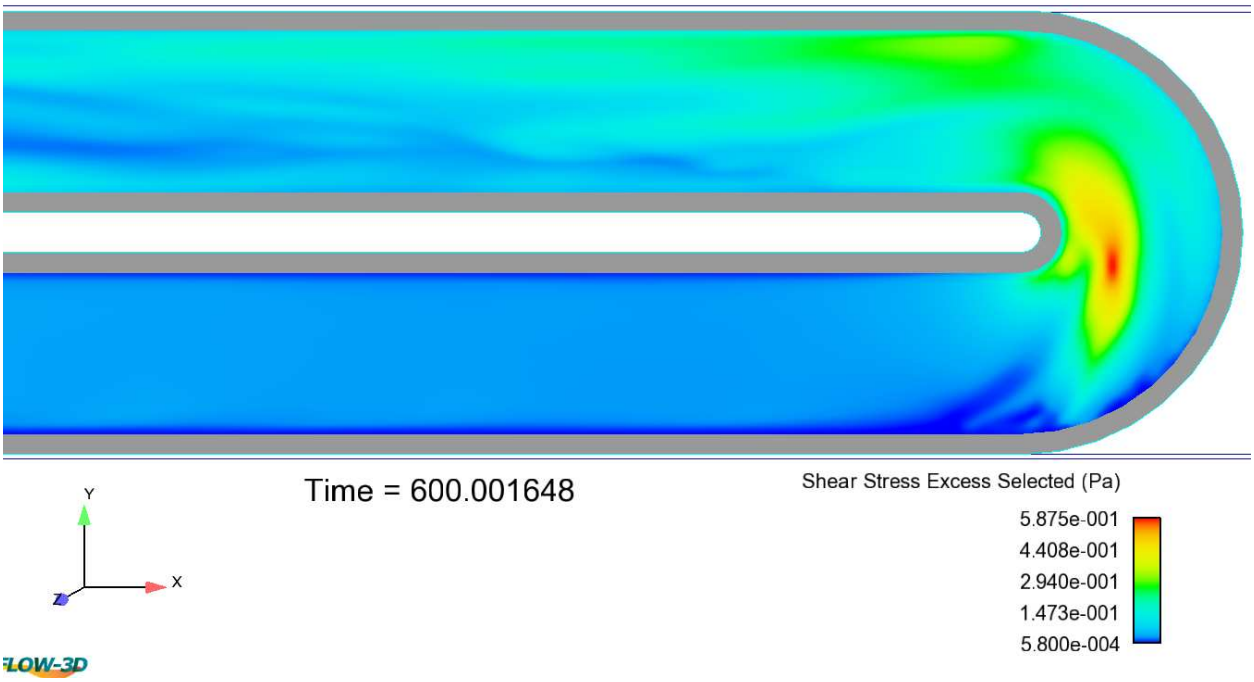

Figure 4.1: Bed Shear Stress distribution for the tight curve ($R/T_w = 0.75$). All radius are defined from the channel center line.

Figures 4.1 to 4.4 only provide the general trend of the bed shear stress distribution. In order to see the details of the shear force dynamics, various line plots in different dimensions have to be examined. The detailed exploration of the four channels begins at the inlet to the curve with Figure 4.5 showing the shear stress distribution. It is clear from this diagram that the maximum shear stress at the inlet to the curve is located close to the inner bend regardless of the curvature. This shear stress distribution at the inlet (for all the four channels) is indicative of the fact that the largest velocity gradients are situated close to the inner wall. The physical reasons why this is so will be explored in the next chapter of this thesis. The wall shear stress distribution follows the same patterns with the maximum wall shear stress exerted on the inner wall at the inlet.

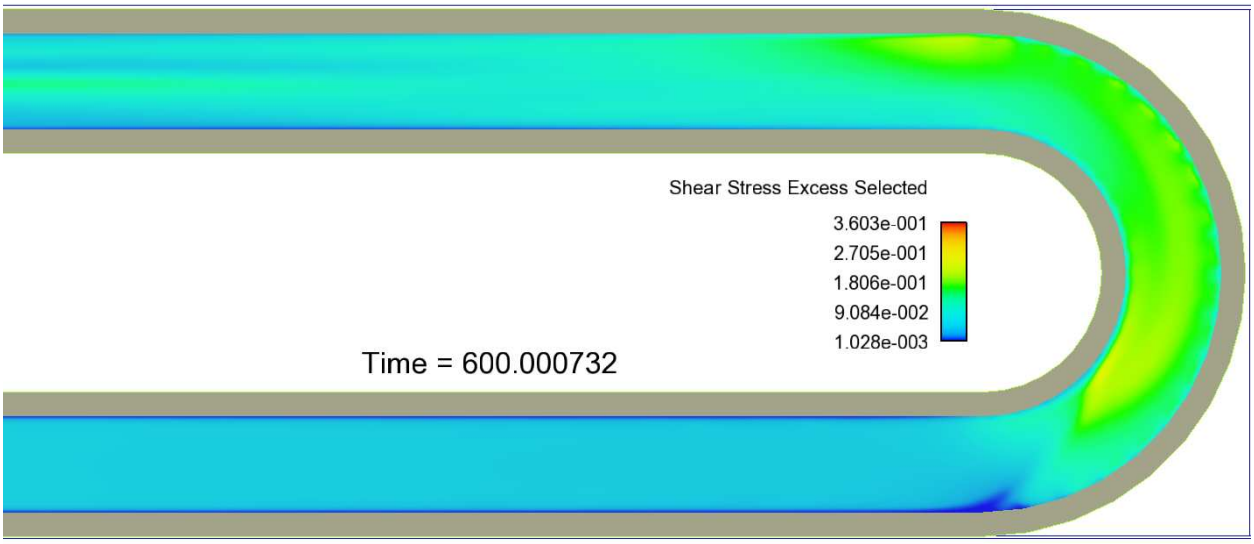

Figure 4.2: Bed Shear Stress distribution for the tight curve ($R/T_w = 2.0$).

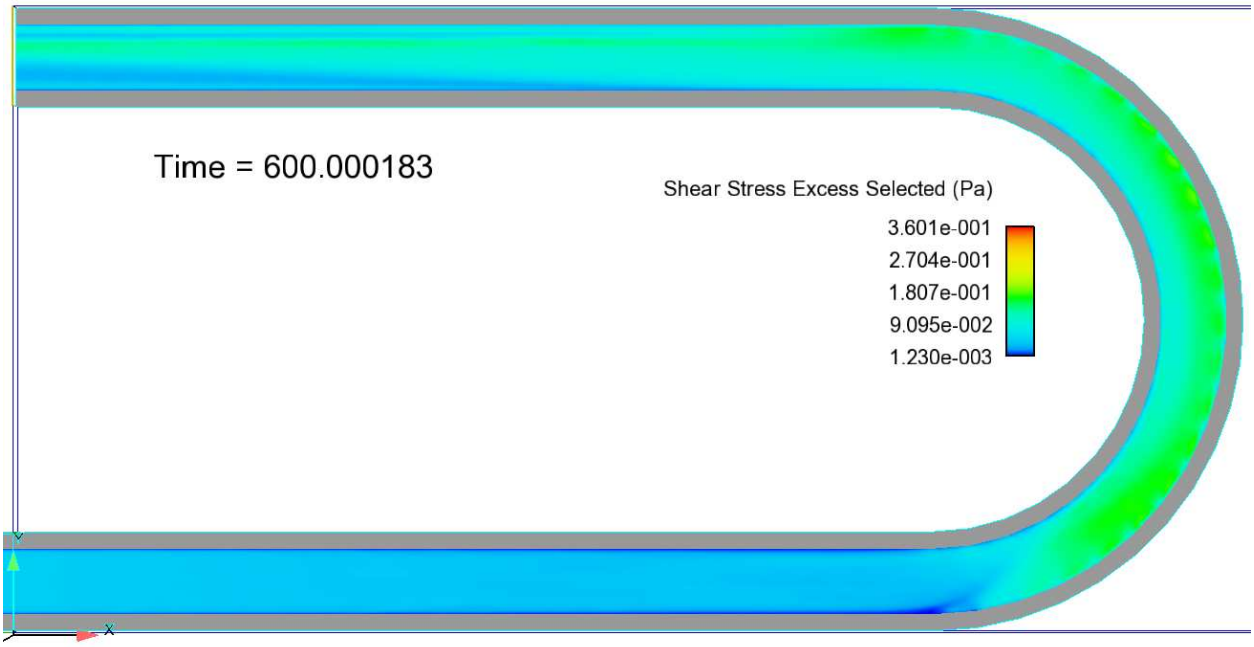

Figure 4.3: Bed Shear Stress distribution for the mild curve ($R/T_w = 4.0$).

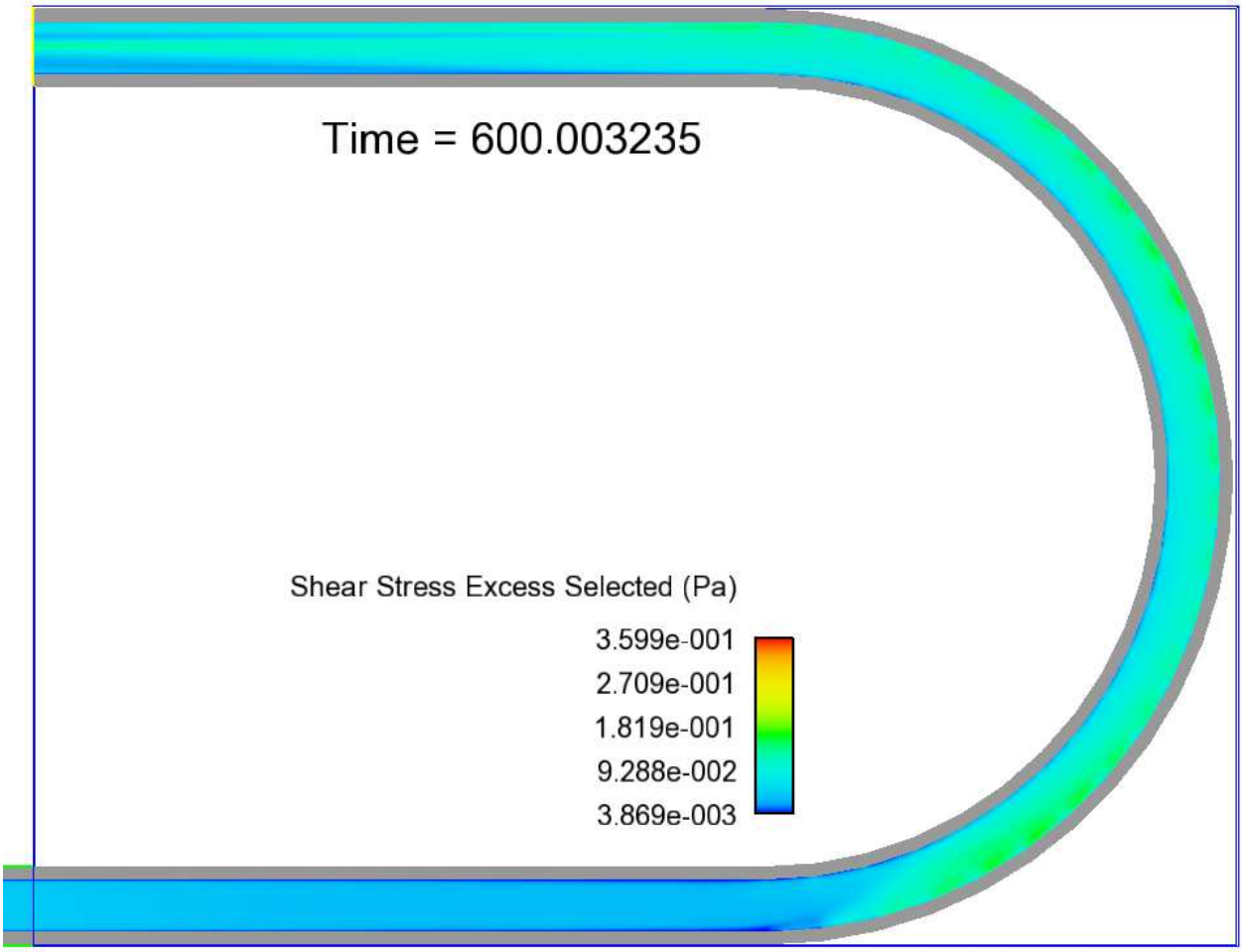

Figure 4.4: Bed Shear Stress distribution for the mild curve ($R/T_w = 8.2$).

Moving away from the inlet into the bend, the bed shear stresses begin to exhibit different characteristics. The mild bends $'EM'$ and $'M'$ (recall that a mild bend is one where $R/T_w > 3$) have their maximum bed shear stress shift quickly to the outer bend regions (see Figure 4.6). This is indicative of a shift in the region of high velocity gradients to the outer bend due to the effect of centrifugal acceleration and other forces as predicted by the standard theory of bend channel circulation (Blanckaert and De Vriend 2004). The tight bends $'ET'$ and $'T'$ however, exhibit a different shear stress distribution as already hinted above with both (initially close to the inlet) having their maximum far away from the outer bend. For the bend $'T'$ what the general trend (Figure 4.2) does not reveal is that the channel has its maximum

shift gradually from the inner bend at the zero degrees plane to the middle of the channel at about the 30° plane (see Figure 4.6a) after which the maximum begins to migrate again back to the inner wall and is at the inner wall by the 60° plane (Figure 4.6b). The bed shear stress then begins to adjust toward that of a zero shear gradient profile with the maximum shear stress values on the inner bend reducing and the values at all other positions increasing to form an almost horizontal shear stress distribution by about the 95° plane . Afterwards the outer shear stress begins to grow and becomes the maximum till the bend exit (see Figure 4.6c and d). In essence the tight channel 'T' has the same stress distribution as the mild channel beyond about the 120° plane.

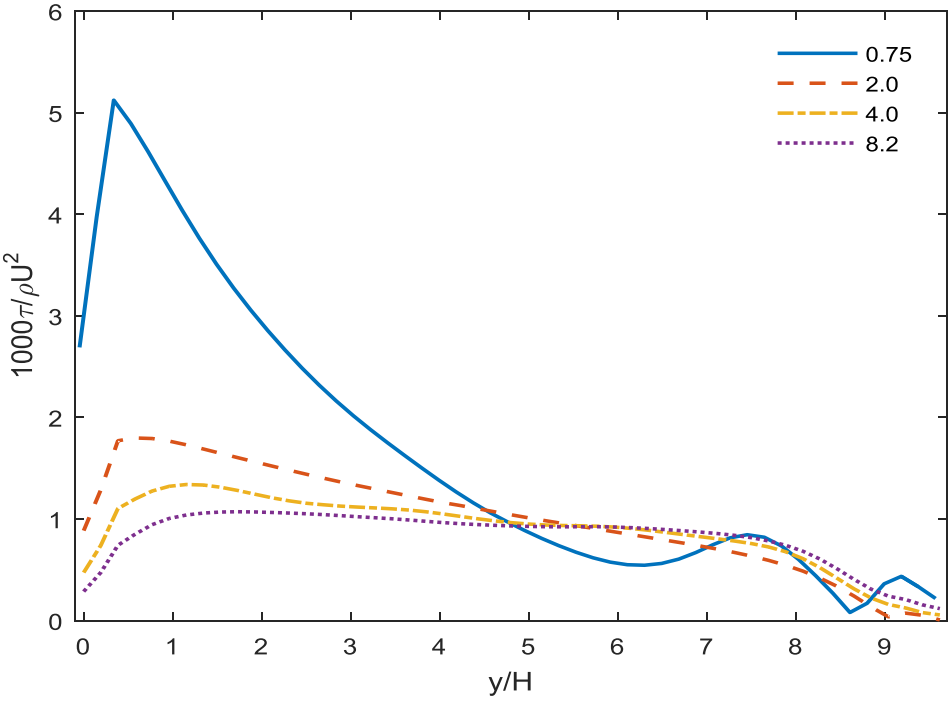

Figure 4.5: Bed Shear Stress distribution at the inlet to the bend. Note H is the flow depth.

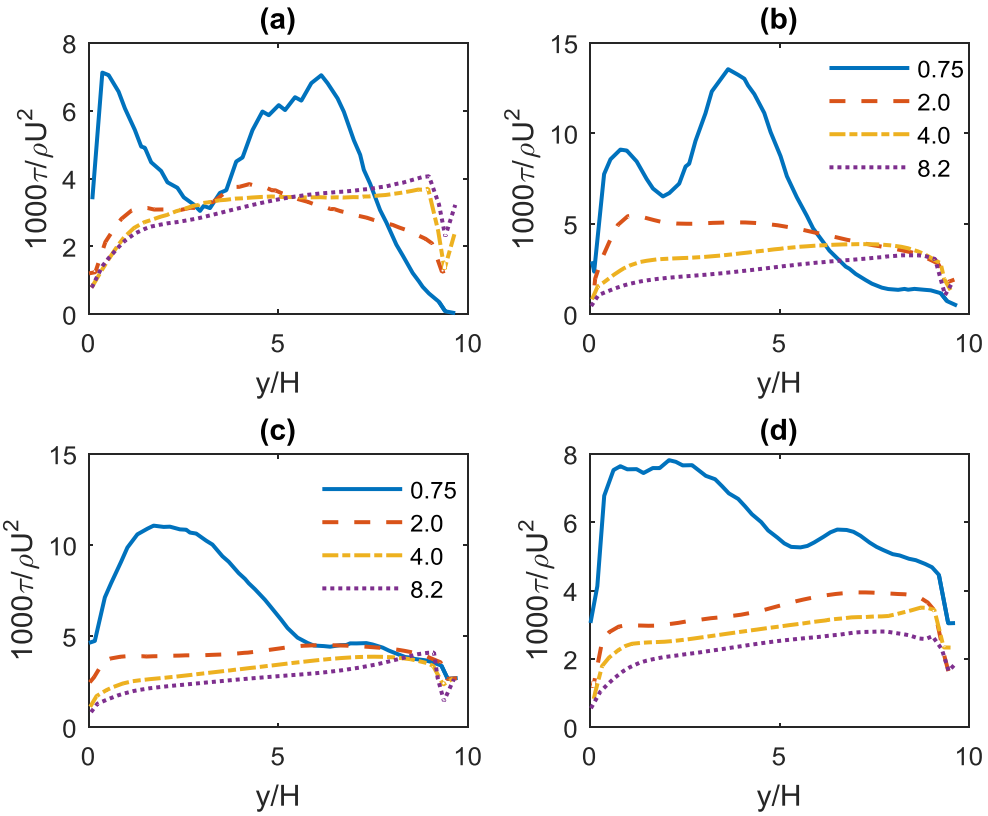

Figure 4.6: Bed Shear Stress distribution. Panel (a) shows the bed shear stress at the 30° plane , panel (b) show the bed shear stress at 60° plane , panel (c) show the bed shear stress at 120° plane , while panel (d) show the bed shear stress at 160° plane.

The tightest channel on the other hand starts with a maximum close to the inner bend and begins to develop an area of local maximum. This region of local maximum grows such that by the 30° plane a 'bi-modal' bed shear stress profile emerges (see Figure 4.6a). This region of local maximum keeps growing such that by the 60° plane it has become the global maximum as shown in Figure 4.6b. This new maximum starts moving toward the inner wall and stays there till the bend exit. Therefore for the tightest channel $'ET'$, at no position in the bend is the maximum bed shear stress ever at the outer bend, a peculiar shear stress distribution when compared to the other channels. The various wall shear stresses follow closely the distributions of their respective bed shear stress (see Figure 4.7). It is clear that for the most part in

the mild channels $'EM'$ and $'M'$, the maximum wall shear stresses are exerted on the outer wall while for the tight channel $'T'$ its maximum is exerted on the inner wall for about 75% of the curve length and then shifts to the outer wall for the remainder of the channel length. The tightest channel $'ET'$ has its maximum exerted on the inner wall (Figure 4.7).

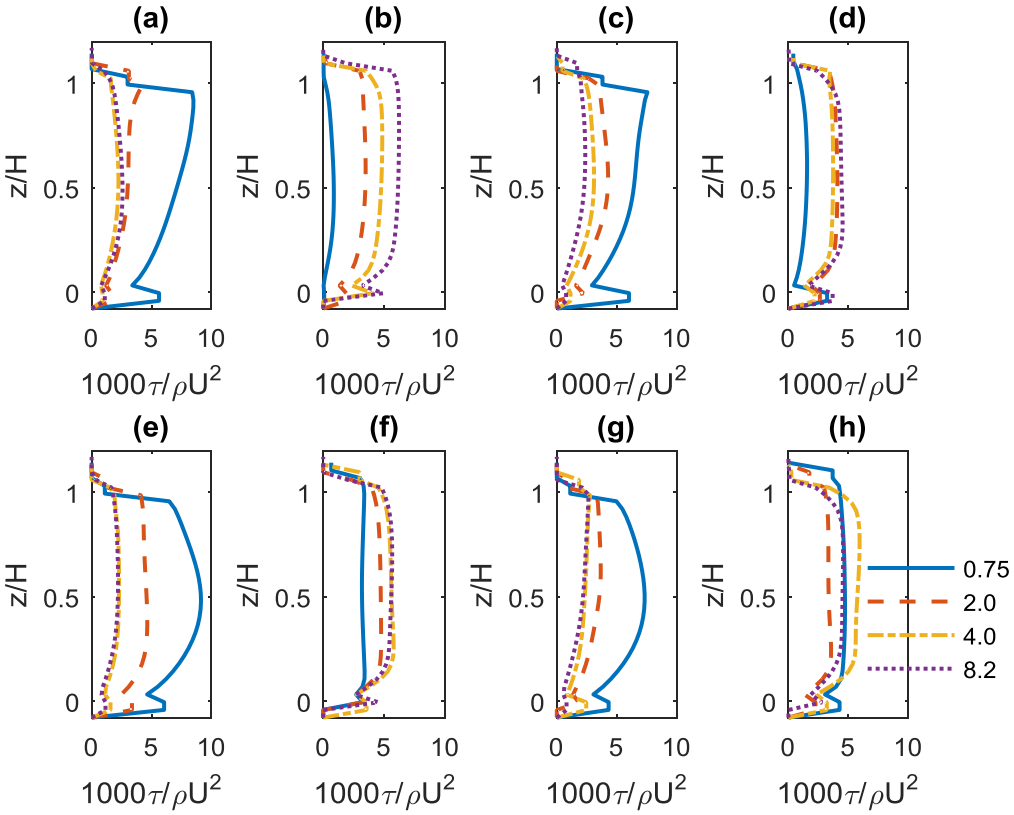

Figure 4.7: Wall Shear Stress distribution. Panels (a), (c), (e), (g) show the inner wall velocities for 30,60,90 and 120 degrees while panels (b), (d), (f), (h) show the outer wall shear stresses for 30,60,90 and 120 degrees.

Despite the fact that this section has described fully the evolution of the boundary shear stress from curve entry to outlet, the details of the dynamics that drive this behavior has yet not been detailed. This is because more information is required to make sense of the various shear stress patterns that has been observed from our simulation results. Since the shear stress is a direct consequence of the velocity

gradient distribution, better insight can come from an examination of the velocity distribution. Therefore, in our journey towards understanding the physics of bend channel dynamics the velocity distribution will be examined in the next section.

4.4 Velocity distribution

An examination of the distribution of velocity can help explain the pattern of boundary shear stress observed in the previous section in the respective channels. Figures 4.8 to 4.11 show the distribution of velocity on vertical planes spaced at 5 degree intervals. It is clear from these results that the distribution of velocity is dependent on the curvature of the channel. Thus, in the mild channels $'EM'$ and $'M'$ (Figures 4.8 and 4.9) the velocity distribution is such that at a short distance from the inlet, the streamlines (or regions) of higher velocities are skewed towards the outer bend regions while streamlines of lower velocities are packed close to the inner bend region. This is due to differential advection of the velocity by the effect of the centrifugal acceleration and the radial pressure gradient which, close to the free surface, pushes more energetic fluid towards the outer bend leaving less energetic fluid close to the inner bend. The tighter channels however seem to have different velocity distributions. For instance, the tight channel $'T'$ (Figure 4.10) seems to have its streamlines of higher velocity start close to the inner wall at the entrance to the curve, this distribution then shifts with the streamlines of higher velocities moving to the middle of the channel (occurring between about the 40 degree and the 90 degree plane). Finally, in the fully developed region of the flow (beyond 90 degrees) the streamlines of maximum velocities shifts to the outer bend for the remainder of the channel. The curve $'ET'$ has a similar velocity distribution with the other curves only in the developing region (0 to 90 degrees). However, beyond 90 degrees the region of maximum velocity stays close to the middle or inner wall region (Figure 4.11). Hence, in the curve $'ET'$ at no point is the region of higher velocity (and hence velocity gradients) ever close to the outer walls.

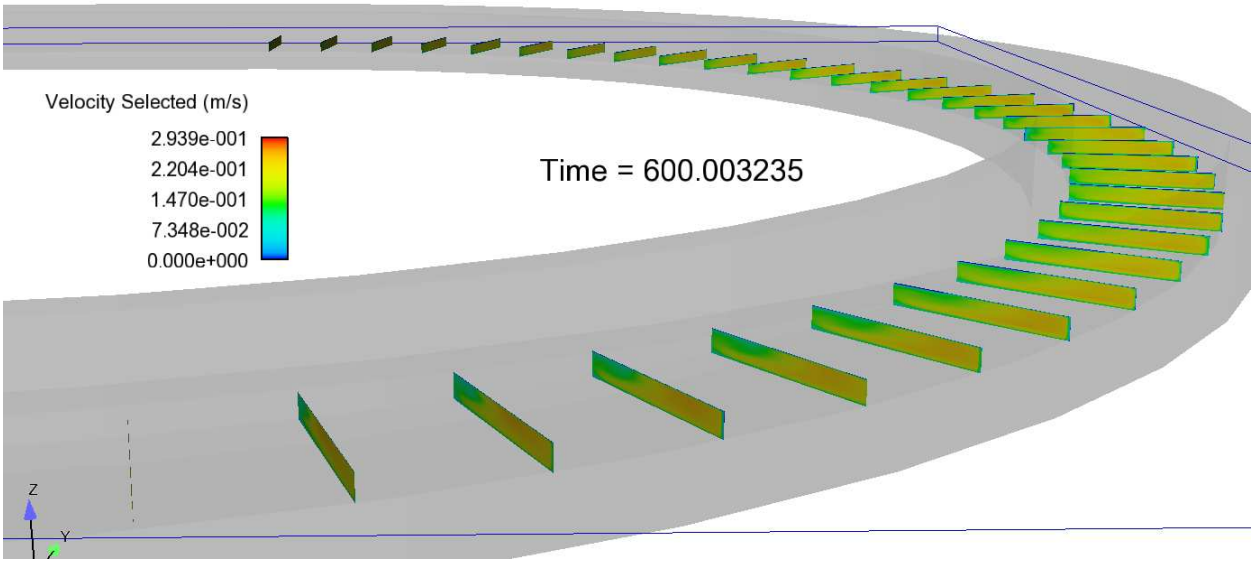

Figure 4.8: Velocity distribution in the mild channel R/Tw = 8.2.

While Figures 4.8 to 4.11 shows the velocity distribution, these results also reveal clear signs of flow separation in certain parts of the bend in all the channels (both mild and tight). Since understanding the pattern of flow separation is critical to gaining better insight into the fluid mechanics of bend channel flows the next section is devoted to a detailed study of the flow separation patterns both in the convex inner bank region and the concave outer bank region and its implication for the flow physics in a river bend.

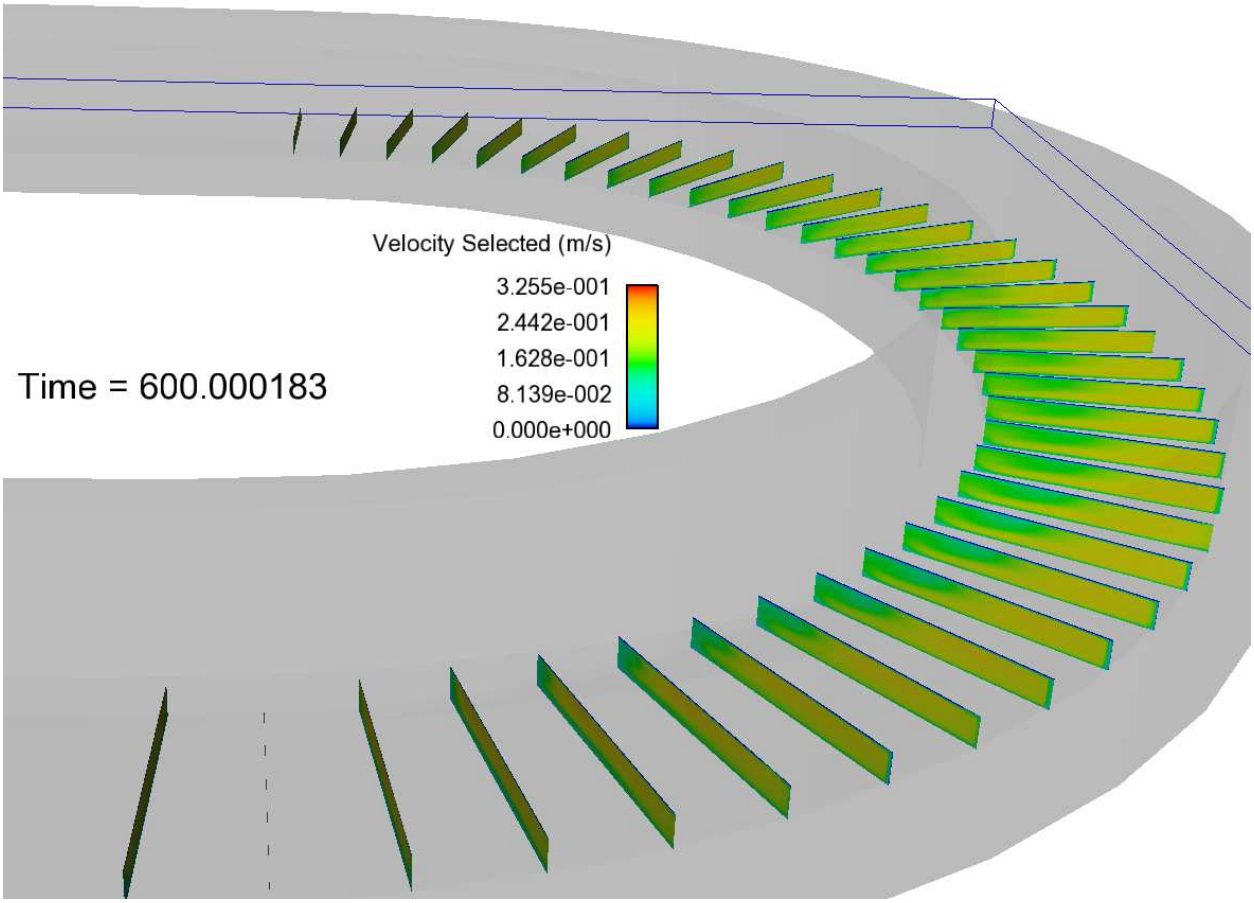

Figure 4.9: Velocity distribution in the mild channel R/Tw = 4.0.

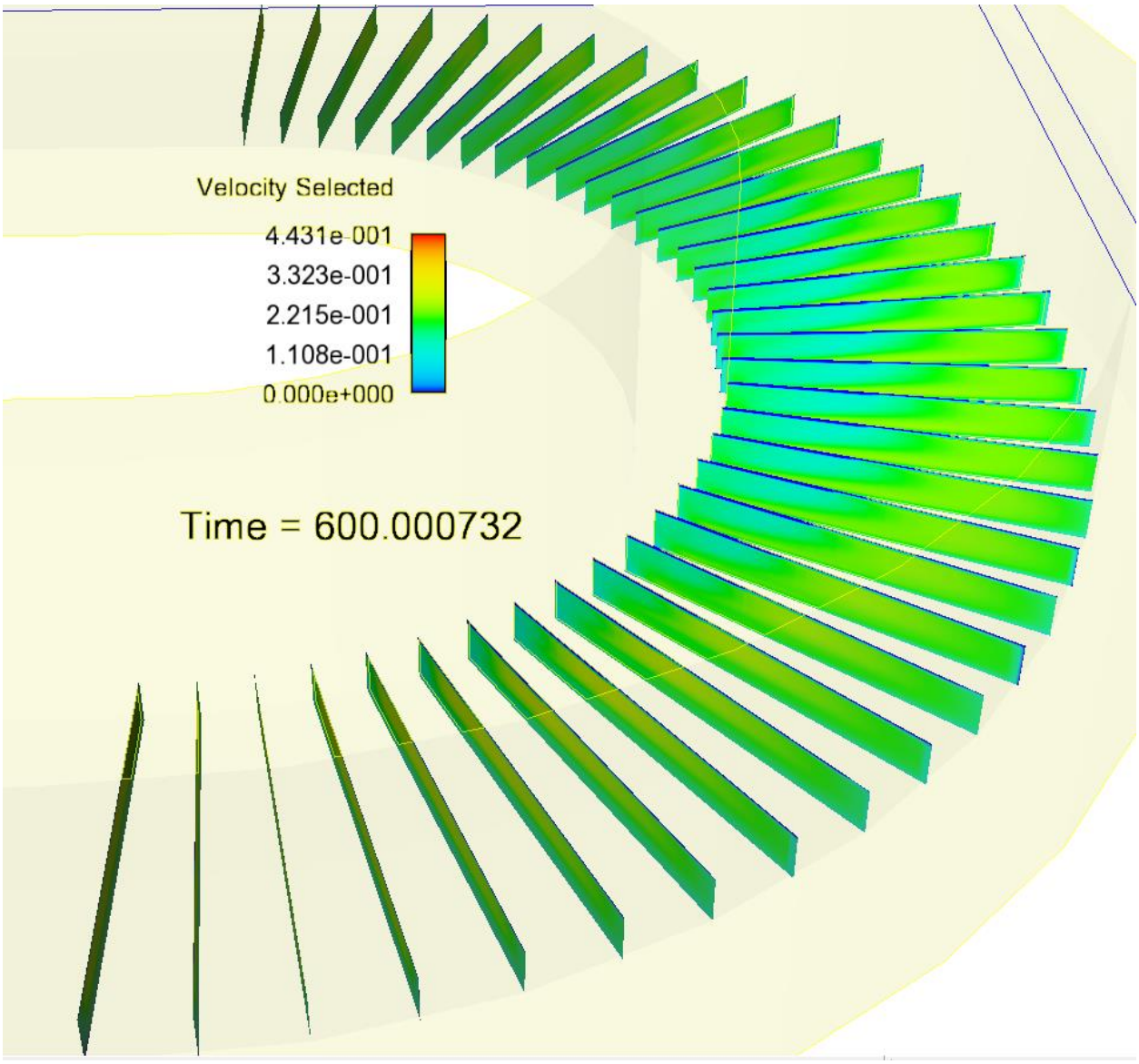

Figure 4.10: Velocity distribution in the mild channel R/Tw = 2.0.

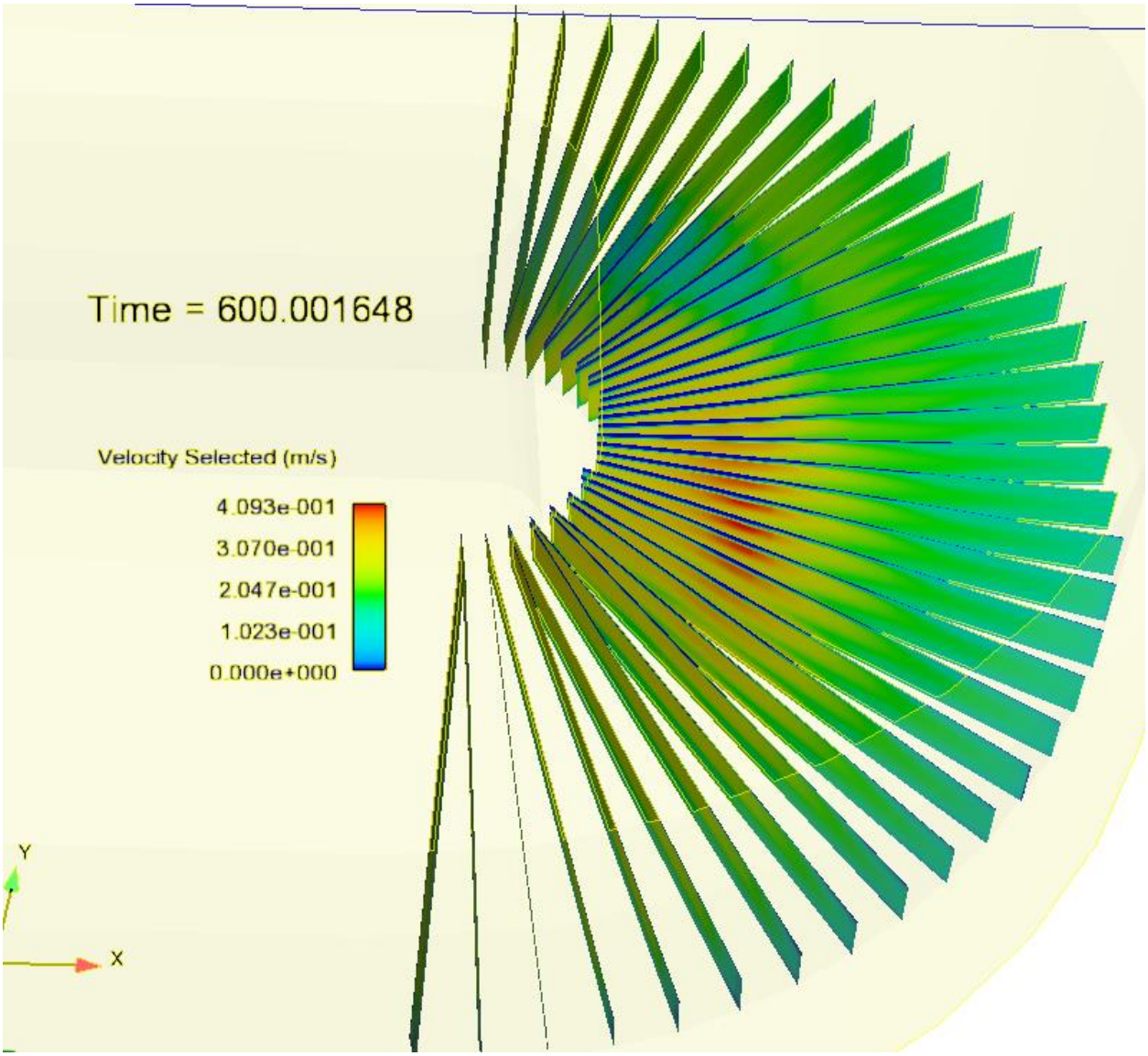

Figure 4.11: Velocity distribution in the mild channel R/Tw = 0.75. Note the dark blue colors are at the surface.

4.5 Flow separation in an open channel bend

An abrupt change in curvature due to the geometry of a bend channel with a straight entrance can induce a boundary layer separation that could significantly shape the physics of an open channel bend. Understanding the effects of these boundary layer separation patterns could provide further insight concerning the events that occur when a fluid encounters a bend. It is for this reason that this section looks at flow separation in the four open channel bends in this section.

Flow separation in natural meandering channels has been studied by Ferguson et al (2003), Frothingham and Rhodes (2003), Nanson (2010), Schnauder and Sukhodolov (2012) and in laboratory scale models of a tight bend by Blanckaert (2015). Despite the many studies that have appeared in literature, there is still no consensus as to the definition of what flow separation is. One popular definition is that proposed by Simpson (1989, 1996) which defines flow separation as a region in a fluid with a significant increase in the normal (away from) to the boundary component of velocity, which causes a shear layer and a thickening of the region of rotational flow between the boundary and the free stream. Using this definition, Simpson (1989,1996) identified two stages of flow separation in a bend channel flow based on a two-dimensional depth averaged analysis as shown in Figure 4.12. The first stage (or type) of flow separation occurs when there is a region of retarded flow in between the channel boundaries and the region of high speed velocity (this region of high velocity is referred to as the free stream velocity for the purpose of our discussion in this section). This is characterized by an inflection point in the velocity profile and the presence of a visible shear layer (see Figure 4.12a). Further downstream from the position of the flow separation, this shear layer diffuses such that there is a blurring of the line between the slow moving fluid and the free stream velocity (Figure 4.12c). In the second stage (or type) of flow separation the velocity profile drops below zero (Figure 4.12b) and a region of re-circulating flow emerges in the space between the channel boundaries and the free stream velocity (Figure 4.12d).

Blanckaert (2015) extended the definitions of flow separation to a three-dimensional paradigm, in which he described flow separation as a region of significant velocity gradients perpendicular to the main stream velocity. This region is characterized by slow moving fluid sandwiched between the boundaries and the free stream velocity. Despite the apparent consensus in literature (Bagnolds 1960 and Blanckaert 2015) that no flow separation or development of an internal shear layer occurs in a mild bend ($R/B > 3.5$ in Blanckaert 2015), the numerical results discussed in this section reveals that this might not necessarily be true. This consensus on flow separation being an exclusive property of tight channels may be the

reason why there has been no systematic study of the effect of curvature on flow separation patterns in a bend. This section aims to fill that knowledge gap.

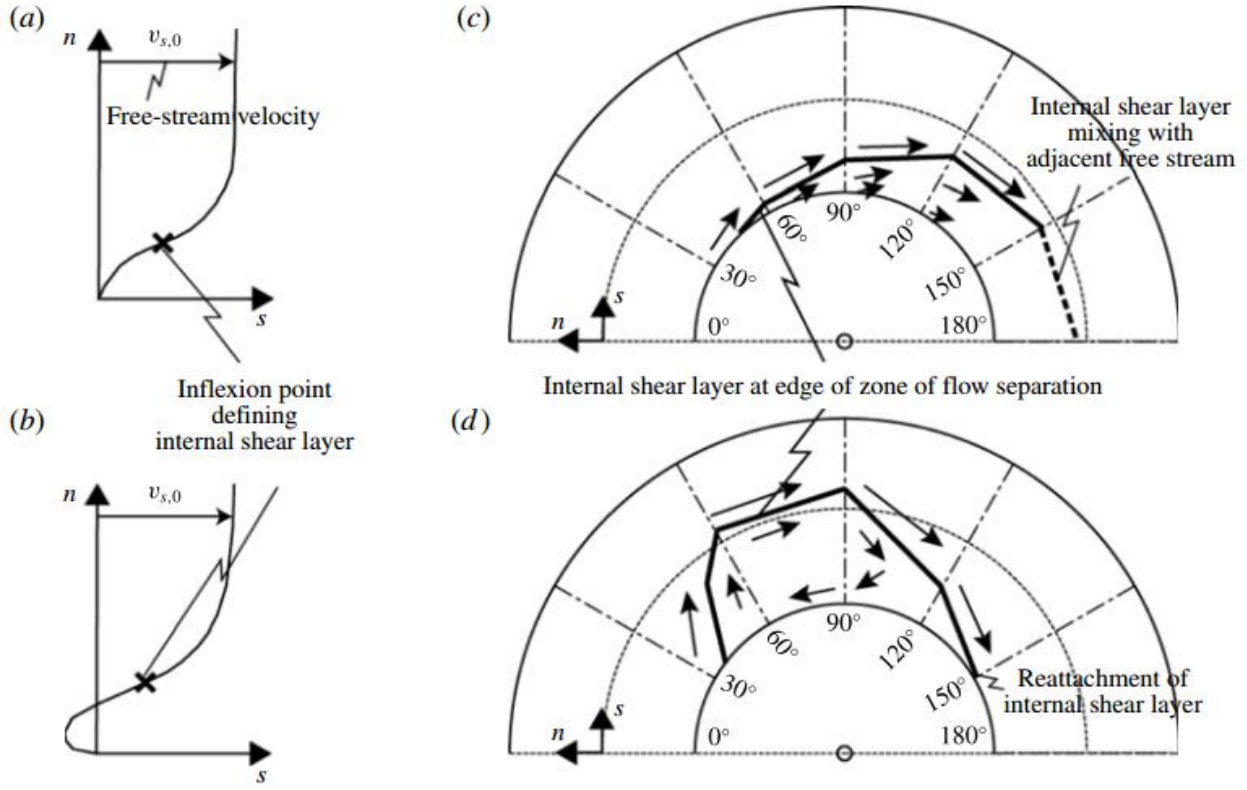

Figure 4.12: Definition sketch of flow separation. Panels (a) and (c) depicts flow separation of the first stage (or type) while panels (b) and (d) shows flow separation of the second stage (or type). Reproduced from Blanckaert (2015).

In channels $'EM'$, $'M'$,and $'T'$ when a fluid coming from a straight channel encounters the bend, the momentum of the fluid tends to continue in its straight trajectory until it encounters the outer (concave) curve boundary. This continuous straight trajectory combined with the centrifugal acceleration ensures that there is differential advection of fluid towards the outer bank causing a tilting of the traverse free surface and hence a radial pressure gradient. Such a free surface configuration guarantees that fluids coming into the bend on the outer wall side experience an adverse mainstream pressure gradient while fluids entering the curve on the side of the inner (convex) wall accelerate as they are subject to a favorable

pressure gradient. Hence there is a transport of momentum towards the inner wall region at all parts of the water column close to the curve entrance except at the free surface. This guarantees that there cannot be a flow separation at the inner wall close to the entrance since the radial pressure gradient and the momentum transport towards the inner wall oppose it. As the fluid moves deeper into the bend it begins to feel the effect of the centrifugal force and develops enough inertia to overcome the radial pressure gradient. This means the fluid breaks away from the inner wall as it is advected towards the outer wall causing a boundary layer separation. As shown in Figure 4.13, as this detached flow moves further into the bend, it merges with the 'free stream' flow in what is clearly a first stage flow separation. An examination of the details of the flow separation from these results show clearly that it starts with a distortion of the vertical plane velocity and formation of a region of extremely slow fluid near the inner wall (see figure 4.15 b, c and d).

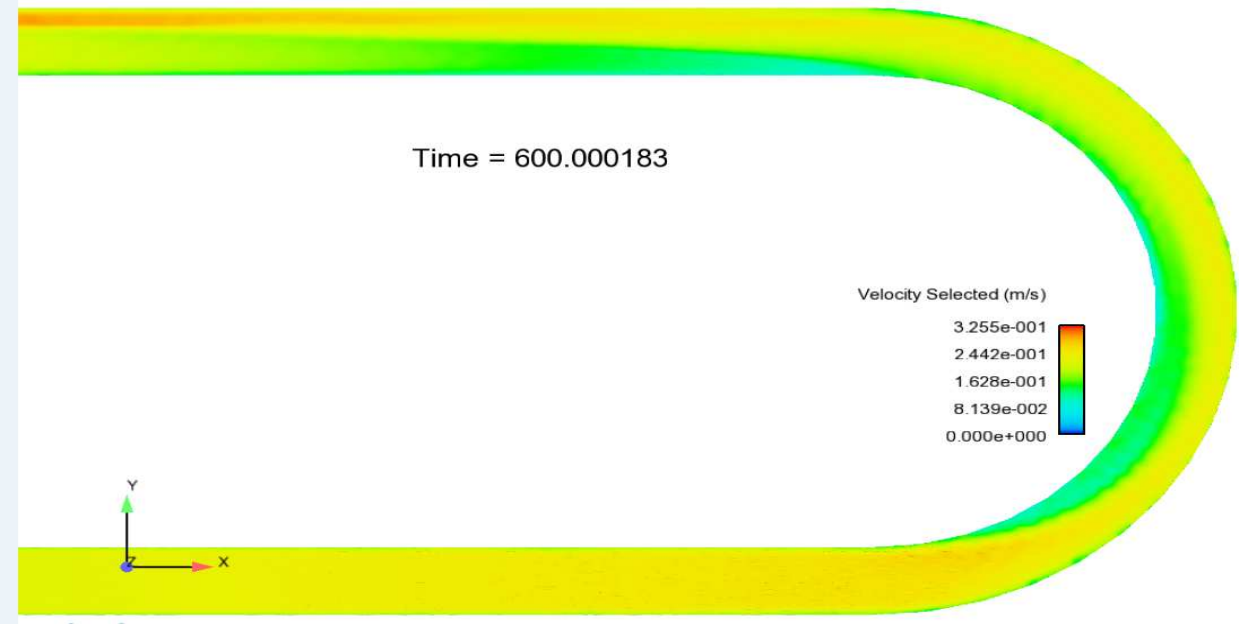

Figure 4.13: Showing the surface velocity distribution and flow separation in a typical channel.

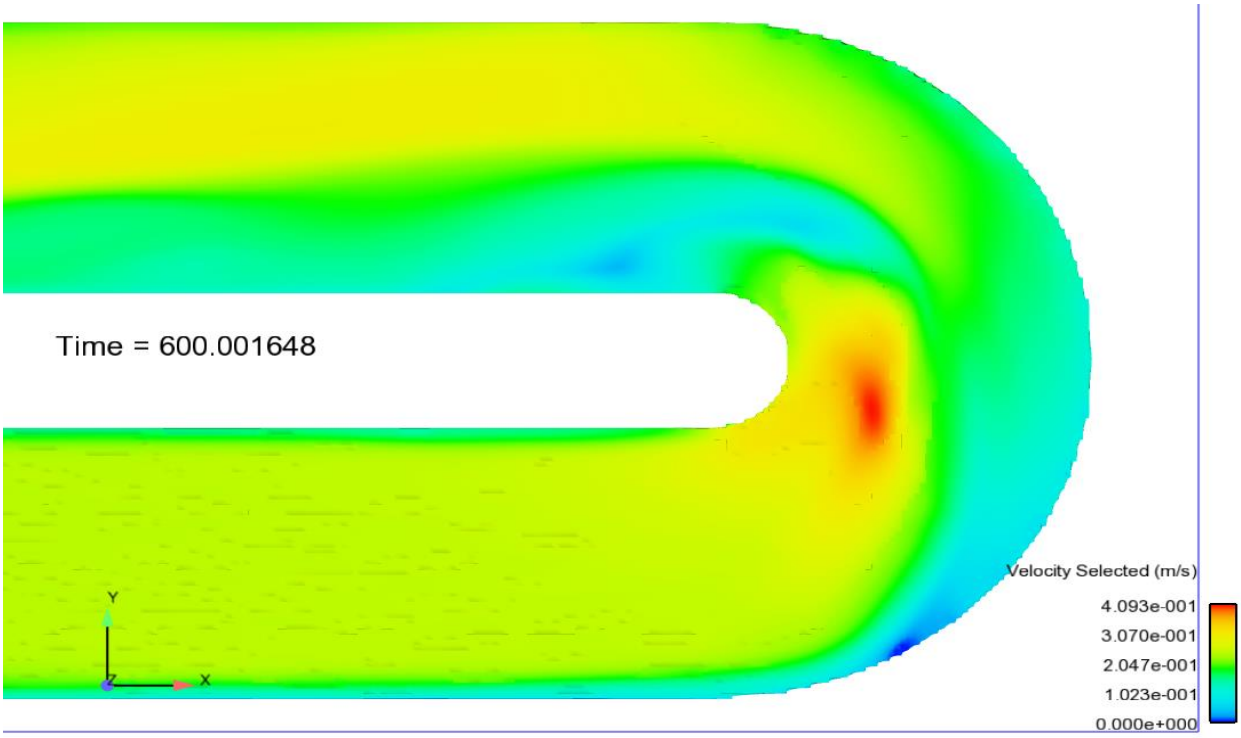

Figure 4.14: Showing the surface velocity distribution and flow separation in the tight curve R/Tw = 0.75.

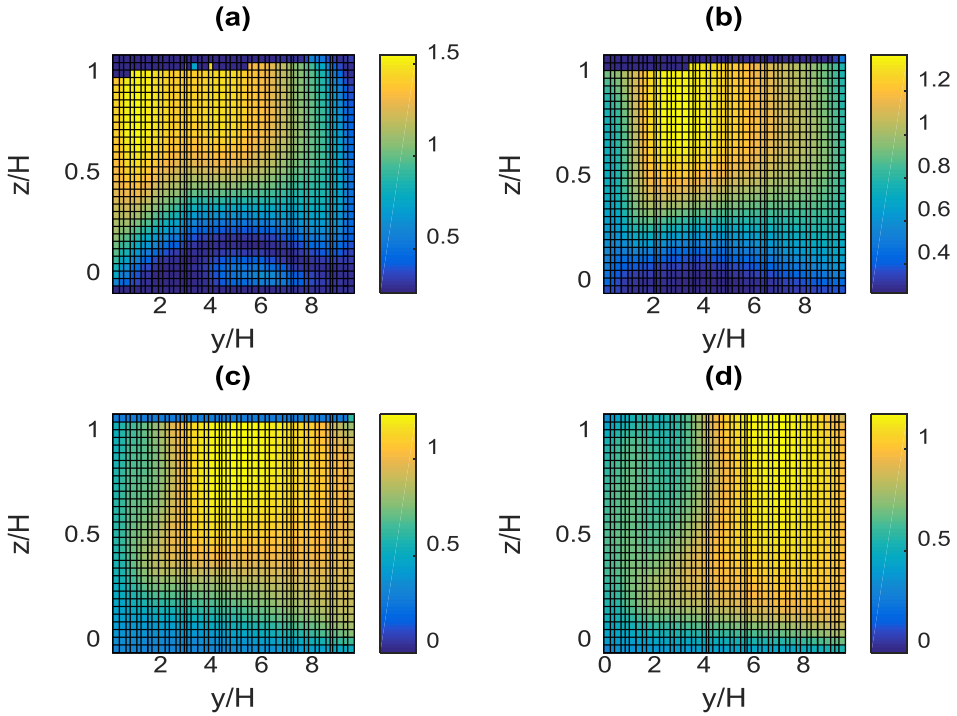

Figure 4.15: Transverse velocity distribution at the 30^{o} plane . Panel (a) channel with curvature 0.75, panel (b) channel with curvature 2.0, panel (c) channel with curvature 4.0 and panel (d) channel with curvature 8.2

While there is also a visible region of retarded flow close to the channel bed forming a visible shear layer, this does not qualify as flow separation because there is no significant component of normal to boundary velocity perpendicular to the bed. The flow separation on the inner wall region then continues to develop until it becomes invariant with space beyond the 90 degrees plane. It should be noted that the region of flow separation (seen close to the inner bank in all three channels) does not extend from the surface to the bed (see Figures 4.15 b, c, d and 4.16 b, c, d). This separation pattern creates a peculiar velocity distribution in the depth plane that is not present in other parts. Hence in the separation region, the velocity close to the surface is slow while the region beneath the flow separation close to the bed is fast in contrast with what is known for a channel without a flow separation. These results have been confirmed by other researchers including Blanckaert (2015). However, the story is quite different for the tightest curve $'ET'$. When the flow encounters the tightest channel, there is mass transport due to the adverse outer wall pressure gradient as explained earlier. This, unlike the other channels, causes a visible boundary layer separation on the outer wall shown in figure 4.15a, as opposed to the boundary layer separation on the inner wall observed in the other bends. This outer boundary layer develops into a peculiar double region pattern previously unreported in literature (see the interior of the curve in Figure 4.14). This boundary layer separation pattern creates two regions of high velocity, one extending from the inner wall to about half the width of the flow channel while the other is close to the bed almost completely surrounded by slow moving fluid (Figure 4.15a). These two regions of high velocity fluid eventually merge as the region of outer bank flow separation grows taking up more than half of the channel width by the 60 degree plain.

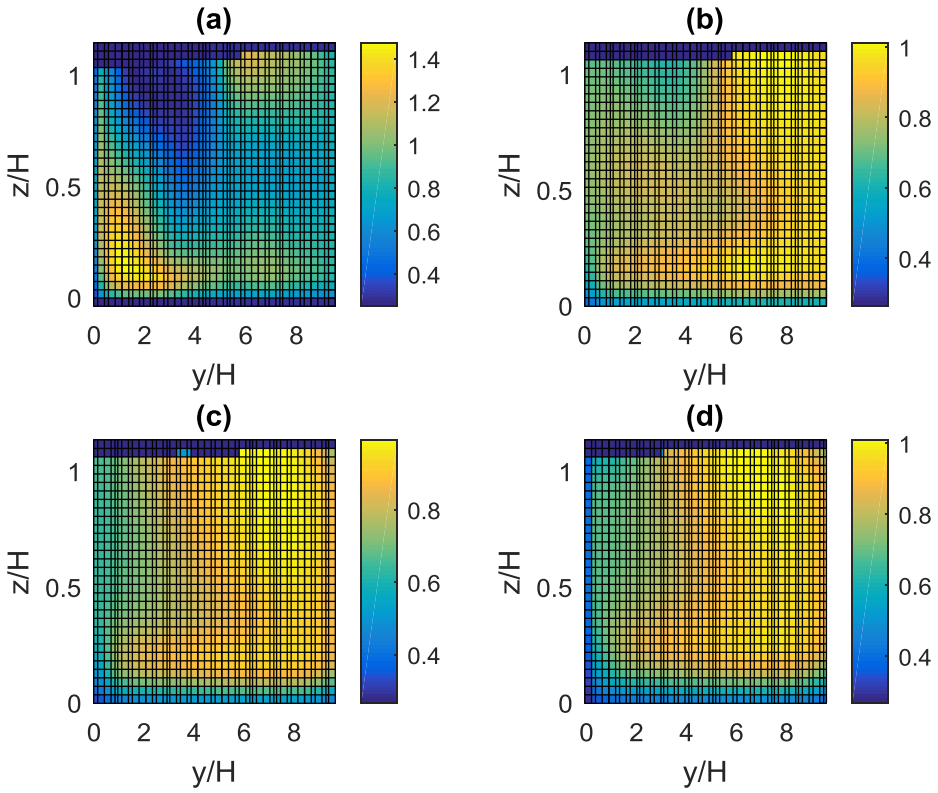

Figure 4.16: Transverse velocity distribution at the 145^{o} plane . Panel (a) channel with curvature 0.75, panel (b) channel with curvature 2.0, panel (c) channel with curvature 4.0 and panel (d) channel with curvature 8.2

Eventually (very close to the channel outlet) the boundary layer pattern collapses to that of a v shape close to the inner wall similar to what is observed in the developing stages of the mild bends (see Figure 4.16a). The flow separation patterns observed have significant consequences for mixing and the distribution of suspended sediments in the fluid.

Nevertheless, while it is clear that the three-dimensional velocity distribution plays a critical role in these observed patterns, it is still not clear why the more energetic fluid stays close to the inner bank for the most part in the tightest bend. Perhaps an examination of the vorticity distribution and the three-dimensional vortex pattern may lead to unravelling this mystery.

4.6 Vorticity pattern in an open channel bend

An examination of fluid rotation can help illuminate unresolved knowledge gaps in the dynamics of open channel bend flows. All studies of angular motion in fluids begin with looking at the velocity gradient. The velocity gradient which is a second order tensor can be decomposed into a symmetric part S_{ij} known as the strain rate tensor and a skew symmetric part known as the vorticity tensor ω_{ij}. Aside from decomposing the velocity gradient tensor, a characteristic equation can be written for this tensor (equation 4.1).

$$\varphi^3 + P\varphi^2 + Q\varphi + R = 0 \ldots\ldots\ldots\ldots\ldots\ldots\ldots\ldots (4.1),$$

where P, Q and R are invariants of the velocity tensor.

While the vorticity which is defined as the curl of the velocity vector is a very popular measure of flow rotation in fluid dynamics, this section begins its inquisition into rotation patterns by looking at the Q criterion. The second invariant of the characteristic equation (4.1) forms the basis of this Q criterion method and can be expressed as

$$Q = \frac{1}{2}\left(tr(\bar{D})^2 - tr(\bar{D}^2)\right) = \frac{1}{2}\|\bar{\omega}\|^2 - \|\bar{S}\|^2 \ldots\ldots\ldots\ldots\ldots\ldots\ldots\ldots (4.2),$$

where Q is the Q criterion,

$\bar{D}$ is the velocity gradient tensor,

$tr(\bar{D})$ is the trace of the velocity gradient tensor.

All other terms are as previously defined.

The Q criterion identifies a connected fluid region with a positive second invariant of the velocity gradient tensor (Holmen 2012). This criterion also requires that the local pressure be lower than the ambient pressure in the vortex. Thus the Q criterion essentially seeks regions in the fluid where the vorticity (or rotation) tensor is greater than the mean strain rate defining such a region as a vortex.

Our results show that there are two distinct patterns of fluid rotation depending on the curvature and position in the channel. The mildest channel for instance has a relatively weak vorticity distribution as shown in Figure 4.17. In Figure 4.17, the mild channel vorticity is so weak that only little traces of the mainstream and counter rotating circulations close to the outer bank are visible which suggests that the strongest vortices are in the outer bend regions in the channel (at an iso-surface value for Q criterion of 250). However, as the channel tightness increases, the Q criterion shows that the vorticity in the main channel increases and is skewed towards the outer bank except in the tightest channel where it is skewed towards the inner and middle regions of the channel and is never at the outer bank (see Figures 4.18 to 4.20).

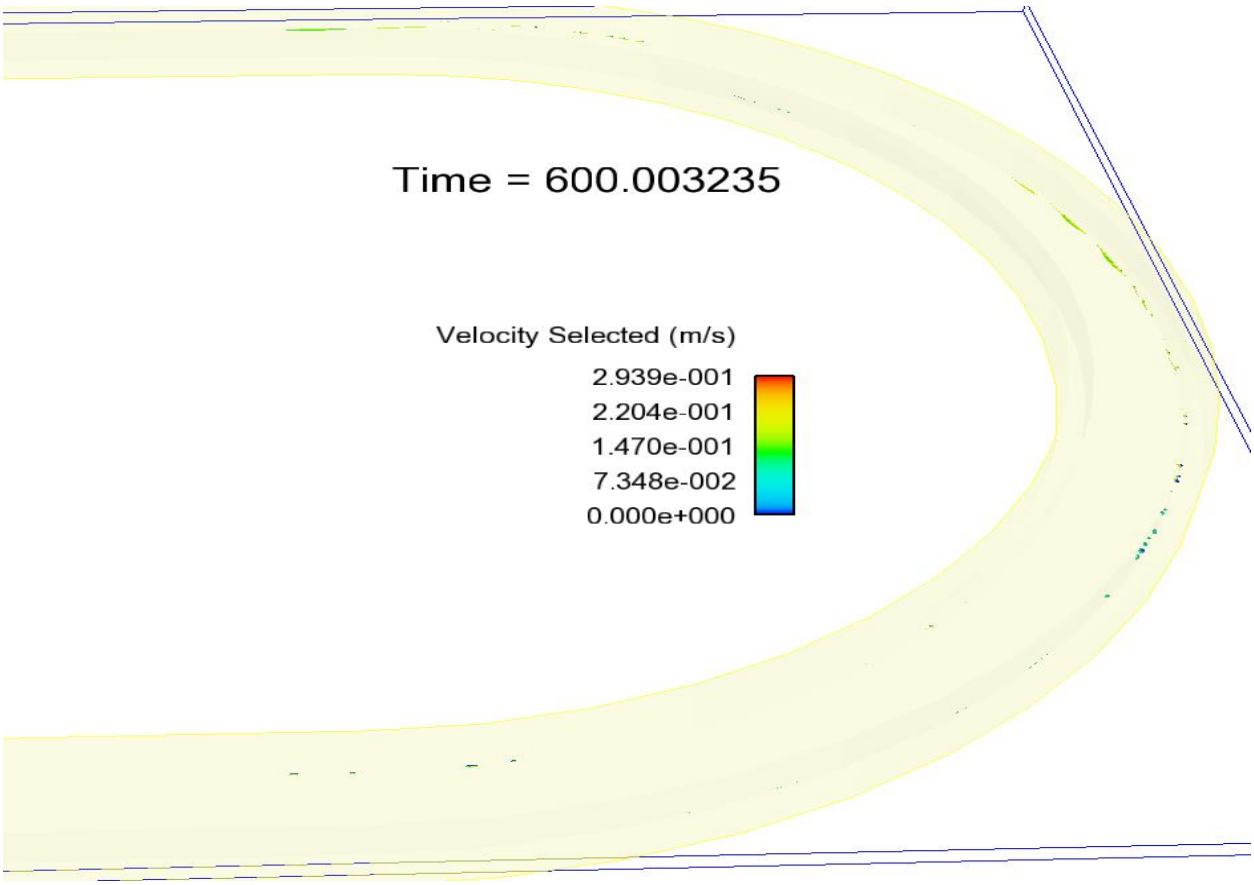

Figure 4.17: A plot of the Q criterion iso-surface colored with velocity magnitude for the mild channel $R/T_w = 8.2$

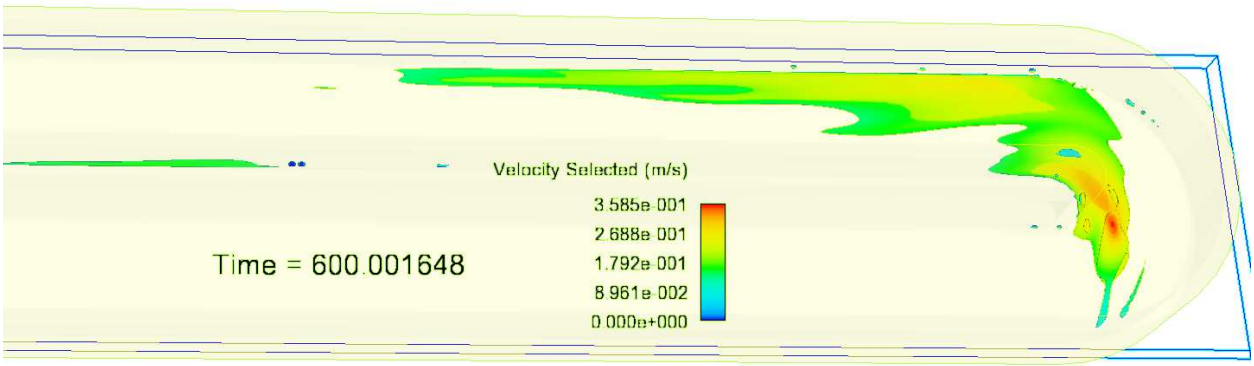

Figure 4.18: A plot of the Q criterion iso-surface colored with velocity magnitude for the tight channel $R/T_w = 0.75$

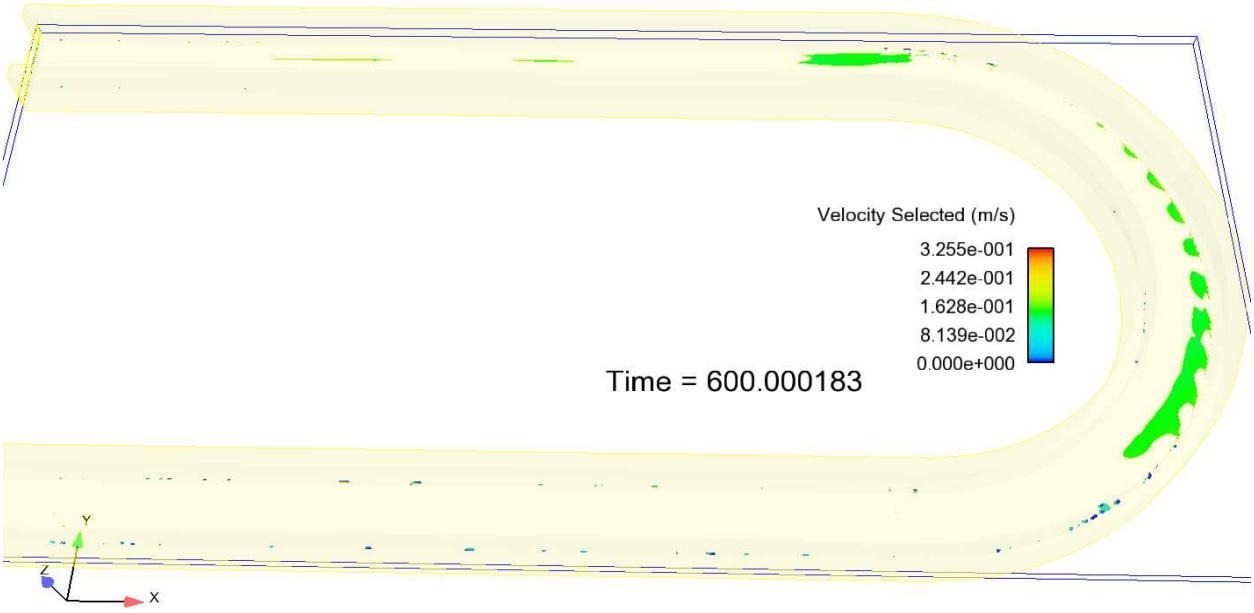

Figure 4.19: A plot of the Q criterion iso-surface colored with velocity magnitude for the mild channel $R/T_w = 4.0$

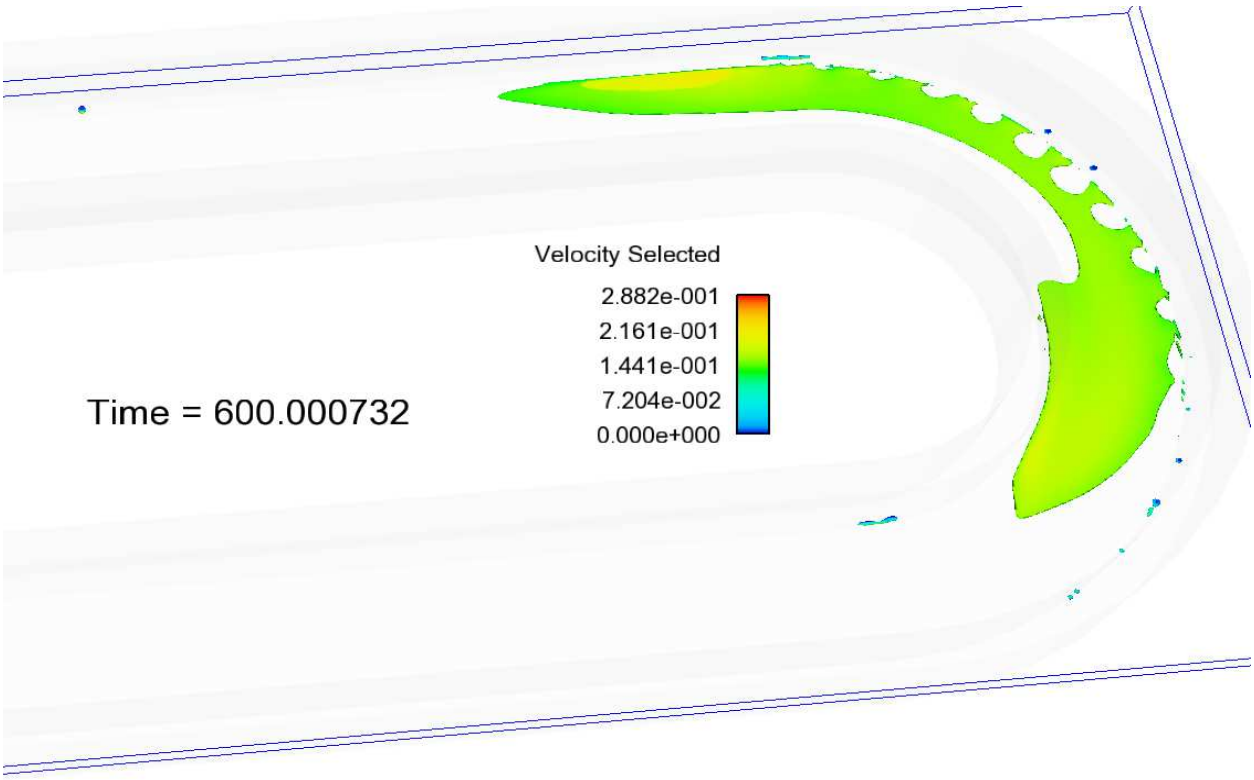

Figure 4.20: A plot of the Q criterion iso-surface colored with velocity magnitude for the tight channel $R/T_w = 2.0$

Even greater details can be obtained from looking at a two dimensional planar circulation plots. Based on these circulation plots (as shown in Figures 4.21 and 4.22), there seem to also be two distinct regions of circulation in the channel. The first region is a region of developing flow where the fluid velocity changes with position (the range of angles for this region depends on the curvature). The second is the fully developed region beyond the 90^o plane (this criterion was chosen based on the results of many simulations and literature) where the flow patterns are spatially invariant. Therefore, after a thorough examination of both sets of plots, it is now clear that in a mild channel, when a flow encounters a bend, it is subjected to a centrifugal acceleration (in addition to a radial pressure gradient). Because of the sudden change in direction, the parcel of fluid reacts to the new external forces (centrifugal force and the radial pressure gradient force) slowly so that the inertia of the fluid begins to change gradually to a circular pattern and the full centrifugal acceleration is not felt in the entrance regions. Further downstream into

the bend this creates the main cell circulation which from the plots of traverse velocity (Figure 4.21) is the only circulation cell present in the developing region (approximately 0 to 90 degrees) of the mild curves. Further in the curve, after the full magnitude of the centrifugal acceleration is felt, a combination of the Q criterion and the two dimensional plot shows that its value is still weak relative to those of the tight channel so that the single cell circulation occupies the bulk of the fluid cross section throughout the channel in the developing and the fully developed regions of the bend. In addition to this main cell, a counter rotating cell close to the outer bank surface is also observed. It should be noted that our results show that this outer rotating cell occurs only in the ''fully developed'' region of the channel. This outer cell has been studied in literature and has been attributed to the complex interaction between the centrifugal acceleration and the Reynolds stresses. Taken together, the results shows that in mild channels, a single cell circulation develops with a mild vorticity close to the bend entrance and spins up to its full value. However, because of the small value of the centrifugal acceleration at mild curvatures, this single clock wise cell is the only circulation cell present in the developing region. In the fully developed region, a second counter clockwise rotating cell develops close to the outer wall near the surface in addition to the main cell circulation forming the famous two cell circulation that has appeared in literature and is the basis for many reduced order models in river simulations.

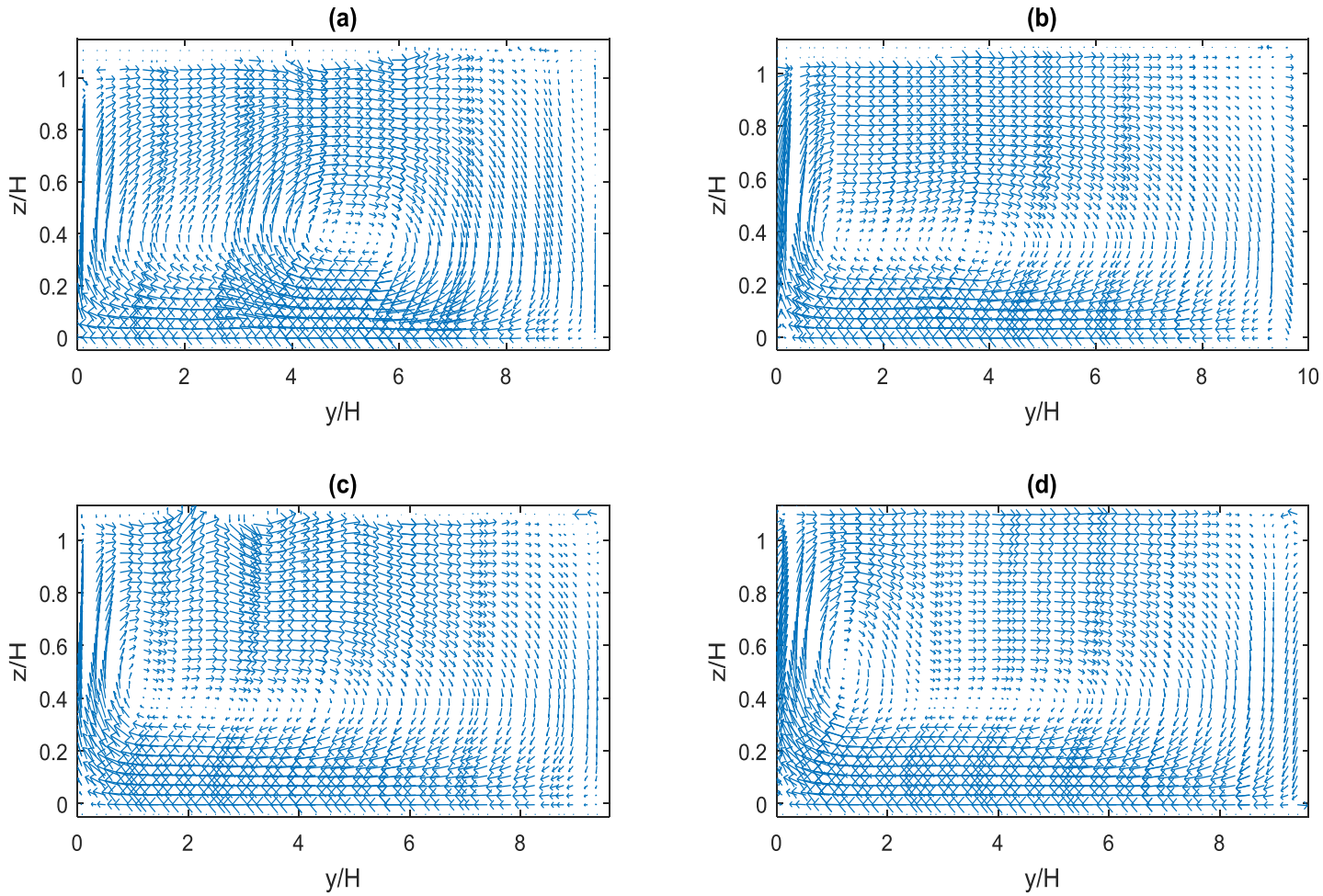

Figure 4.21: Transverse velocity vector plots at the 30^{o} plane. Panel (a) is for channel with curvature R/Tw = 0.75, panel (b) is for channel with curvature R/Tw = 2.0, panel (c) is for channel with curvature R/Tw = 4.0 and panel (d) is for channel with curvature R/Tw = 8.2

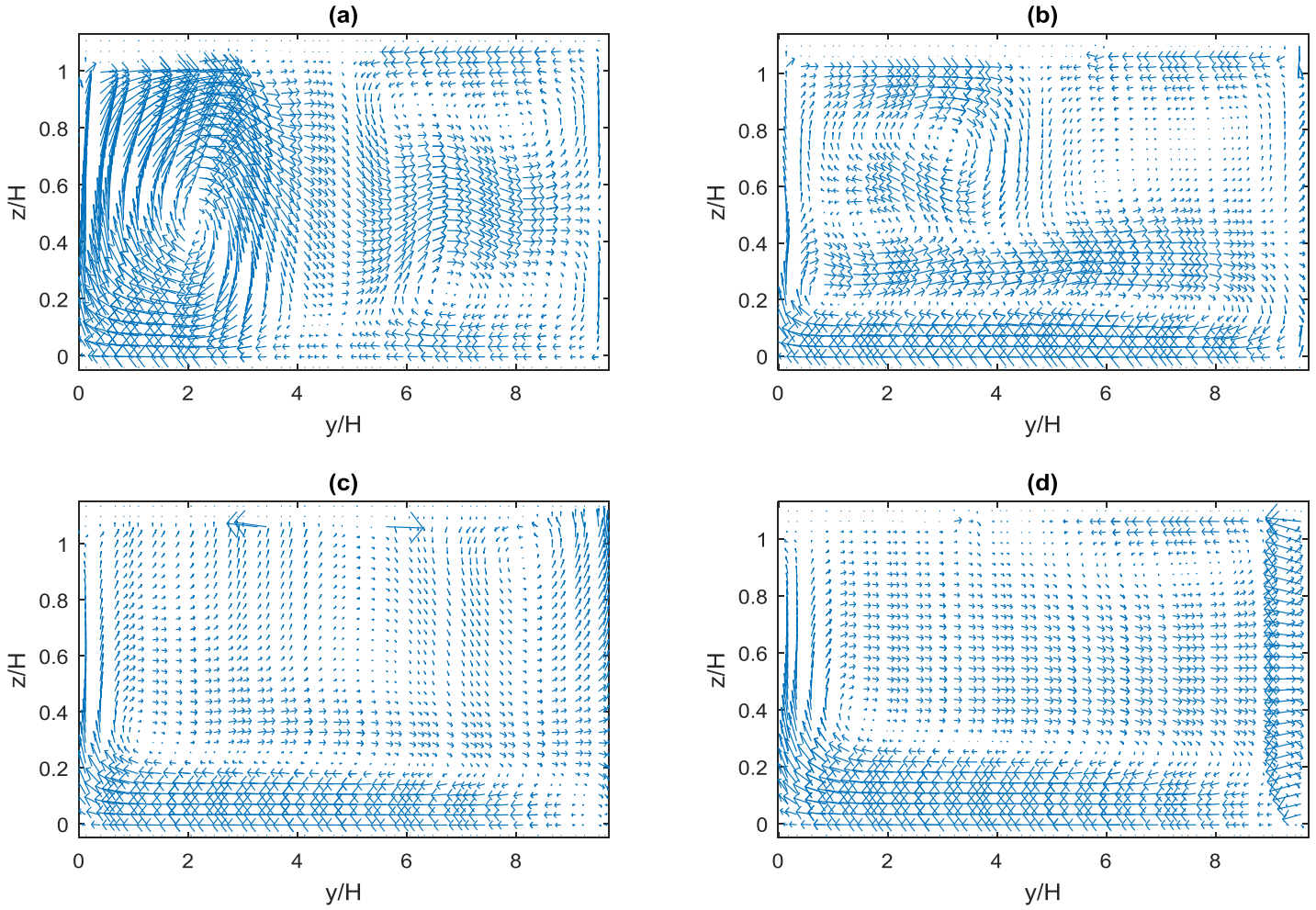

Figure 4.22: Transverse velocity vector plots at the 145^{o} plane. Panel (a) is for channel with curvature R/Tw = 0.75, panel (b) is for channel with curvature R/Tw = 2.0, panel (c) is for channel with curvature R/Tw = 4.0 and panel (d) is for channel with curvature R/Tw = 8.2.

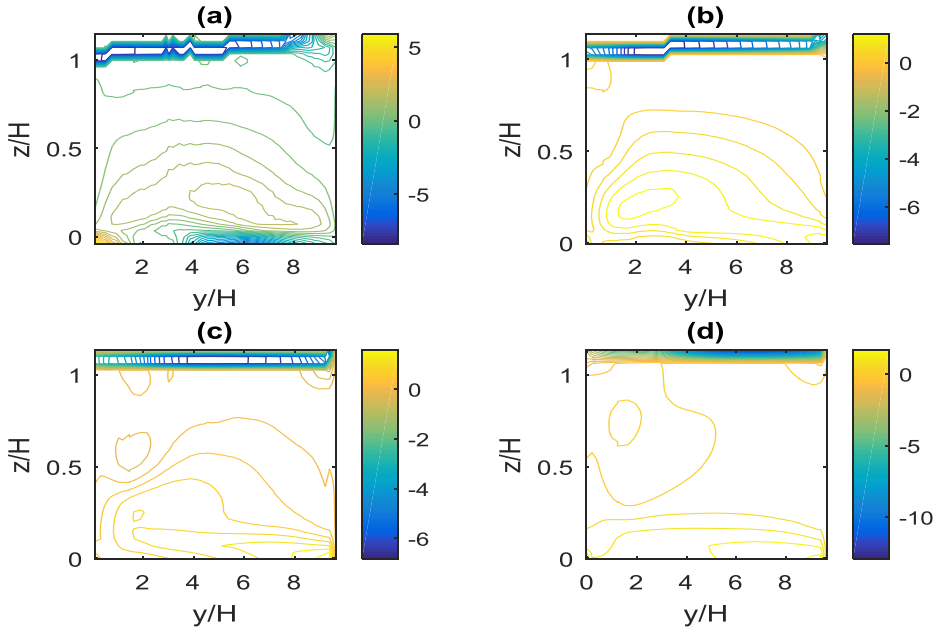

Figure 4.23: Vorticity distribution contours at the 30° plane. Panel (a) channel with curvature 0.75, panel (b) channel with curvature 2.0, panel (c) channel with curvature 4.0 and panel (d) channel with curvature 8.2

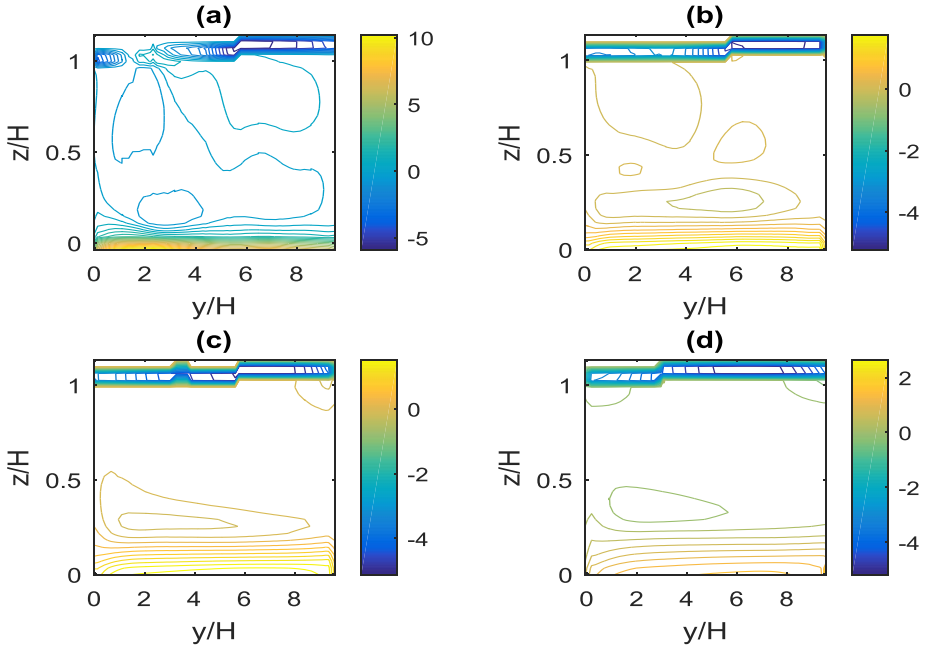

Figure 4.24: Vorticity distribution contours at the 145° plane. Panel (a) channel with curvature 0.75, panel (b) channel with curvature 2.0, panel (c) channel with curvature 4.0 and panel (d) channel with curvature 8.2.

The case of the circulation pattern for the tight channel is different when compared with that of the mild channel. In order to understand the physics, a plot of the contours of vorticity in the developing and fully developed regions is shown in figure 4.23 and 4.24. These diagrams show that at the initial stages, the vorticity is developing with relatively low values for both the mild and tight channels (compared with the developed regions). Note that unlike the tight channels, the mild channels have their vortex contours confined closer to the boundaries leaving the bulk of the mid-section of the flow with no vorticity. Essentially the relatively small vortex magnitude (compared to the fully developed regions) creates the single cell circulation similar to that in the developing region of the mild channels. Notice however that the highest vortex strength in the developing region (while still relatively small compared to the fully developed region) in the tightest channel is more than three times that of the mildest channel. As the flow proceeds to its fully developed state, the vortex strength has almost doubled for all channels (as shown in figure 4.24). However, with the vorticity in the tightest channel still about 3 times greater than other channels, a single cell circulation in the tightest channel is no longer feasible. In addition to the magnitude, the distribution of the contours of high vorticity also contributes to the three cell circulation structure seen in the tightest bend. This is evident by comparing vorticity plots for 'T' and 'M'. Hence, it is clear that in the tight curve when the fluid encounters the bend, it is subject to a centrifugal acceleration and a radial pressure gradient. This force imbalance between the centrifugal acceleration and the radial pressure gradient creates a single cell circulation in the regions from the entrance to about the 60^o plane. Initially because of the sudden change in direction, the fluid parcel adjusts slowly so that it takes some time for the centrifugal acceleration to fully impact the inertia of the fluid. However, unlike the case of the mild channel the magnitude of the centrifugal acceleration is far greater for a tighter bend such that when the fluid parcel is subject to the full effect of its magnitude, the initial single cell circulation developed at the initial stages of the flow between the entrance and the 60^o plane (part of the developing region) cannot be sustained. The single cell circulation therefore breaks into two clockwise circulation cells and is

maintained throughout the developed region of the flow. A counter rotating cell just like the one encountered in the mild channel develops for the same reasons explained earlier in the fully developed flow region of the tight bend. Together these results paint a picture of a single cell circulation in the developing regions of a tight channel and a three cell circulation in the developed region of the bend. While this has been hinted at in literature, there has been no explanation provided for the existence of this circulation structure. Our results show (especially in the tightest curve) that it is the magnitude of the centrifugal acceleration that is responsible for the intensity of the vorticity such that the single main cell clockwise circulation splits into two clockwise circulation cells in the developed region of the channel.

4.7 A new type of flow regime

A recurring theme in this study is the distinct character of flow in the curve $'ET'$ from the other three curves. A couple of examples include the shear stress where all other channels have their maximum move towards the outer bend as the fluid moves into the curve except the curve $'ET'$ where the maximum shear stress stays on the inner bend the entirety of the curve. Another example is the velocity distribution where the region of flow separation is on the inner (convex) wall except in the curve$'ET$. Several more examples exist of the peculiar character of the curve $'ET'$ which curvature effects alone cannot explain. This raises more questions concerning the dynamics of the flow in this particular curve and further examination aimed at revealing the details of the flow physics revealed a new type of flow regime. This regime is characterized by an unsteady type of periodic motion even after the simulation has run long enough for the flow to have reached steady state. A thorough study of our results showed that this flow character emerged (at a turbulent Reynolds number) due to the tightness of the bend and its complex interaction with a strong centrifugal acceleration. These complex interactions result in a unique flow separation pattern where two adverse pressure regions exists on different sides of the curve (see Figure 4.14). Therefore, there is a region of flow separation in the near field region close to the outer bend and a second large region of flow separation close to the inner bend in the far field. These two regions

represent a space of extreme shear at which the flow configuration breaks down to instability. Eventually the flow finds a new equilibrium downstream in the form of a periodic motion similar to that of a Von Karman vortex street in the immersed two dimensional cylinder problem. Further visualizations (not shown here) of the results indicate that (because the flow is sub-critical) information is propagated back upstream thereby modifying the flow conditions in a periodic fashion. This creates a very complex flow that is varying in time which (to the knowledge of this author) has never been reported in literature. One immediate implication of this result is that below certain curvatures the flow is never strictly steady as the flow structure and dynamics of such bends is a function of time.

4.8 Summary

In this chapter the effect of curvature on the three-dimensional flow structure and dynamics of open channel bend flow was investigated. The investigation was carried out with large eddy simulations of four open channel bends with curvatures ranging from mild $\frac{R}{T_w} = 8.2$ to tight $\frac{R}{T_w} = 0.75$. Care was taken to resolve the free surface with the volume of fluid method to improve accuracy of simulation results. The results obtained from this chapter confirm some of the results that are already known from literature but more importantly, provide new insights into the dynamics of bend flows previously unreported in literature.

The simulation results confirm, among other things, the two cell circulation structure that has previously appeared in literature (Van Balen 2009, Blanckaert, and de Vriend 2004) and lend credence to the fact that indeed the main circulation cell is caused by the complex interaction between the centrifugal acceleration and the radial pressure gradient. Also, results from the simulations in this chapter confirm that differential advection caused by the imbalance of forces acting on the bend channel control volume plays a crucial role in the distribution of the bed and wall shear stresses. In addition, a couple of new insights emerged. One such new insight is that regardless of the curvature of a bend, the maximum bed

and wall shear stresses at the channel inlet and regions close to the inlet, (0 to about 15^{o}) are exerted on the inner bed and wall region respectively. It should be noted that past isolated studies had shown larger inner bend shear stress at the inlet to the curve but did not cover a sufficiently broad range of curvatures to show that this shear stress behavior was independent of curvature. While the two cell circulation structure has appeared in literature and is known to researchers in the hydraulics community, findings in this chapter provides new understanding on the two cell circulation structure. The present results show that in the developing region of a bend channel (regardless of curvature), the flow structure is that of a single cell circulation (and not the two cell circulation). In the fully developed region of the bend flows, the circulation structure depends on the curvature with the mild channel exhibiting the standard two cell circulation structure and the tight channel exhibiting a three cell circulation structure. Even though the study Koken et al., 2013 (the only study to our knowledge) hinted at the possibility of a three cell circulation, the physics behind this circulation structure was previously unclear. It is now clear from a thorough examination of the transverse velocity distribution and the magnitude of the vorticity contours at various planes for all the channel that in a tight bend the centrifugal acceleration is far greater than for corresponding positions in a mild bend. This high magnitude of the centrifugal acceleration impacts a vorticity of high magnitude on the fluid in the given control volume such that a single main cell circulation (as was observed in the mild channel) is unsustainable. The dynamics therefore responds to this high vorticity by splitting the main cell circulation into two clockwise circulations. This combined with the outer wall counter rotating cell that has been attributed in literature to an-isotropy of the turbulent stresses gives rise to a three cell circulation structure in a tight bend.

In all the channels simulated, the Q criterion suggest that the highest vorticity is skewed towards the outer bend except in the tightest curve $'ET'$ where it is either on the inner bend or in mid cross section of the flow. Similarly the bed shear stress distribution of all the curves are “uni-modal” with the maximum shear stress shifting to the outer bend region at some point in the curve except the tightest curve $'ET'$

where the maximum shear stays on the inside. This consistent peculiar behavior of the tightest curve $'ET'$ led to a separate examination of its dynamics. This separate examination revealed a unique flow separation pattern at both wall boundaries of the tightest curve. This flow separation pattern causes extreme perturbation of the fluid flowing through the bend such that the flow breaks down to instability. This instability leads the whole flow system to settle into a new equilibrium which is of a periodic motion in the outlet channel similar to that of a Von Karman vortex street in the two dimensional immersed cylinder problem. Because the flow is subcritical, information can propagate back upstream hence the periodic equilibrium flow in the outlet periodically modifies the hydraulics conditions upstream leading to a complex time varying flow regime which to the knowledge of this author has never been reported in literature. Finally, while it is widely accepted in literature (Blankert 2015) that convex (inner) bank flow separation occurs exclusively in tight bend channels, the simulation results in this chapter combined with physical reasoning has shown that this cannot be true as flow separation of various kinds (including from the concave bank) occurs at every curvature.

Several questions still exist that this chapter has not yet answered. One such question is why the region of high velocity gradients and shear stresses stay close to the inner bend only in the tightest curve $'ET'$ for the entirety of the channel length. Perhaps more information and insight needed to answer this and more questions concerning bend channel flows can be obtained examining the effect of curvature length (which is the second dimensionless group in equation (3.10) in the research framework section) on the dynamics and flow structure of bend channel flows. This is the subject of the next chapter of this dissertation.

Chapter 5

The effect of curvature length on the flow structure and dynamics of open channel bends.

5.1 Preamble

This chapter examines the effect of variation in curvature length on the three dimensional flow structure and dynamics of bend channel flows. In order to accomplish this task 12 simulations of various channel lengths were carried out using the computational fluid dynamics code already detailed in Chapter 3. After a brief description of the various geometric and dynamics conditions in Section 5.2, Section 5.3 examines the evolution of the shear stress distribution as the curvature length changes. Section 5.4 studies the characteristics of the velocity distribution as the curvature length varies while Section 5.5 explores the free surface dynamics in an attempt to explain distribution of shear stress and velocity observed in Sections 5.3 and 5.4. In Section 5.6 the evolution of the circulation structure as channel length changes is thoroughly examined. This chapter aims to provide a better understanding of the effect of curvature length on the dynamics of bend channel flows.

5.2 Background

The study of the curvature effects in the previous chapter (chapter 4) provided new insights into the dynamics of bend channel flows. It also raised a couple of questions that cannot be answered by just varying the curvature. For instance, varying the channel curvature did not immediately reveal why the maximum shear stress in the tightest channel stayed close to the inner bend for virtually the entirety of the bend length. A particularly interesting question pertains to the vortical structure in a bend. In the mildest channel, there is a developing flow region (from the 0^O entrance plane to the 85^O plane) where a single cell circulation exists. However, as the fluid moves through the channel, it gets fully developed reaching a spatially invariant two cell circulation at about the 90^O plane (see chapter 4 for details). What happens if the channel length is shortened (keeping the radius unchanged) such that there is no 90^O

plane? For example, what would the flow structure look like if the curve (bend) length is shortened to say a 30^O mild bend? Does the flow still have a developing region with a single cell circulation and a fully developed region with a spatially invariant circulation structure as seen in the 180^O bends studied in chapter 4? If so, is that fully developed vortical state a two cell circulation that exists in a 180^O mild bend? In order to answer these and other related questions, the effect of a variation in curvature length on the three dimensional flow structure and dynamics of open channel bend flows is investigated using numerical simulations.

As has already been detailed in Chapter 2, several bend channel studies exist in literature. Some were experimental studies of mild channel with rigid beds (Booij 2003) while others were experimental studies of mild channels with erodible beds (Odgaard & Bergs 1988). There have also been experimental studies of tight bends with erodible beds, (Blanckaert & Graf 2001, Blanckaert & De Vriend 2004). Complimenting experimental studies are various types of numerical studies looking at various aspects of bend channel dynamics such as those by Engelund (1974), De Vriend (1977), Odgaard (1986) Jin and Steffler (1993), Yeh and Kennedy (1993), Booij (2003), Stoesser *et al.* (2008), Van Balen (2009) and Blankert (2009). Despite the large body of work on bend channel dynamics in literature there has been no systematic study on the effect of variation of curvature length on the three dimensional flow structure and dynamics of open channel bend flows. It is therefore the aim of this chapter to fill in this knowledge gap. In an attempt to close the knowledge gap enumerated above, large eddy simulation of bend channel flows of various curvature lengths using a volume of fluid free surface solver as already detailed in Chapter 3 were carried out. Based on equation (3.10) in Section 3.5, and the fact that the curvature length is a function of two parameters as shown in equation 5.1, two curvature radii were chosen to constrain the number of simulations required for this study.

$$L = R\theta, \ldots\ldots\ldots\ldots\ldots\ldots\ldots\ldots (5.1)$$

where L is the curvature length,

R is the radius of curvature,

θ is the curvature angle.

Hence one set of simulations were run with a mild curvature of $\frac{R}{T_w} = 8.2$ and another set with a tight curvature of $\frac{R}{T_w} = 0.75$. Effectively, constraining the curvature radius means the length of curvature can be varied by just changing the bend channel angle (as can be seen from equation 5.1). Therefore for each curvature radius, 6 simulations were run at $0^o, 30^o, 60^o, 90^o, 120^o, 150^o$ and 180^o for a total of 12 simulations, to study the effect of variations in curvature length on the flow structure of bend channel flows.

To make our discussion easier, in this chapter each channel would have an alias just like in the previous chapter, with MB for mild bend and TB for tight bend. Attached to this two letter code would be the channel length in degrees, thus the 180 degrees mild channel in this chapter would be referred to as MB180 while the 30 degrees tight channel would be referred to as TB30.

To facilitate the isolation of cause and effect in this study similar upstream and downstream geometries were used for all the 12 channel simulations carried out. For each channel there is an upstream straight inlet of 11 m chosen to make sure that the fluid reached a fully developed state before encountering the bend. Downstream of each curve is a straight outlet of length 6.7 m. For both inlet and outlet straight channel the flow cross section is that of a rectangle with a width of 0.5 m (see Figure 5.1 for the details of a typical channel used). In all the simulation runs carried out, the same initial and boundary conditions were imposed for reasons already highlighted above. Thus at the entrance to the straight inlet channel a volume flow rate boundary condition of 0.0052 m^3/s was imposed while atmospheric boundary condition was imposed at the downstream outlet and the free surface of the fluid. Because the side wall and bed were assumed smooth, a no slip boundary condition without a roughness component was imposed on the walls and bed. All simulations were initialized as stationary with a flow

depth of 0.052m and allowed to run up to steady state before simulation results were collected. Hydraulic details of all the simulations carried out in this chapter are provided in Tables 5.1, 5.2 and 5.3. Using these numerical simulations, physical and dimensional reasoning, this chapter would attempt to provide some insights into the effects of varying curvature length on open channel bend flow dynamics.

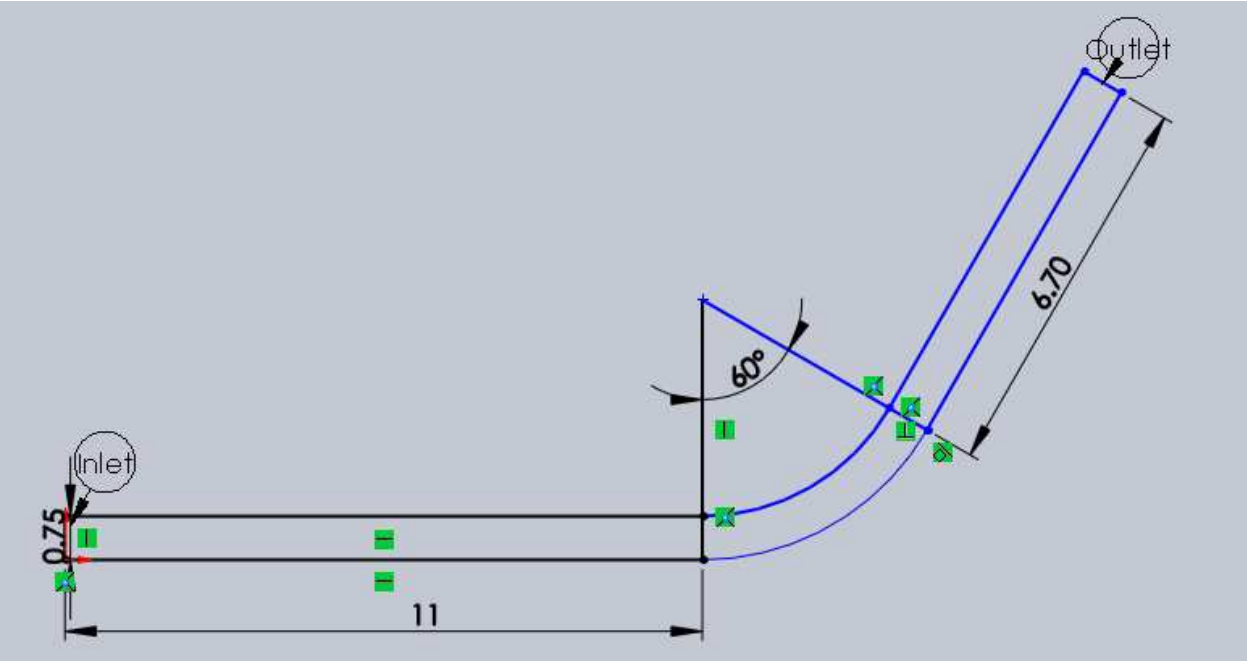

Figure 5.1: Schematic diagram of the typical mild channel used in this chapter. The bend angle (60^O in this particular case) is varied from 30^O to 180^O to analyze the effect on bend flow structure. Note all linear length measurements in the diagram are in meters and all angular length measurements are in degrees.

Table 5.1: General hydraulic details for all 12 simulations conducted in this chapter.

B(m)	H(m)	Q(m^3/s)	U_{avg}(m/s)	Re	Fr
0.5	0.052	0.0052	0.2	10400	0.28

Note B (m) is the channel width, H (m) is the flow depth, Q (m^3/s) is the volume flow rate, U_{avg} (m/s) is the average velocity, Re is the Reynolds number and Fr is the Froude number.

Table 5.2: Geometric parameters for varying the length at the mild curvature (R/Tw = 8.2).

	L(m)	L/T_w(degrees)	Mesh Dimensions	Total cell count
Simulation 1	2.15	30	2015 x 50 x 27	2720250
Simulation 2	4.30	60	2230 x 50 x 27	3010500
Simulation 3	6.44	90	2444 x 50 x 27	3299400
Simulation 4	8.59	120	2659 x 50 x 27	3589650
Simulation 5	10.73	150	2873 x 50 x 27	3878550
Simulation 6	12.88	180	3088 x 50 x 27	4168872

Note L (m) is the arc length and L/T_w is the dimensionless arc length in degrees.

Table 5.3: Geometric parameters for varying the length at the tight curvature (R/Tw = 0.75).

	L(m)	L/T_w (degrees)	Mesh Dimensions	Total cell count
Simulation 1	0.20	30	1820 x 50 x 27	2457000
Simulation 2	0.39	60	1839 x 50 x 27	2482650
Simulation 3	0.60	90	1860 x 50 x 27	2511000
Simulation 4	0.79	120	1879 x 50 x 27	2536650
Simulation 5	0.98	150	1898 x 50 x 27	2562300
Simulation 6	1.18	180	1918 x 50 x 27	2589300

5.3 Shear Stress

The distribution of shear stress plays a critical role in the dynamics of bend channel flows, especially in revealing the forces the flowing fluid exerts on its boundaries (the bed and side walls). While this study is strictly about bend channel flows in rigid boundaries, shear stress results obtained from this study can reveal potential erosion and deposition patterns in erodible channels of similar geometry. Thus the shear stress results would be useful from an engineering design perspective and in revealing the physics behind the flow structure that would be observed as this chapter proceeds.

A specific examination of the series of numerical experiments carried out in this chapter reveals two distinct shear stress distribution patterns in the bend channel at various curvature lengths. In the mild bend (recall that the mild bend has $\frac{R}{T_w} = 8.2$) regardless of curvature length the pattern of maximum shear stress distribution is towards the inner bend in the region close to the entrance to the curve and towards the outer bend as the fluid moves further into the channel (see figures 5.2 to figure 5.4). A

thorough review of all results shows that when the fluid coming from the straight inlet channel encounters a bend, it experiences an adverse pressure gradient on the outer wall side and a favorable pressure gradient on the inner wall side. This is due to the slow speed of the fluid inertia adjusting to the curved geometry and the influence of the centrifugal acceleration which causes fluid in the bend to accumulate at the outer wall causing a tilting of the traverse free surface. Thus, the momentum coming from the straight inlet encountering the bend is pushed towards the inner wall at the entrance region as that region experiences an acceleration because of a favorable pressure gradient. This results in situating the streamlines of higher velocity close to the inner wall at the entrance region. Because the velocity must vanish at the wall (no slip boundary condition) this implies that the regions of higher velocity gradients are close to the inner wall. Since shear stress is a function of the velocity gradient, the maximum bed and wall shear stresses are therefore exerted on the inner bed and wall regions respectively at the entrance region to the curve (see Figure 5.2 (a), (b) and 5.4 (a), (b)). However, as the fluid moves into the bend the effect of the centrifugal acceleration becomes more pronounced and the fluid of higher velocity is advected towards the outer wall region (especially those close to the surface). This sets up an extreme velocity gradient (no slip condition at the bed) in the horizontal plane causing the maximum shear stress to shift towards the outer bend. Similarly, the combination of fluids of higher velocities on the outer bend coupled with the no slip boundary condition at the outer wall is responsible for the position of the maximum wall shear stress being at the outer wall. This shear stress distribution pattern holds for the remainder of the channel as shown in Figures 5.3 and 5.4.

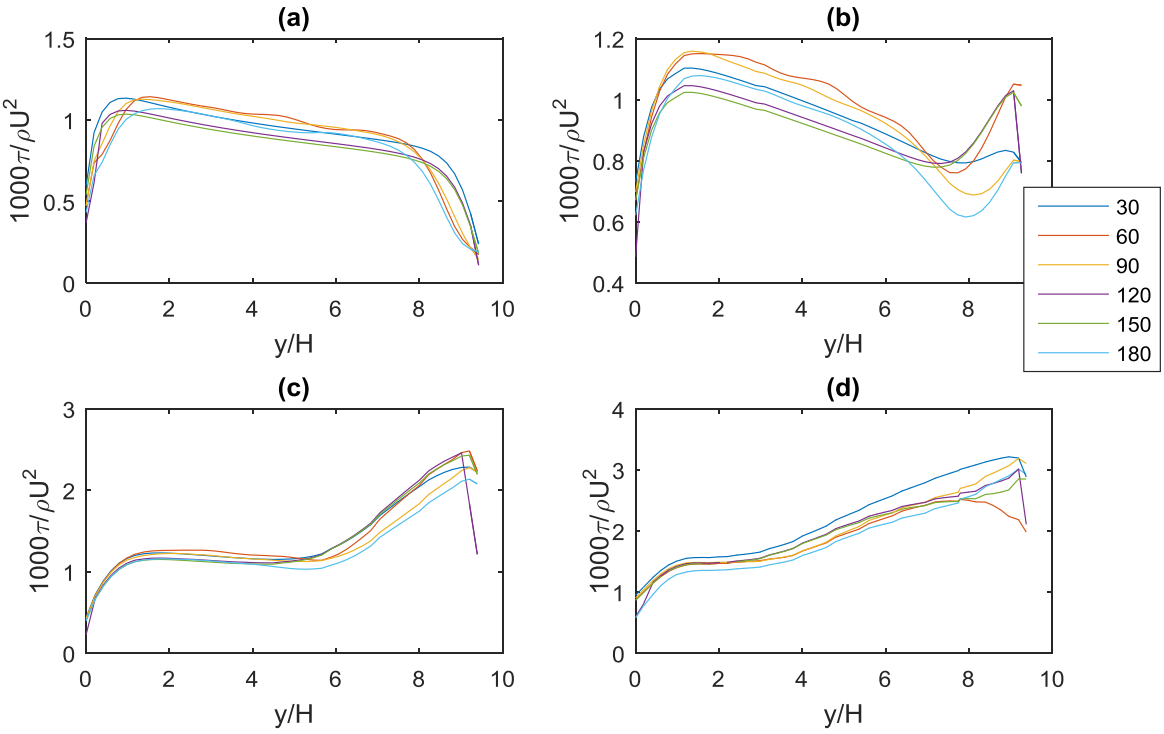

Figure 5.2: Bed shear stress plot of the mild channel $R/T_w = 8.2$. Note the angles in the legend denote the various channel lengths. Panel (a) shows the bed shear stress at the 0^o plane (or curve entrance) while panel (b) shows the bed shear stress at the 5^o plane . Panel (c) shows the bed shear at the 10^o plane while panel (d) shows the bed shear stress at the 15^o plane .

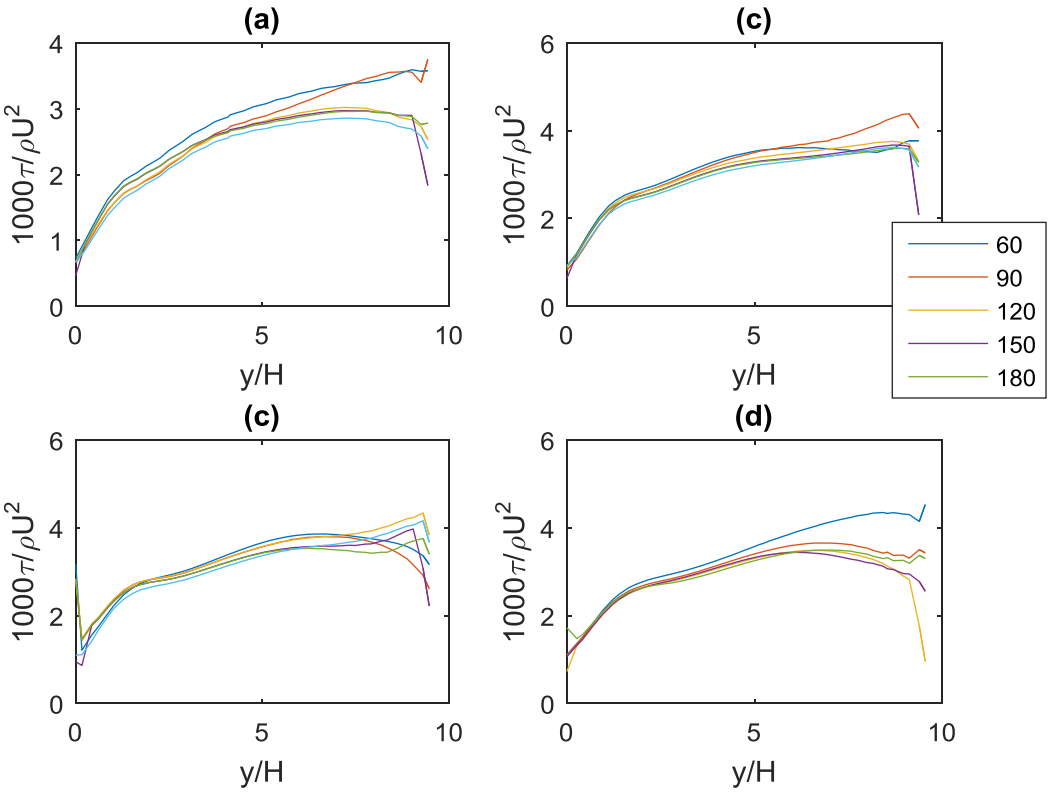

Figure 5.3: Bed shear stress plot of the mild channel $R/T_w = 8.2$. Note the angles in the legend denote the various channel lengths. Panel (a) shows the bed shear stress at the 20^O plane while panel (b) shows the bed shear stress at the 25^O plane . Panel (c) shows the bed shear at the 30^O plane while panel (d) shows the bed shear stress at the 35^O plane. Note the trend of maximum shear stress at the outer bend and minimum shear stress at the inner bend continues till the channel exit.

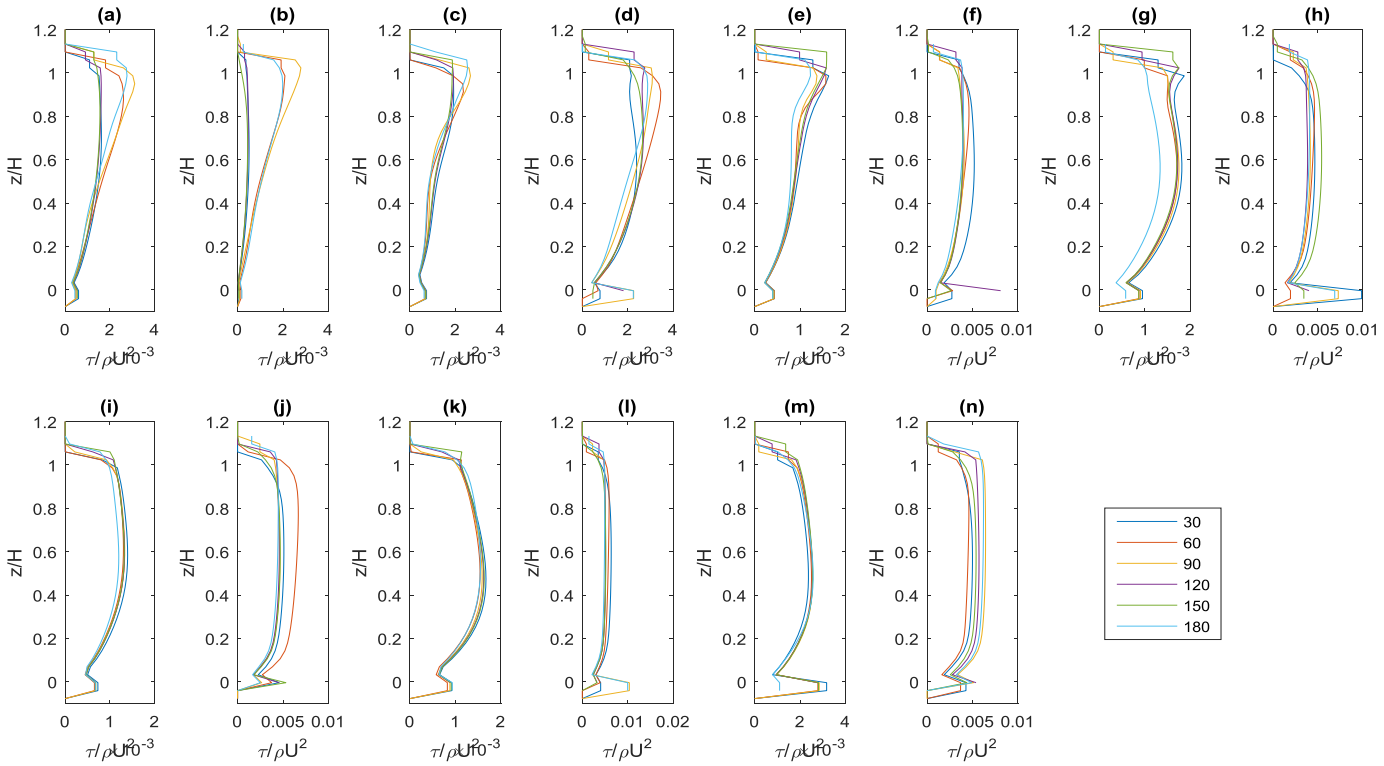

Figure 5.4: Wall shear stress plots for the mild channels $R/T_w = 8.2$. Note the angles in the legend denote the channle length. Panel (a) shows the inner wall shear stress at the 0^O plane, panel (b) shows the outer wall shear stress at the 0^O plane. Panel (c), (e), (g), (i), (k), (m) show the inner wall shear streses at the 5, 10, 15, 20, 25, 30 degree planes. Panels (d, (f), (h), (j), (l), (n) show the outer wall shear streses at the 5, 10, 15, 20, 25, 30 degree planes, respectively.

The shear stress distribution for the tight channel ($\frac{R}{T_w} = 0.75$) showed a different pattern regardless of the curvature length. While the mild channel length exhibited a uni-modal pattern of cross stream shear with a single maximum, the shear stress pattern for the tight channel at all curvature lengths initially exhibited a bi-modal cross sectional shear stress distribution as shown in Figures 5.5 and 5.6. Also, from Figures 5.5 to 5.8, it can be seen that (unlike in the mild channels) at no curvature length was the maximum shear stress close to the outer wall. The maximum stress was always closer to the inner wall. While the results from Chapter 4 hinted at the possibility of this shear stress pattern, neither the plots here or in the previous chapter reveals the physics of this peculiar shear stress distribution. In order to explain why this occurs, an examination of the velocity distribution is done in next section to provide some physical meaning to the shear stress patterns observed in the tight bends at various curvature lengths.

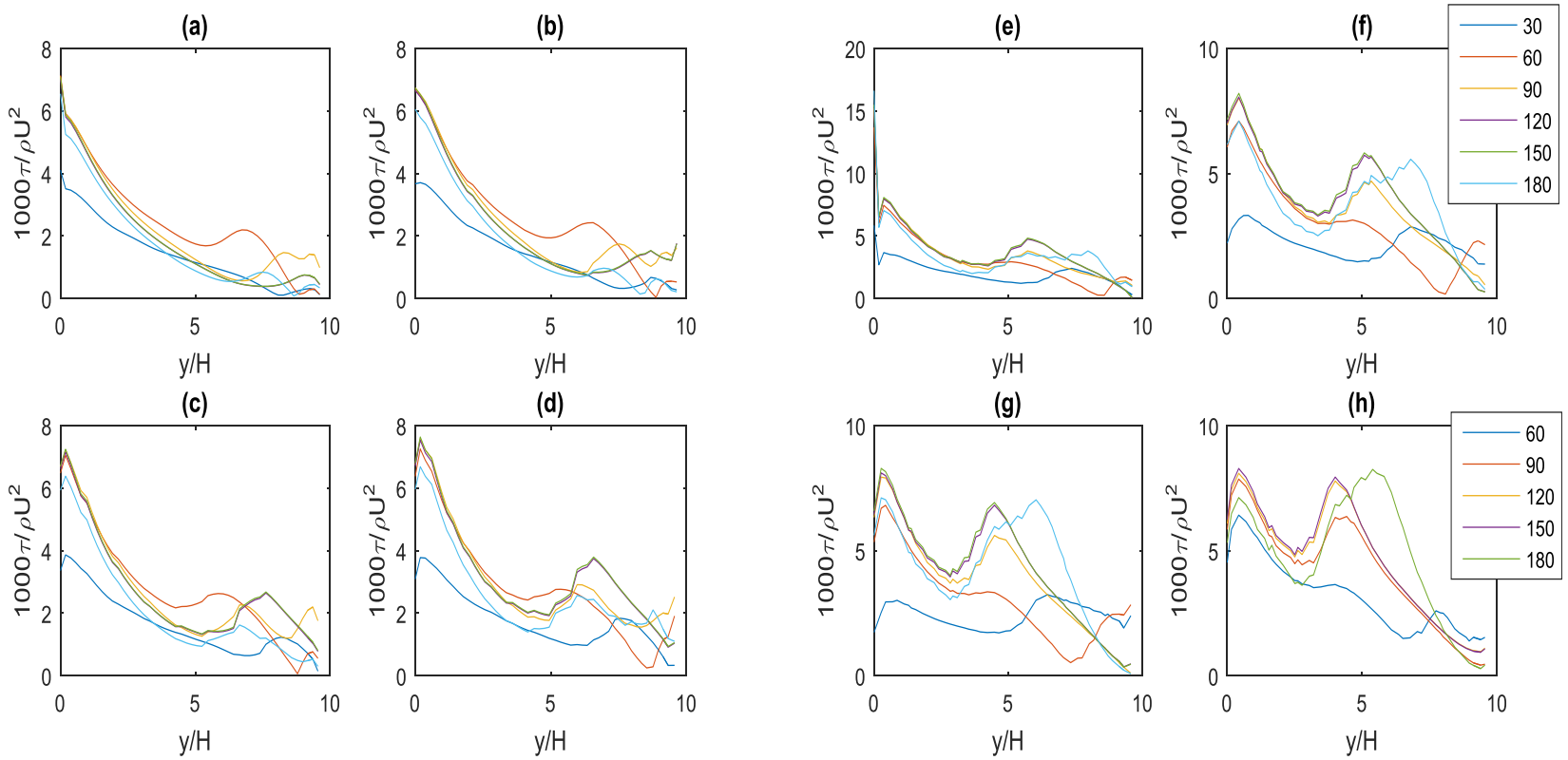

Figure 5.5: Bed shear stress plots for the tight channels $R/T_w = 0.75$ from 0^O to the 35^O planes. Note the angles in the legend denote the channel length. Panel (a) shows the bed shear stress at the 0^O plane, panel (b) shows the bed shear stress at the 5^O plane, panel (c) at the 10^O plane while panel (d) at the 15^O plane. Panels (e), (f), (g), (h) show the bed shear stress at the 20, 25 ,30 ,and 35 degree planes, respectively.

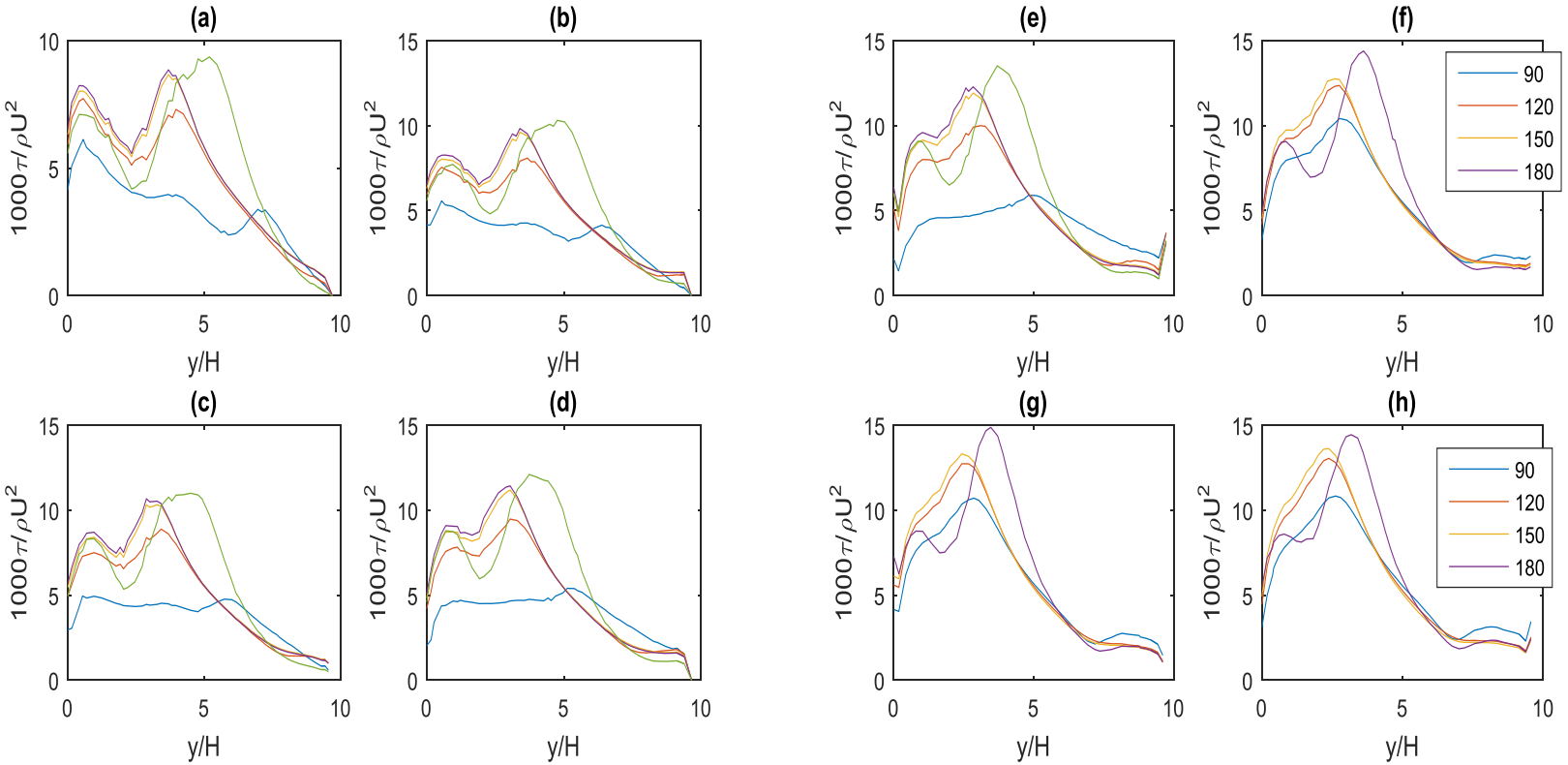

Figure 5.6: Bed shear stress plots for the tight channels $R/T_w = 0.75$ from 40^O to the 75^O planes. Note the angles in the legend denote the channle length. Panel (a) shows the bed shear stress at the 40^O plane, panel (b) shows the bed shear stress at the 45^O plane, panel (c) at the 50^O plane while panel (d) is at the 55^O plane . Panels (e), (f), (g), (h) show the bed shear stress at the 60, 65 ,70 ,and 75 degree planes.

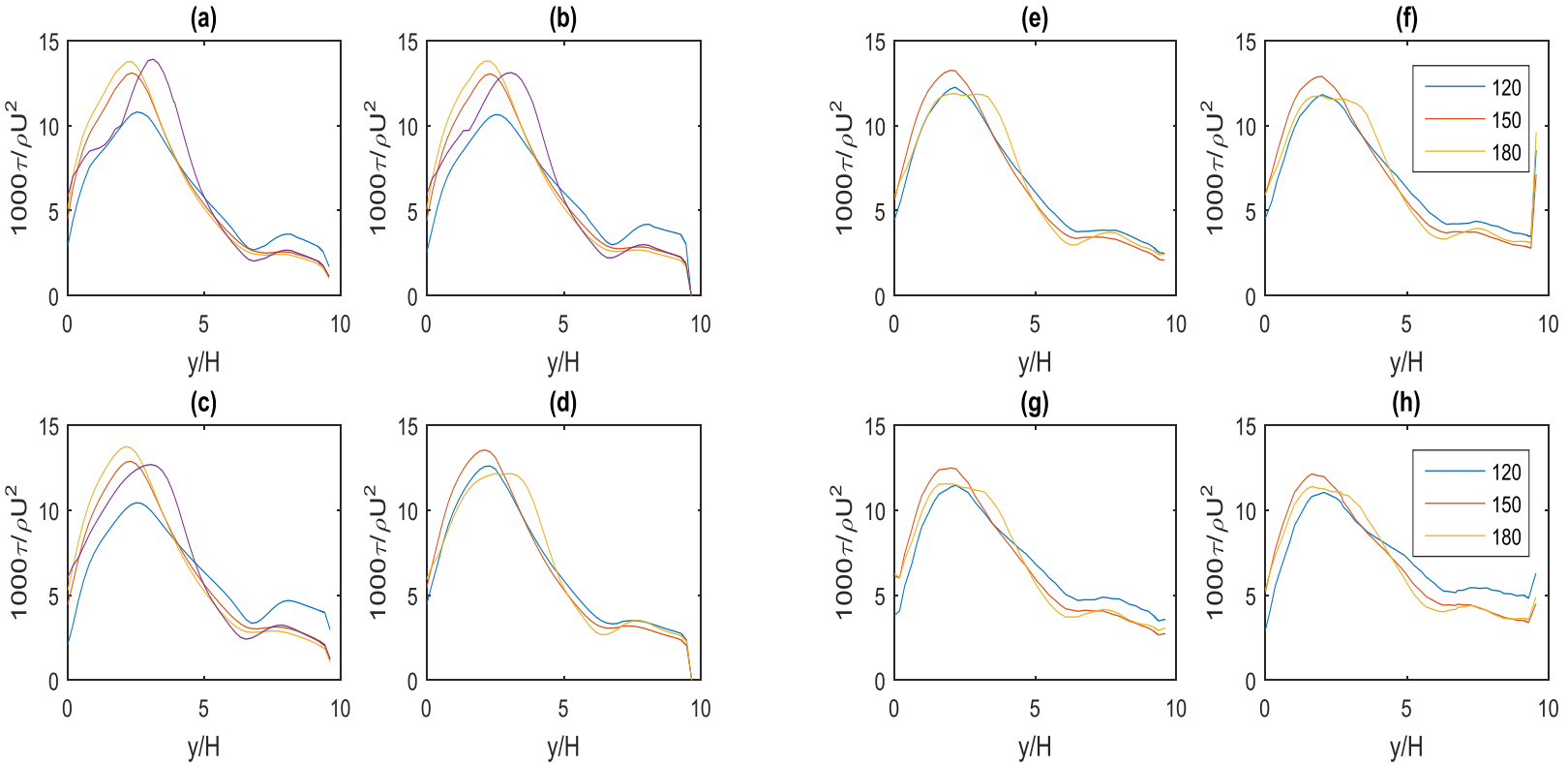

Figure 5.7: Bed shear stress plots for the tight channels R/T_w = 0.75 from 80^O to the 115^O planes. Note the angles in the legend denote the channle length. Panel (a) shows the bed shear stress at the 80^O plane, panel (b) shows the bed shear stress at the 85^O plane, panel (c) at the 90^O plane while panel (d) at the 95^O plane. Panels (e), (f), (g), (h) show the bed shear stress at the 100, 105 ,110 ,and 115 degree planes.

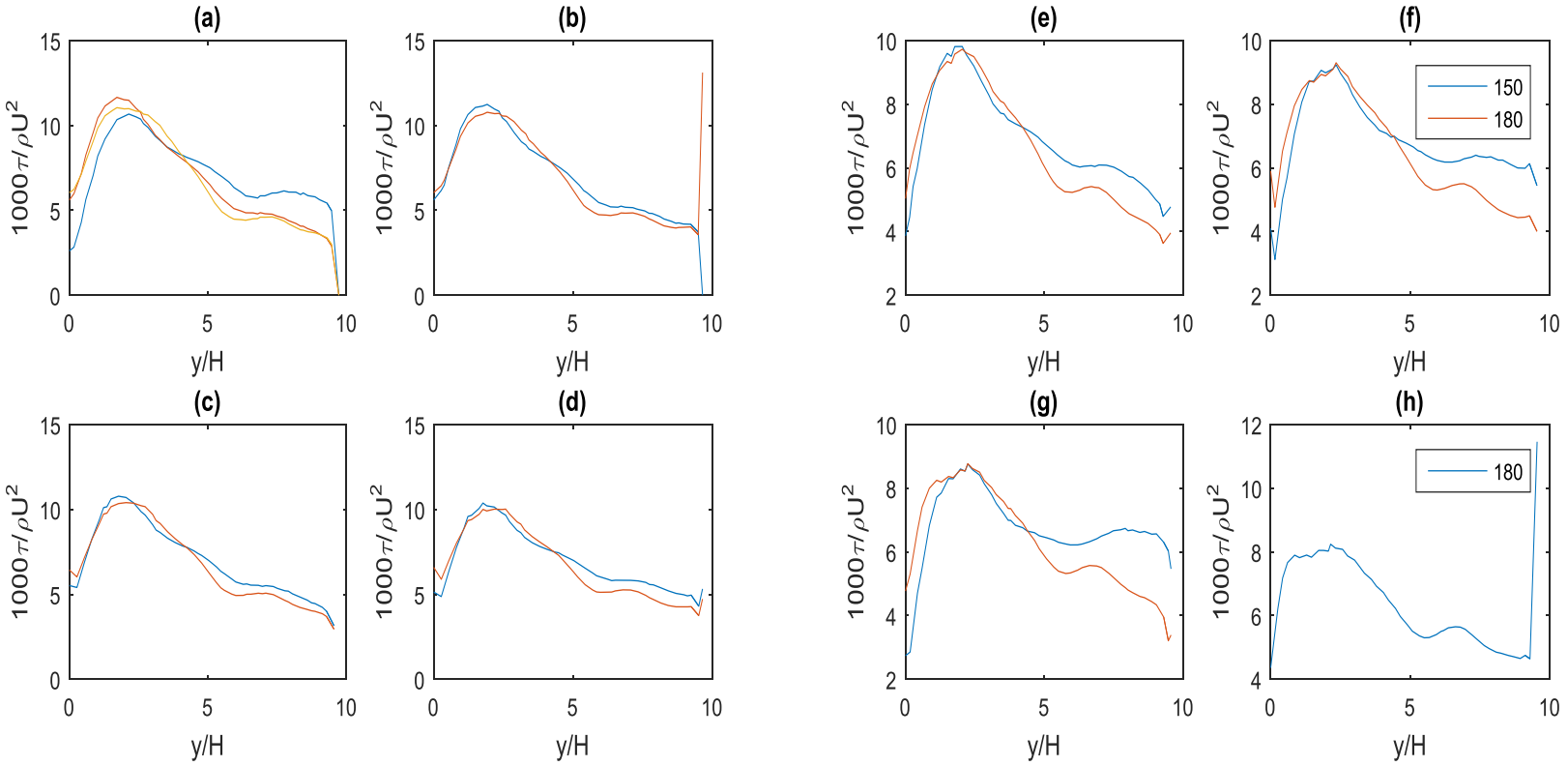

Figure 5.8: Bed shear stress plots for the tight channels $R/T_w = 0.75$ from 120^O to the 155^O planes. Note the angles in the legend denote the channle length. Panel (a) shows the bed shear stress at the 120^O plane, panel (b) shows the bed shear stress at the 125^O plane, panel (c) at the 130^O plane while panel (d) at the 135^O plane. Panels (e), (f), (g), (h) show the bed shear stress at the 140, 145 ,150 ,and 155 degree planes.

5.4 Velocity Distribution

The velocity distribution determines not only the distribution of velocity gradients, but also the distribution of shear stresses in an open channel bend. Therefore, more insight may be gained into events responsible for the various shear stress distributions encountered in the previous section, especially of that in the tight channel.

Figures 5.9 and 5.11 shows the velocity distribution in the mild channels MB30 and MB150. These two channels show velocity distributions that are typical of the mild bends regardless of the curvature length. The velocity distribution shown in these figures is as expected given the known result of the interaction between the centrifugal acceleration and the radial pressure gradient. Hence at the inlet to the curve, an adverse pressure gradient at the outer wall and a favorable pressure gradient at the inner wall ensures that the bulk of the fluids momentum is pushed toward the inner wall (explained in Chapter 4 and in the previous section of this chapter). The streamline plots shown in figures 5.10 and 5.12 help visualize this better. As the fluid moves deeper into the bend, fluid closer to the surface begin to feel the full impact of the centrifugal acceleration and move towards the outer wall while fluid close to the bed move closer to the inner wall because of the reversal of the direction of the centrifugal force at depths close to the channel bed. This creates the distribution of velocity shown in Figures 5.9 and 5.11.

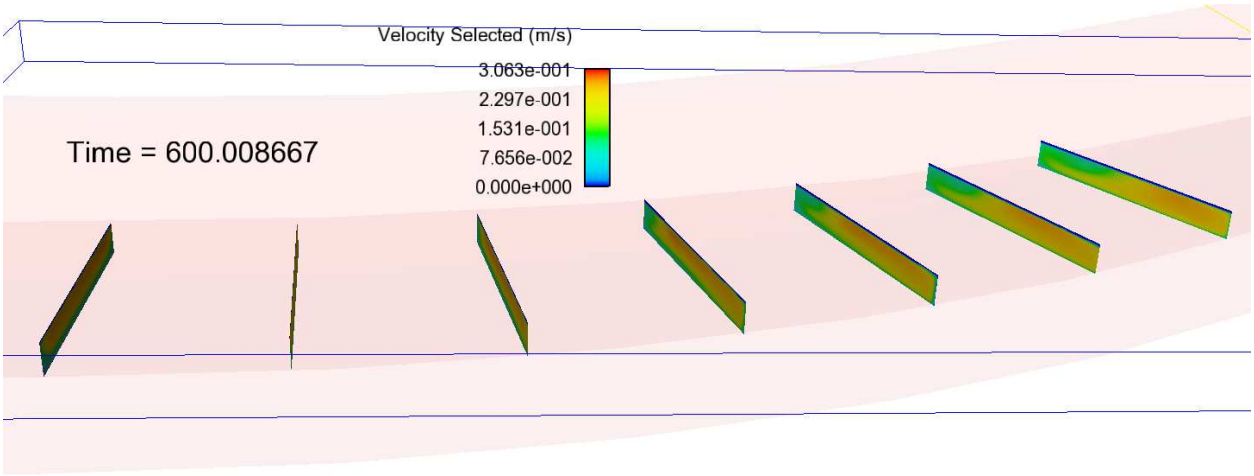

Figure 5.9: Velocity distribution in the mild channel with length 30 degrees MB30.

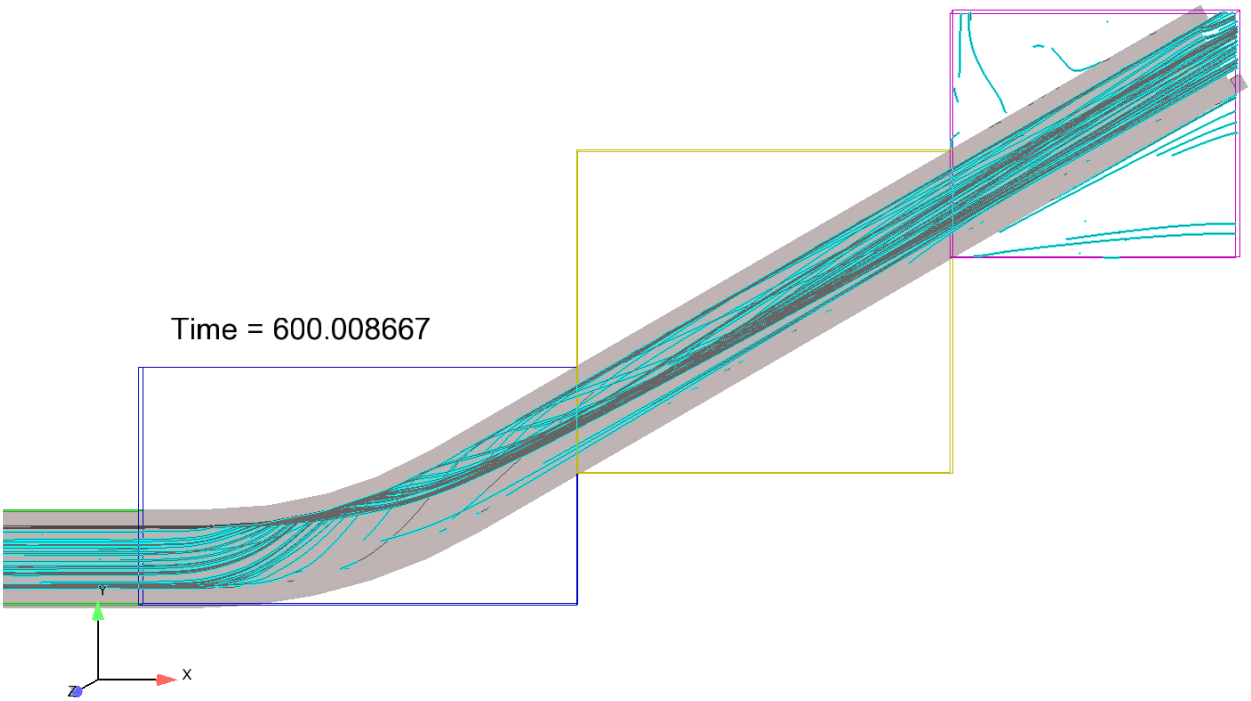

Figure 5.10: Streamlines in the mild channel with length 30 degrees MB30.

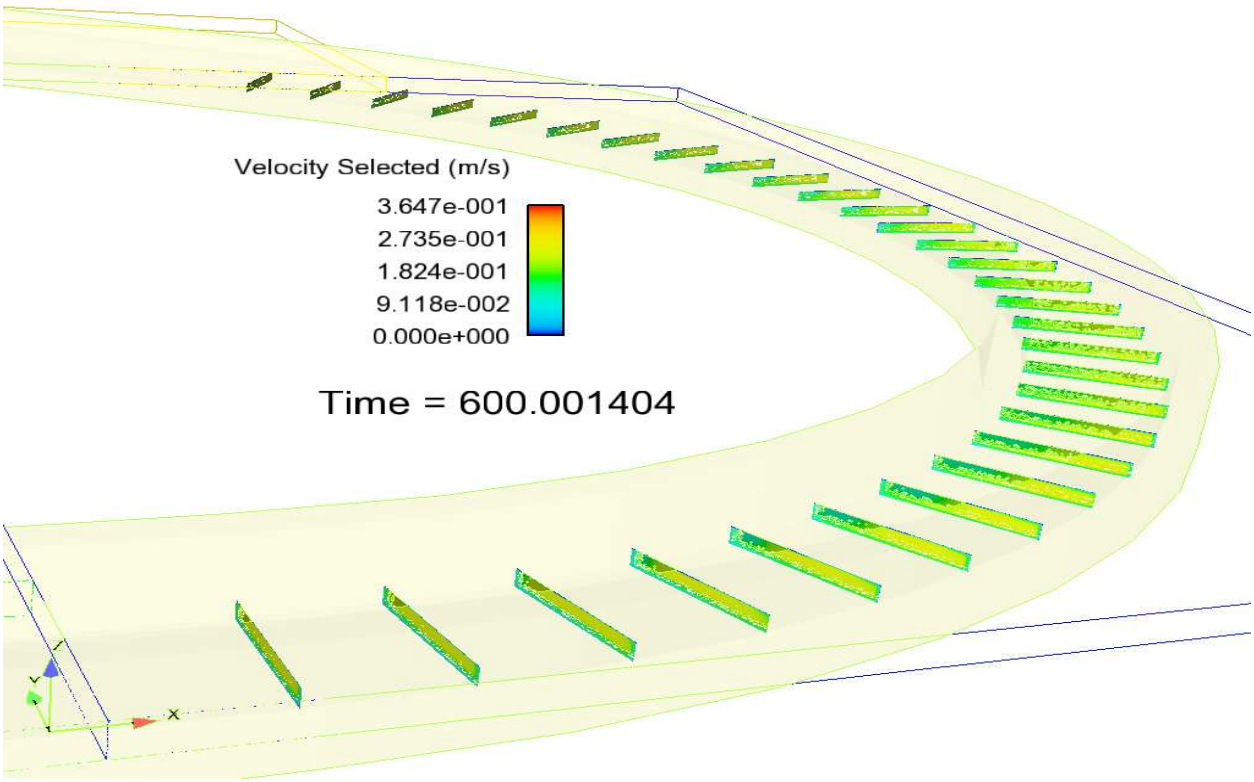

Figure 5.11: Velocity distribution in the mild channel with length 150 degrees MB150.

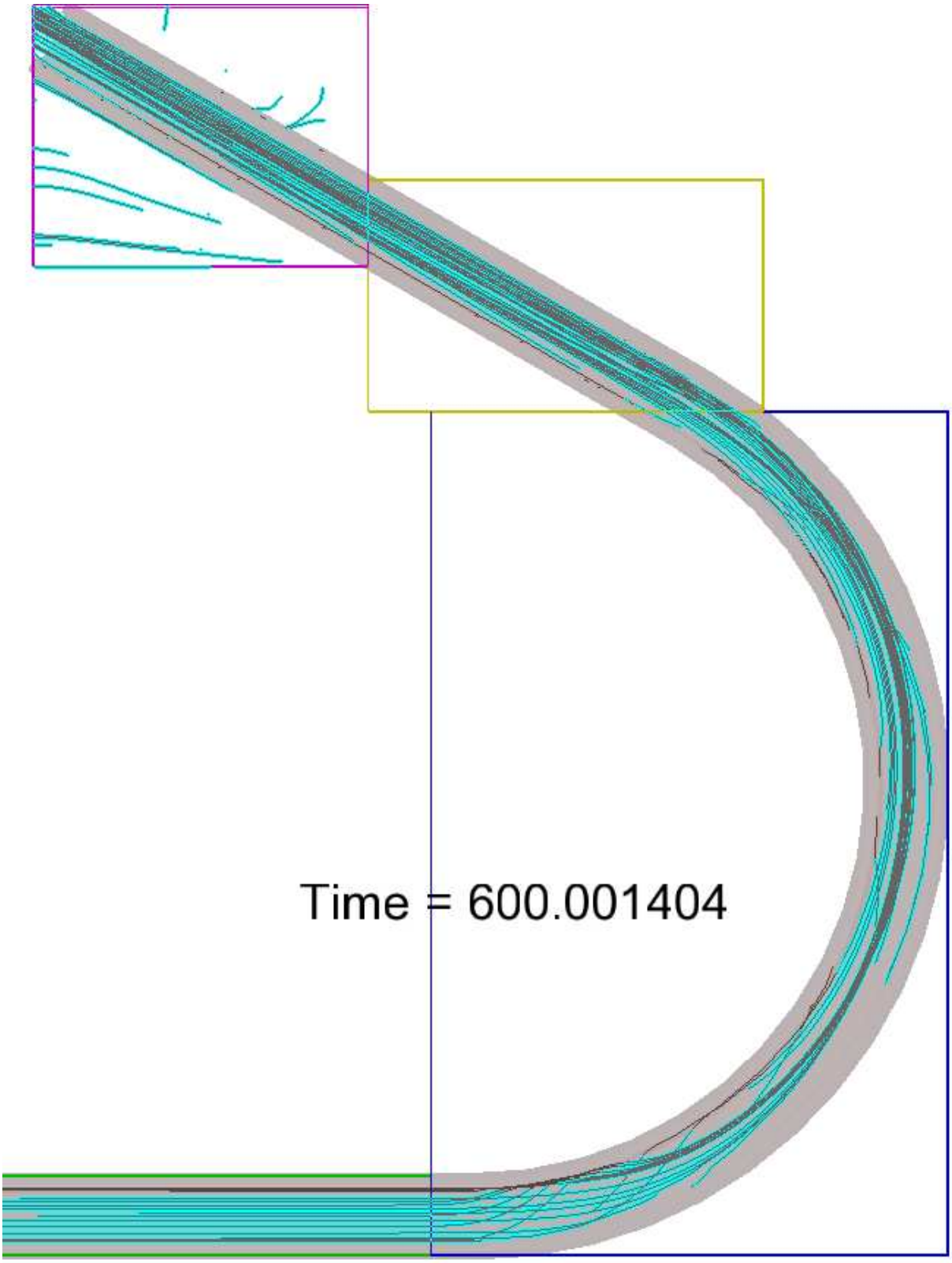

Figure 5.12: Streamlines in the mild channel with length 150 degrees MB150.

In the tight bends, a different velocity distribution is encountered. Surprisingly our results show that two distinct velocity distributions occur depending on the curvature length of the tight channel. In the short channels TB30, TB60 and TB90, the region of maximum velocity streamlines is situated closer to the inner wall for reasons similar to that of the mild channel bends (see Figures 5.13 and 5.14). But unlike in the mild channel as the fluid proceeds into the bend in the short channels (TB30, TB60 and TB90) the streamline of maximum velocity do not shift to the outer wall, this pattern holds for the entirety of the length of the short tight channels. In the longer tight channels, the entrance regions exhibit similar velocity patterns to that of the short channels for reasons similar to the physics of the entrance region of the mild channels. However, unlike the short tight channels the region of maximum velocity streamlines shifts to the middle regions in the channel interior (see Figures 5.15 and 5.16) and then to the outer bend region outside the channel in the outlet. It is speculated that in the short channel there is not enough space for the centrifugal force to develop to such a magnitude that the high velocity fluid region is pushed towards the outer bend while the longer channel manages to provide a little space close to the outlet where the centrifugal acceleration develops enough for the region of high fluid velocity to shift towards the outer bend.

Important as these velocity distribution plots are and the hypothesis they helped create there is still doubt as to how the dynamics can sustain such high velocity gradient on the inner bend for the entirety of the channel in some of the tight curves. In a last ditch attempt to uncover why this is the case the next section examines the free surface profiles and how these may provide some insights into why the flow dynamics of the bend channels are as observed.

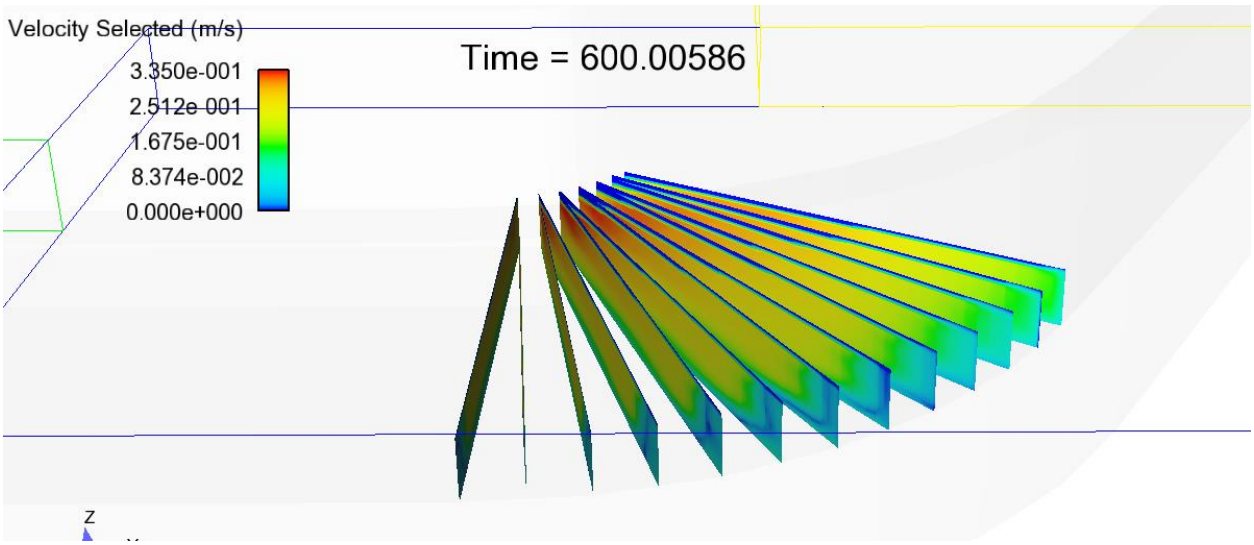

Figure 5.13: Velocity distribution in the tight channel with length 60 degrees TB60.

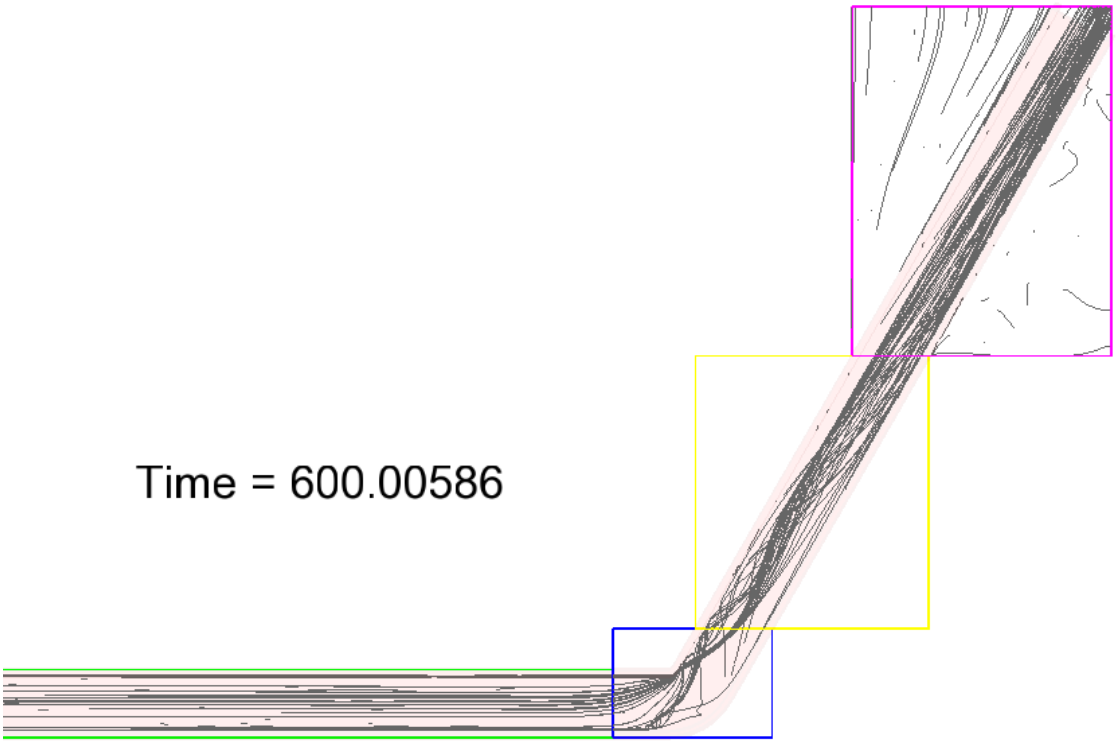

Figure 5.14: Streamlines in the tight channel with length 60 degrees TB60.

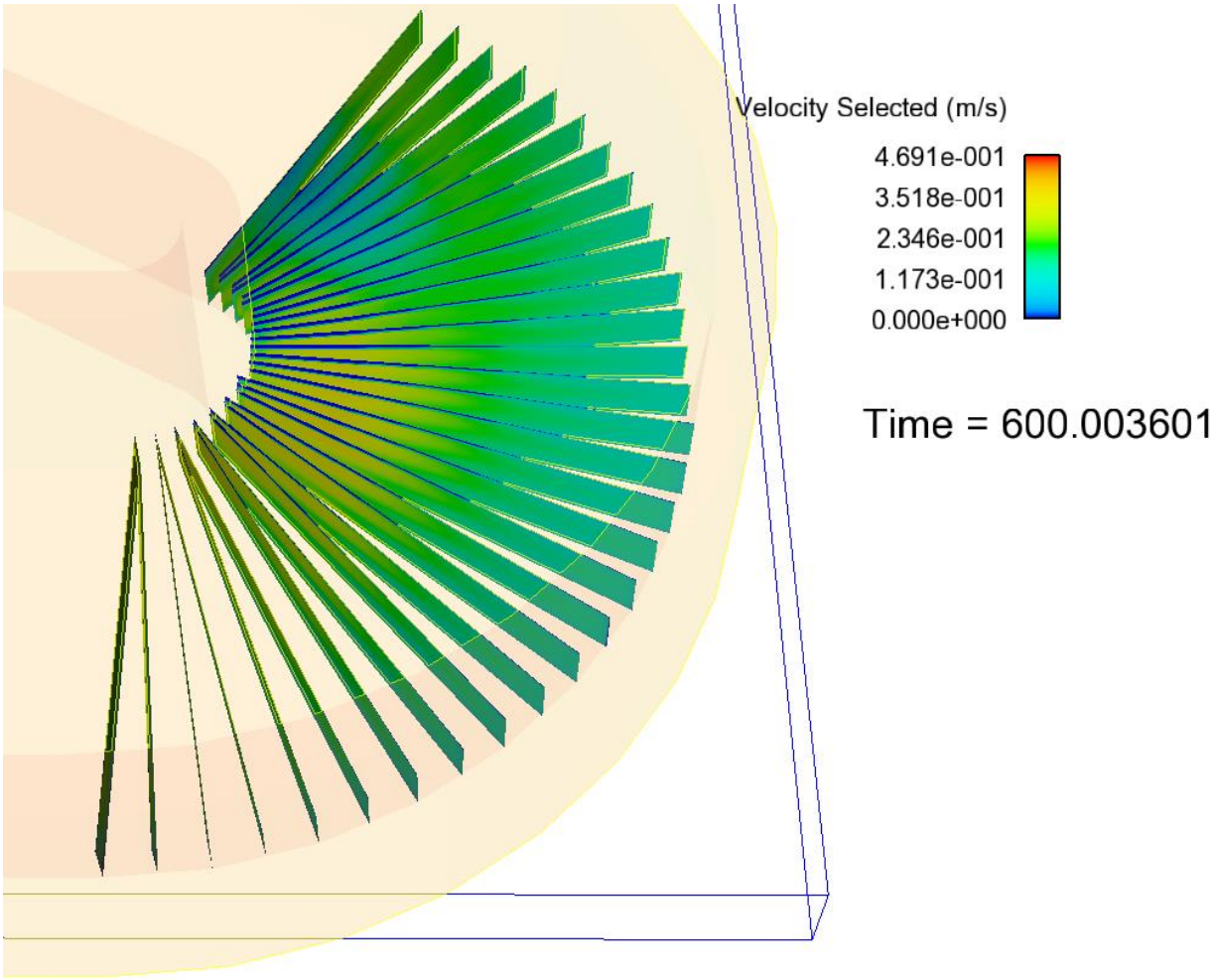

Figure 5.15: Velocity distribution in the tight channel with length 150 degrees TB150.

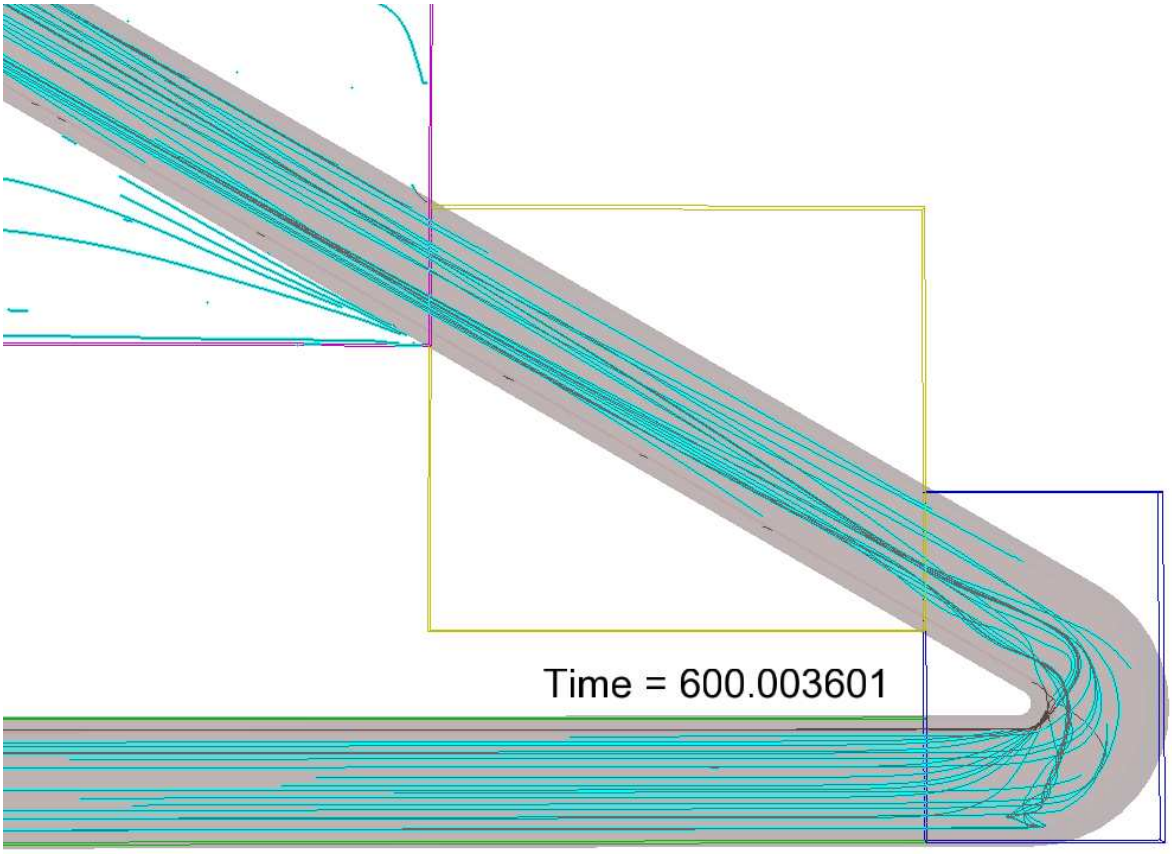

Figure 5.16: Streamlines in the tight channel with length 150 degrees TB150.

5.5 Free Surface Dynamics

The free surface is critical to understanding the dynamics in our present context. Even though all simulations were conducted using the full three dimensional Navier-Stokes equations, the hydrostatic assumption is used to compute the radial pressure gradient. This assumption means that the acceleration in the vertical dimension is negligibly small so that the derivative of the pressure field with respect to depth is a constant (implying that the pressure is a function of depth). This assumption simplifies enormously the calculation procedure for the pressure gradient force per unit mass $\frac{1}{\rho g}\frac{\partial P}{\partial r}$ as in a hydrostatic channel, this force simply reduces to the radial free surface gradient $\frac{\partial H}{\partial r}$.

In any transverse cross-section (or control volume) in the channel bend, the two main external forces are the centrifugal force (per unit mass) and the radial pressure gradient (per unit mass). A critical look at the interaction between these two forces may finally bring some closure to the question of the tight bend dynamics especially concerning the questions that remain unanswered from Chapter 4. In comparing these two forces, attention is paid to the fully developed region only. This is done since according to knowledge gathered so far from this research the flow parameters are invariant with changes in position in this developed regions making it ideal for this analysis. Also care has been taken to select velocities near the surface with the highest magnitude in order to analyze the extreme scenarios. All these were done so that values representative of extreme conditions is captured in our analysis to enhance the quality of the final deductions made.

An examination of the centrifugal forces per unit mass in both the mild and tight channel show that they follow the same trend even though magnitudes may differ. However, the radial pressure gradients for both channels are different with that of the mild channel bend essentially almost constant and that for the tight channel rising almost sharply from the inner wall. The moment of clarity comes when the centrifugal acceleration and the radial pressure gradient are compared for each curvature. It becomes clear from Figure 5.17 that in the mild bend when the flow is developing (beyond the 35 degree plane) the centrifugal force is greater than the radial pressure gradient. The resultant in a mild channel is a dynamic force that pushes fluid above a certain depth towards the outer bend. On the other hand, in a tight bend, the extreme geometry ensures that the free surface gradient is large such that the radial pressure gradient force (which has an inward direction) is always greater than the outward directed centrifugal force (see Figure 5.18). This results in a force strong enough to pin the fluid of higher velocity close to the inner wall for the entirety of the channel. Hence the peculiar dynamics in the tightest channels is due to the extremely high magnitude of the radial pressure gradient forces.

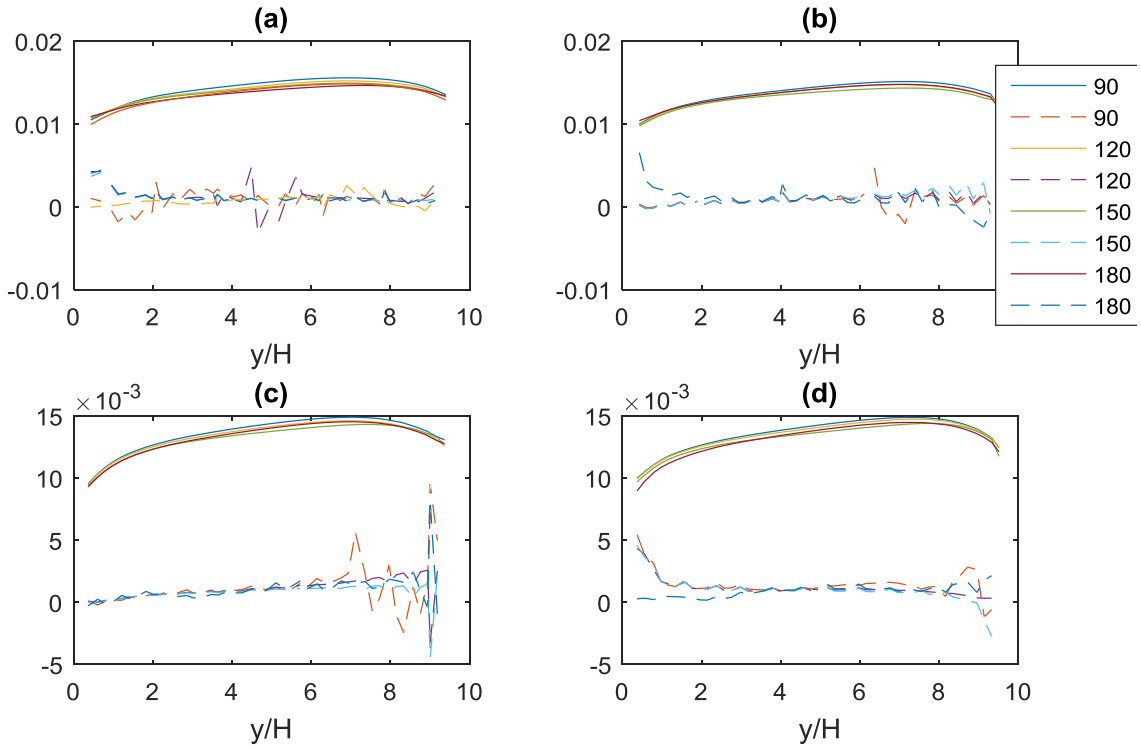

Figure 5.17: Plots of the maximum non- dimensional centrifugal acceleration (unbroken lines) and the non-dimensional radial pressure gradient (broken lines --) at various channel lengths for the mild curvature. Note the centrifugal acceleration was non-dimensionalized as $\frac{H}{U^2}\frac{v^2}{r}$ where H is the flow depth and U^2 is the average velocity squared. The radial pressure gradient is calculated as $\frac{\partial H}{\partial r}$. Panel (a) shows the plots at the 60^O plane while (b), (c), and (d) show the plots at the 65, 70 and 75 degree planes, respectively.

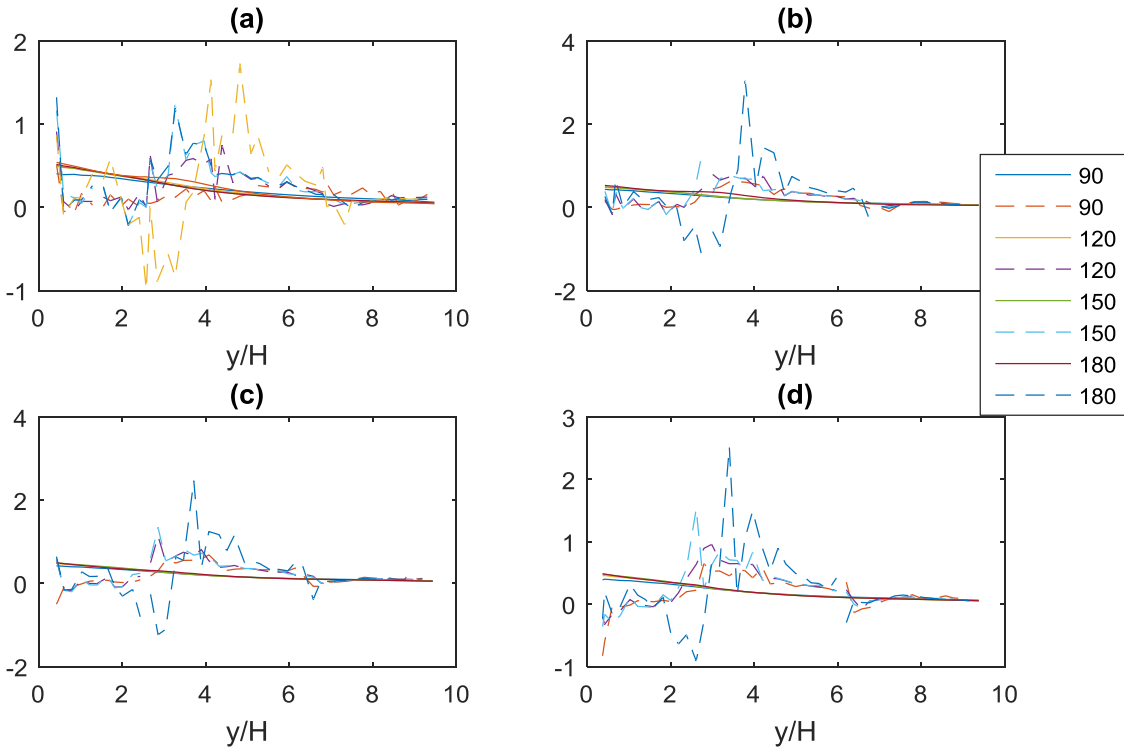

Figure 5.18: Plot of the maximum non- dimensional centrifugal acceleration (unbroken lines) and the non-dimensional radial pressure gradient (broken lines --) at various channel lengths for the tight curvature. Note the centrifugal acceleration was non-dimensionalized as $\frac{H}{U^2}\frac{v^2}{r}$ where H is the flow depth and U^2 is the average velocity squared. The radial pressure gradient is calculated as $\frac{\partial H}{\partial r}$. Panel (a) shows the plots at the 60^O plane while (b), (c), and (d) show the plots at the 65, 70 and 75 degree planes, respectively.

Even though the previous paragraph presents a plausible explanation for a long standing question (that was first posed in chapter 4), there still remains the question pertaining to the different vortical (circulation) structures. In order to answer this, an examination of the circulation structure and vorticity distribution in bends of various curvature length is carried in the next section.

5.6 Vorticity Dynamics

It is known from the study of curvature effects in an open channel bend that there is a spatially developing region (which depends on the curvature $\frac{R}{T_w}$) and a fully developed region in the bend where flow properties are spatially invariant. A specific example is that of the mild channel $MB180$. In the previous chapter, it was observed that for mild curvature ($\frac{R}{T_w} = 8.2$), there was a spatially developing region from the 0^o plane to about the 85^o plane, and a fully developed region beyond the 90^o plane. The question posed at the beginning of this chapter was: how does the circulation structure develop for a bend with similar curvature but with significantly shorter length? Since there is no 85^o plane in a significantly shorter channel, does the flow still evolve to reach a spatially invariant state like in the channel $TB180^o$?. If so, is that spatially developed state still characterized by the two cell circulation structure? In order to answer these questions, the circulation structure for the mild channels (MB30 to MB180) are compared to those of the tight channels (TB30 to TB180).

The transverse velocity plots which shows the circulation structure for the mild channels are shown in figures 5.19 to 5.22 for four of the six lengths (MB30, MB60, MB90, and MB120) at transverse planes ranging from the channel entrance to 30 degrees. These plots show that in regions close to the bend entrance, there is interaction between the centrifugal acceleration and the radial pressure gradient creating a single cell circulation (refer to Chapter 4). This single cell circulation continues to increase in vortex strength (as explained in the vorticity section of chapter 4) as the flow proceeds further into the bend. In addition, as the flow moves deeper into the bend, it seems that the shorter channels have a shorter development length and reach the spatially invariant two cell circulation structure at an earlier stage in the flow than their longer counterparts. A good example of this phenomena is the circulation structure of the shortest (30^o) mild channel (see Figure 5.19 to 5.22 panel (a)). For this case, the spatially invariant two cell circulation structure is fully formed by the 20^o plane (compare figure 5.20 panel (a) with

panels (b) to (d)) as opposed to the 80^o plane in the longer 180^o channel. Hence, this indicates (a somewhat surprising result) that the longer channels develop spatial invariance at later stages compared to the shorter channels.

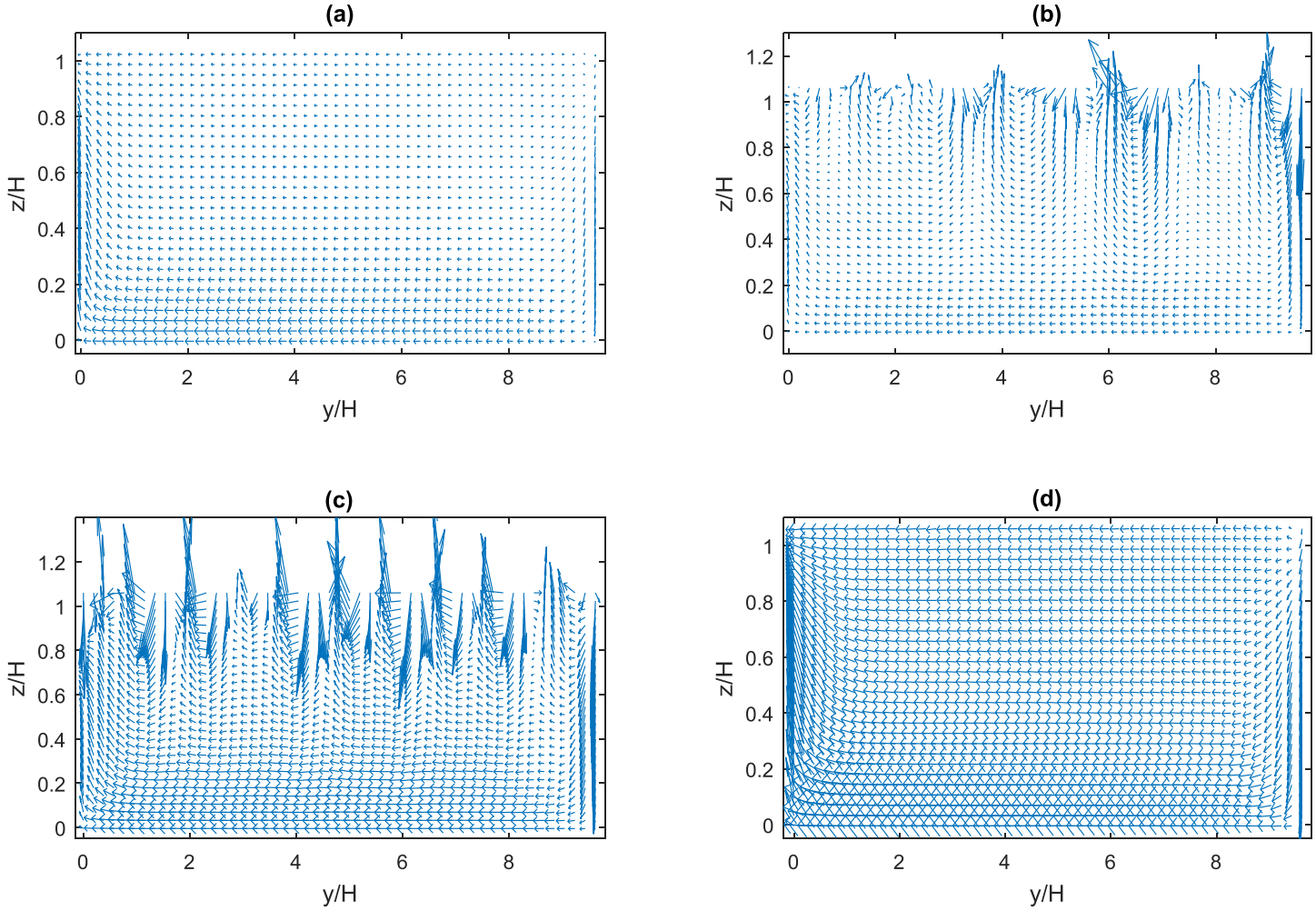

Figure 5.19: Transverse velocity plots at the 0^O plane for the mild channel ($\frac{R}{T_w} = 8.2$) of length 30^O (panel a), length 60^O (panel b), length 90^O (panel c) and length 120^O (panel d).

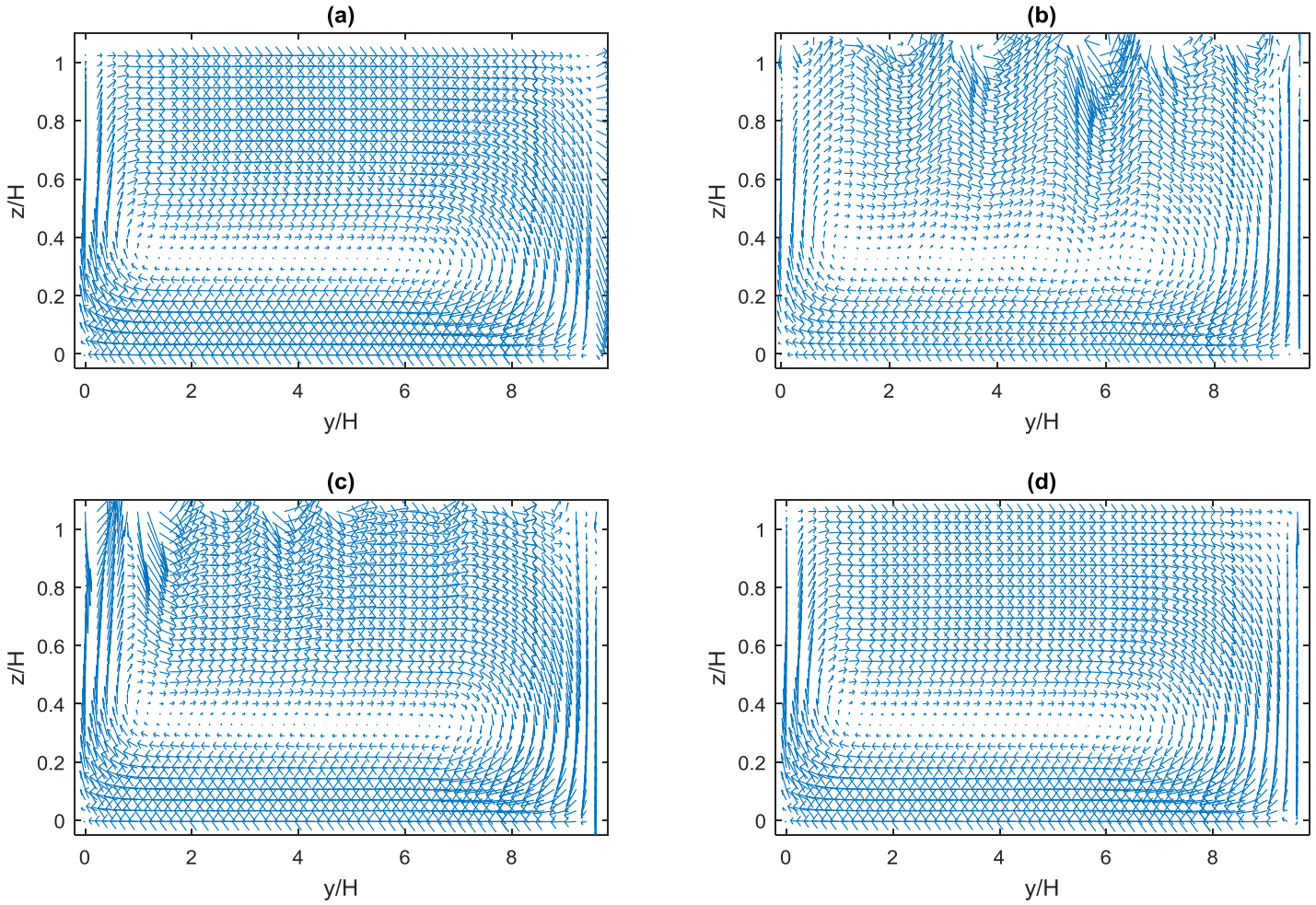

Figure 5.20: Transverse velocity plots at the 10^{O} plane for the mild channel ($\frac{R}{T_w} = 8.2$) of length 30^{O} (panel a), length 60^{O} (panel b), length 90^{O} (panel c) and length 120^{O} (panel d).

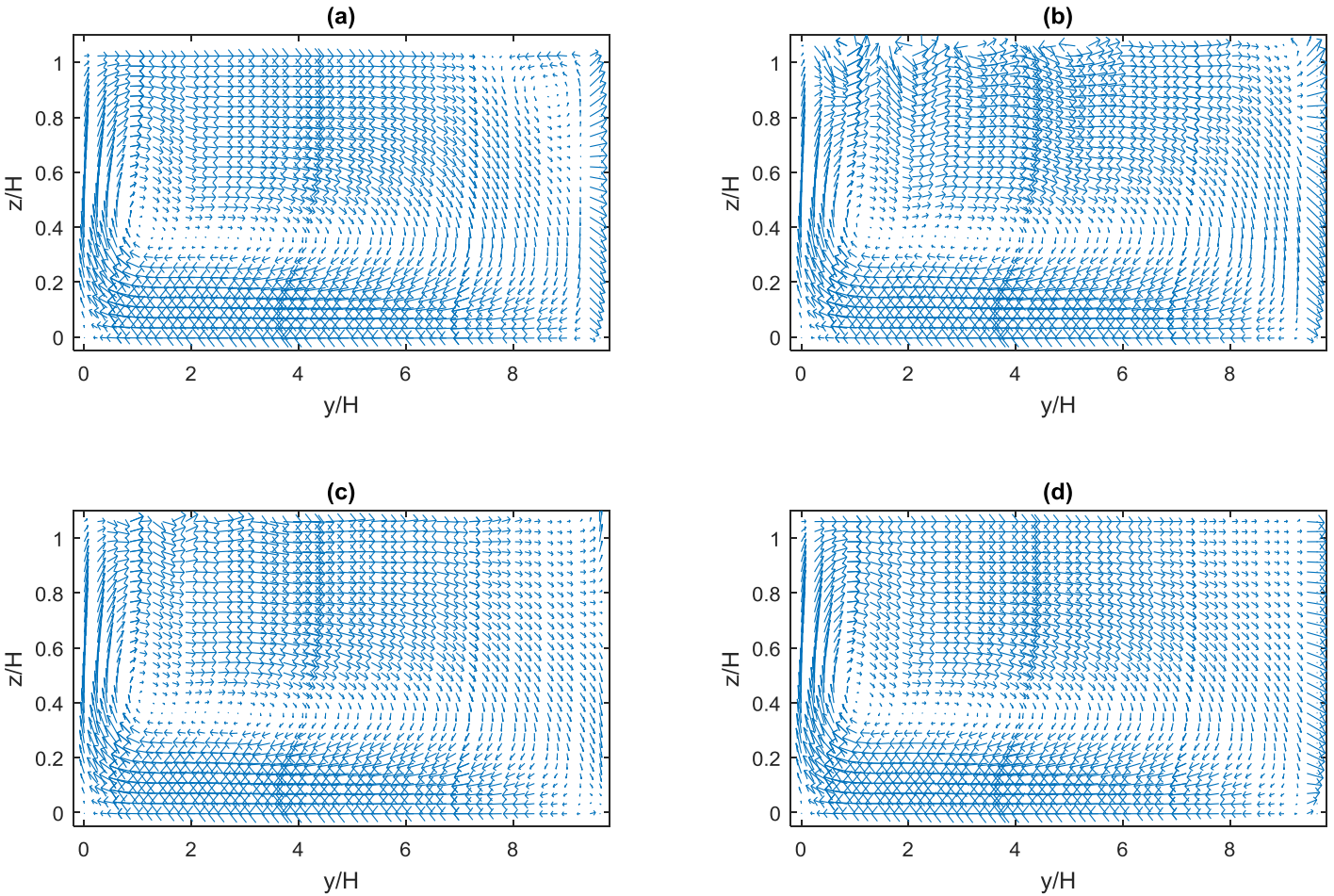

Figure 5.21: Transverse velocity plots at the 20^{O} plane for the mild channel ($\frac{R}{T_w} = 8.2$) of length 30^{O} (panel a), length 60^{O} (panel b), length 90^{O} (panel c) and length 120^{O} (panel d).

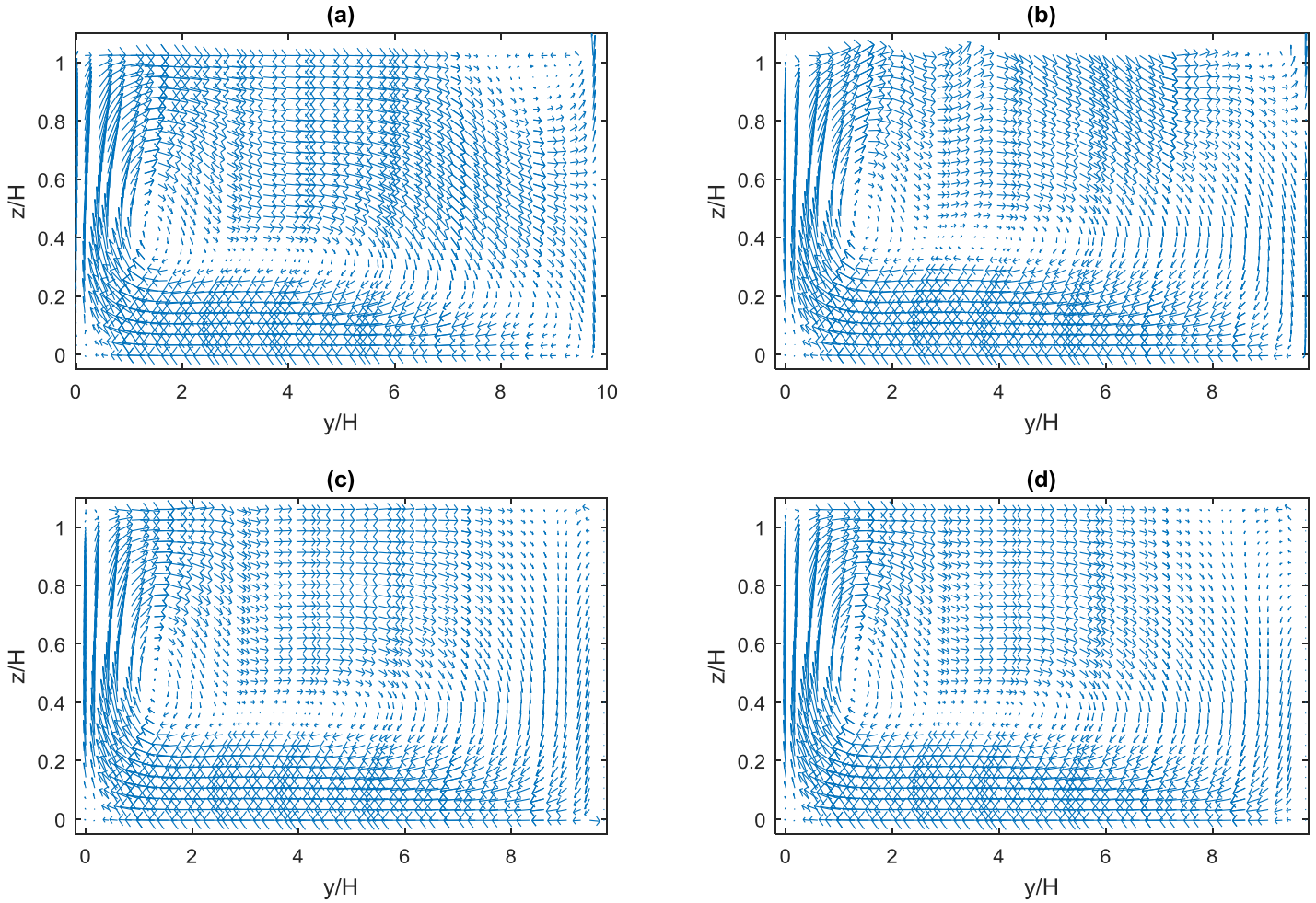

Figure 5.22: Transverse velocity plots at the 30^O plane for the mild channel ($\frac{R}{T_w} = 8.2$) of length 30^O (panel a), length 60^O (panel b), length 90^O (panel c) and length 120^O (panel d).

The tight channels on the other hand exhibit two distinct vortical patterns depending on the length of curvature. In the shorter channels (TB30 and TB60), the circulation structure is that of a single cell for the entirety of the channel length (see Figures 5.23 and 5.24). The complex interaction between the centrifugal acceleration and the radial pressure gradient is also responsible for this circulation. However, given the relatively shorter lengths, the vorticity contours show that the vorticity magnitude never develops to values seen in the longer channels so that the condition for the existence of two clockwise main body cell established in Chapter 4 is never reached. In addition, in the short channels, the outer bank counter rotating cell is missing for the entirety of the channel length (Figure 5.23 and 5.24 panel (a)). In the longer channels (i.e. TB90, TB120, TB150, TB180) there is an initial development region with a single cell circulation structure. As the flow moves deeper into the bend, a second counter rotating outer wall cell develops forming the two cell circulation structure similar to that already observed in a full 180^o mild channel (figure 5.25 panel (c) and (d)). Finally, as the flow reaches its fully developed stage, the main clockwise circulation cell splits into two (due to the extreme values of vorticity magnitude as explained in chapter 4) resulting in the 3 cell circulation structure for a tight bend (Figure 5.26 panels (c) and (d)). This three cell structure however only occurs in the fully developed region of the longer bends (bends of 90^o and above). Unfortunately, the reason why the counter clockwise outer wall circulation develops quicker than expected in the short mild channels and not at all in the short tight channels is beyond the grasp of this research.

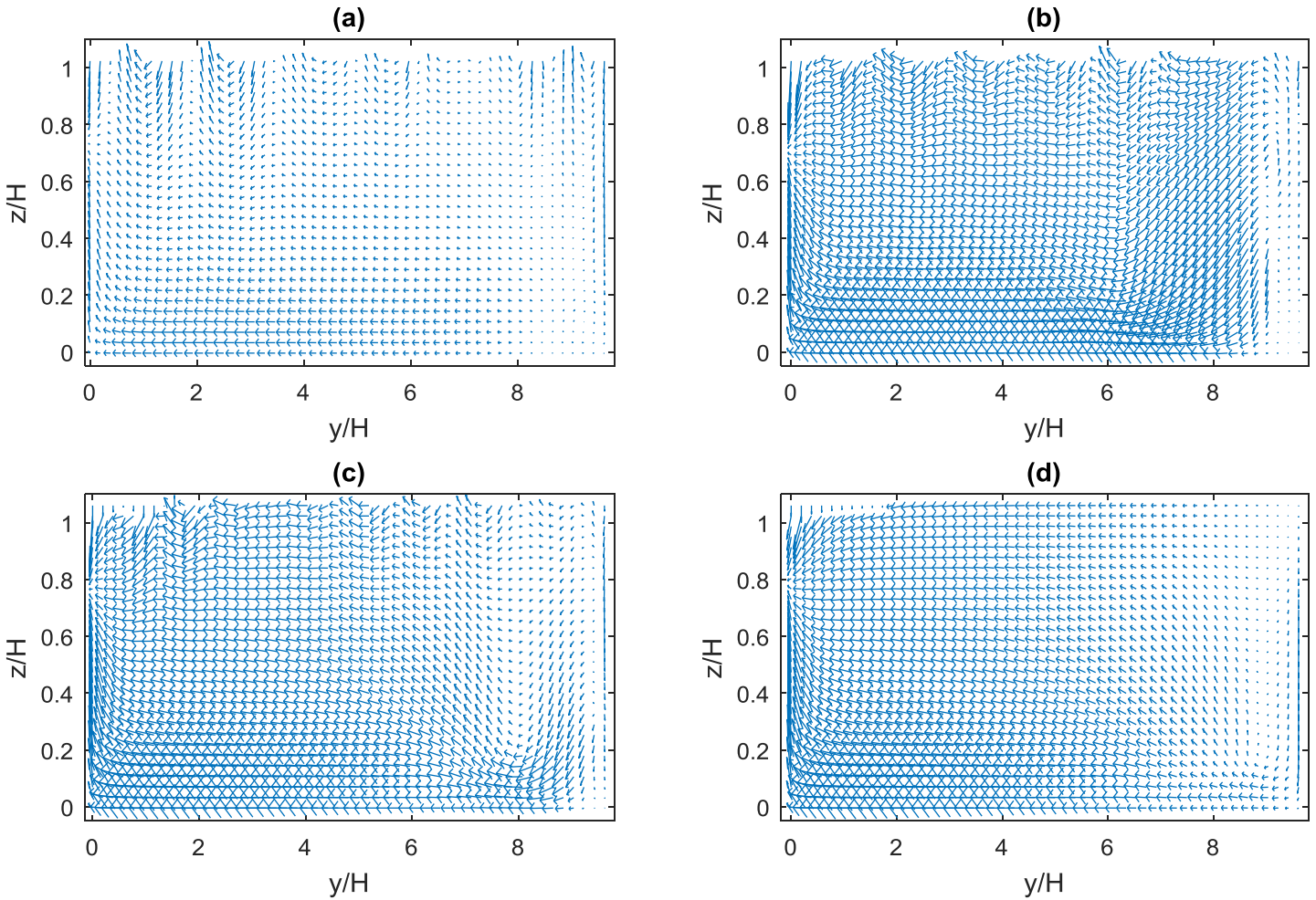

Figure 5.23: Transverse velocity plots at the 0^O plane for the tight channel ($\frac{R}{T_w} = 0.75$) of length 30^O (panel a), length 60^O (panel b), length 90^O (panel c) and length 120^O (panel d).

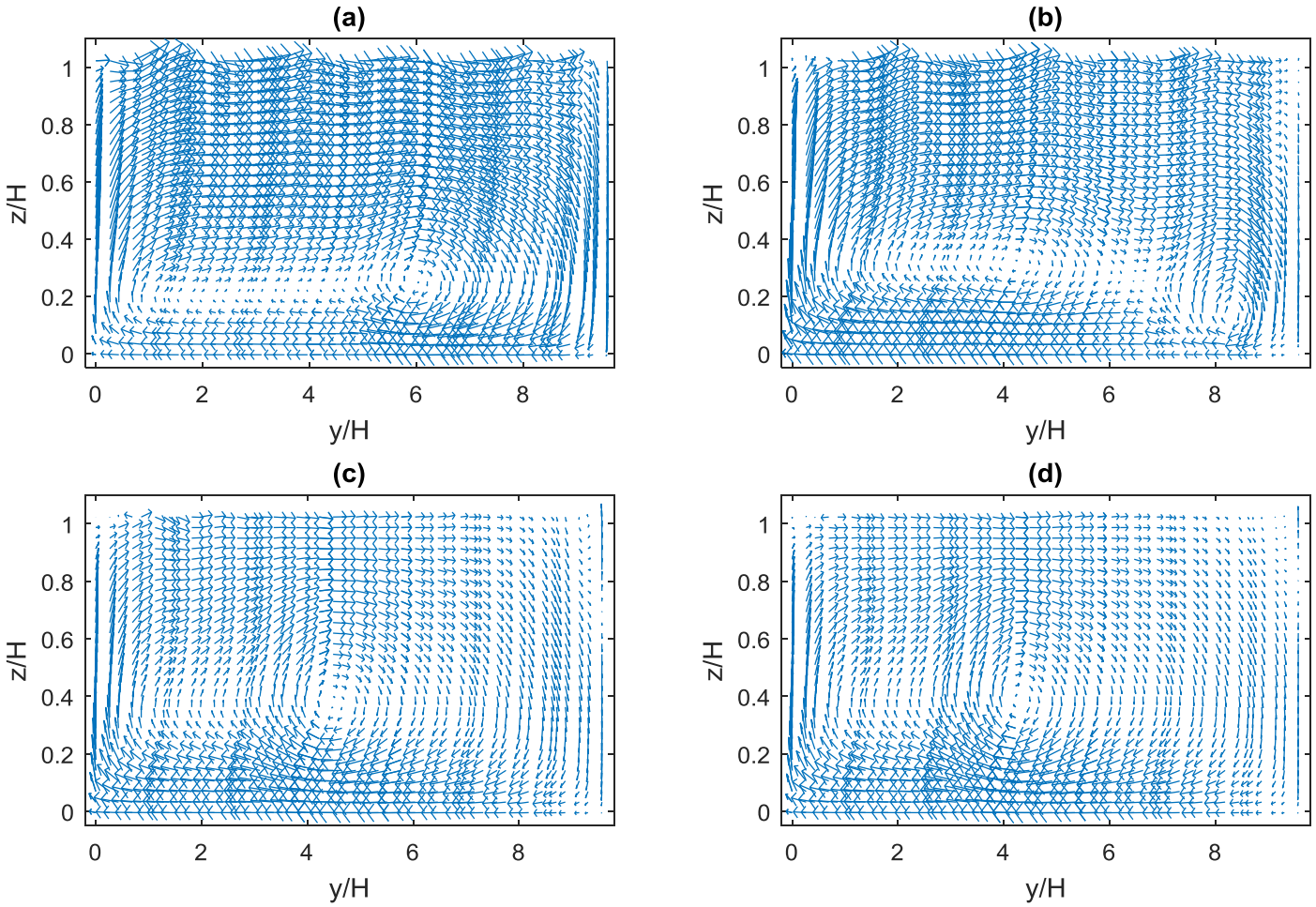

Figure 5.24: Transverse velocity plots at the 30^{O} plane for the tight channel ($\frac{R}{T_w} = 0.75$) of length 30^{O} (panel a), length 60^{O} (panel b), length 90^{O} (panel c) and length 120^{O} (panel d).

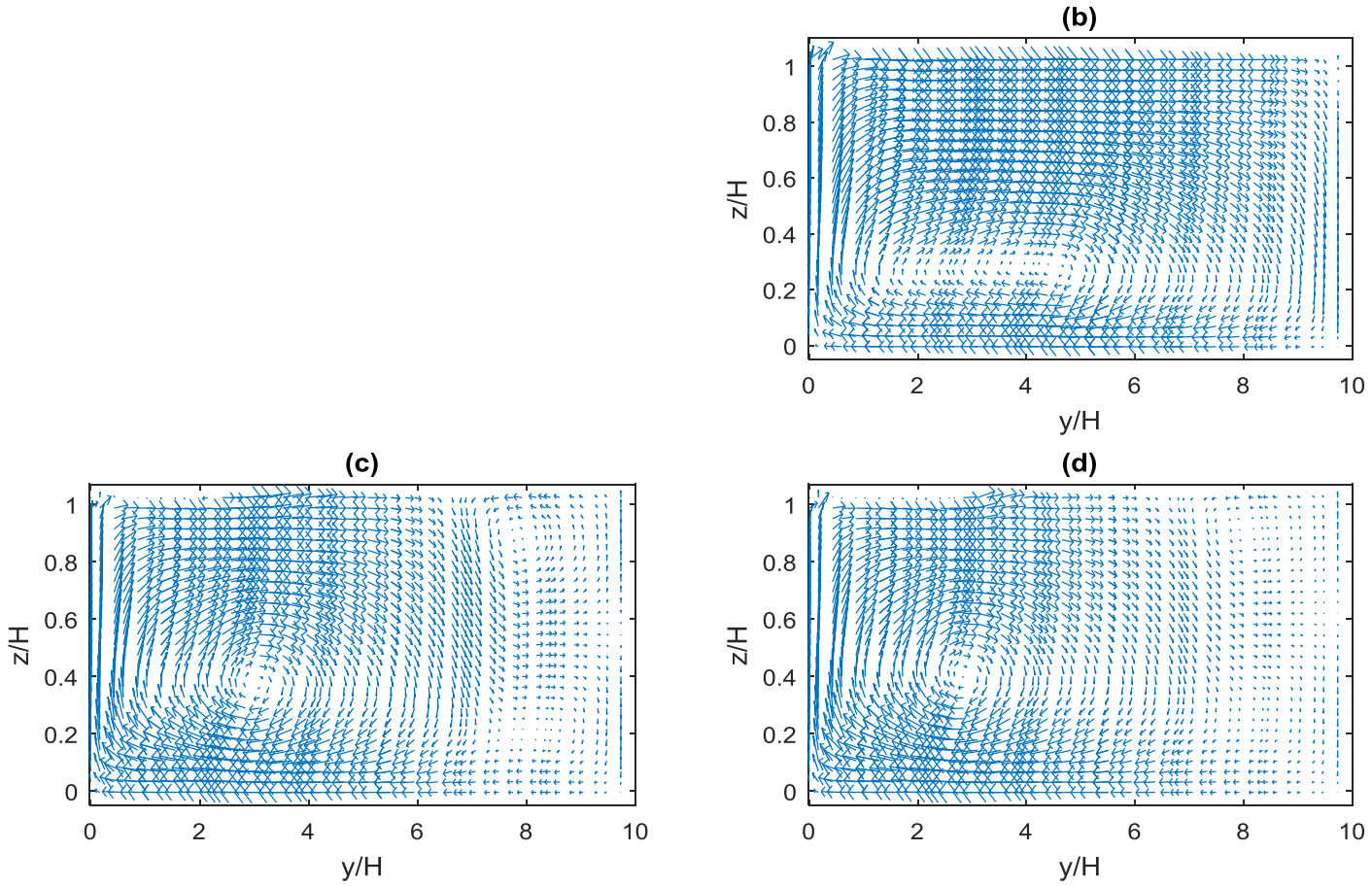

Figure 5.25: Transverse velocity plots at the 60^O plane for the tight channel ($\frac{R}{T_w} = 0.75$) of length 30^O (panel a), length 60^O (panel b), length 90^O (panel c) and length 120^O (panel d).

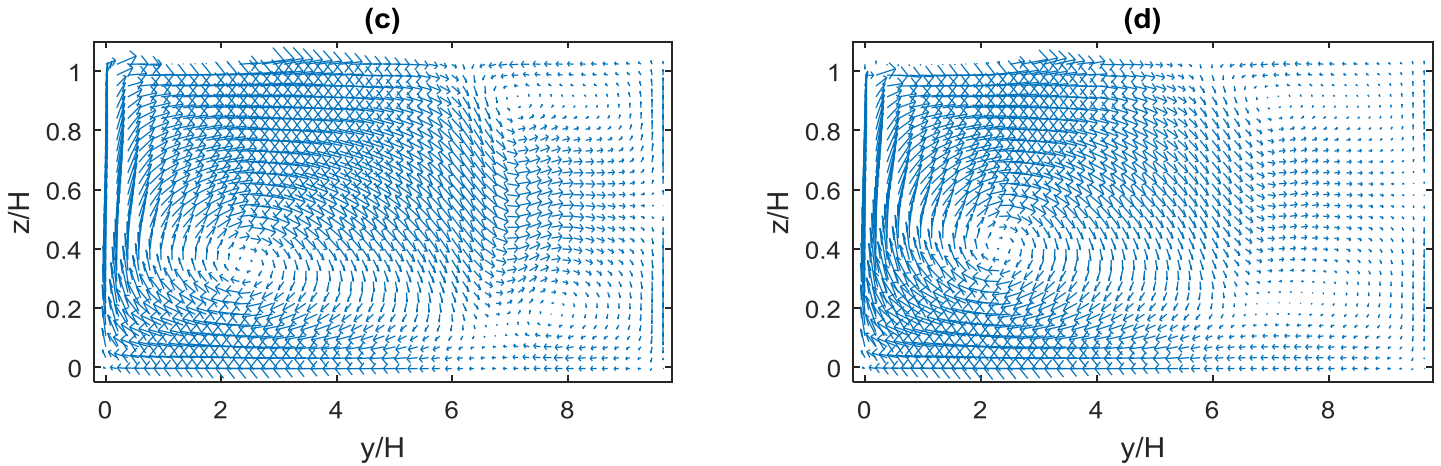

Figure 5.26: Transverse velocity plots at the 85^{O} plane for the tight channel ($\frac{R}{T_w} = 0.75$) of length 30^{O} (panel a), length 60^{O} (panel b), length 90^{O} (panel c) and length 120^{O} (panel d).

5.7 Summary

This chapter studied the effects of curvature length variation on the 3 dimensional flow structure and dynamics of open channel bend flows. This was accomplished using 12 different geometries of curvature length ($30^o, 60^o, 90^o, 120^o, 150^o, 180^o$) at two radii of curvature ($\frac{R}{T_w} = 0.75, \frac{R}{T_w} = 8.2$). In conclusion, we can now better articulate the circulation events in a curved open channel. In mild channels, the circulation starts in the developing region with a single cell circulation and then develops into a two cell circulation structure in the later parts of the channel consisting of a main body circulation cell and an outer wall counter rotating cell. The position where this two cell circulation develops depends on the length of the mild channel as shorter channels attain fully developed conditions at shorter angular distances from the entrance than longer channels. The circulation structure for the tighter channels depend on the channels length with the shorter channels having a single cell circulation only. In tight channels with angular length of 90^o and beyond, the circulation structure starts at the entrance region with a single cell circulation which is followed closely by the formation of the outer wall counter rotating cell and the eventual emergence of the three cell structure in the fully developed part of the tight channel.

It has been known that variations in geometry alone cannot explain the full range of flow phenomena observed in bend channel flows. A second look at equation (3.10) in the research framework section of this dissertation (section 3.5) shows that there is still one more dimensionless group (the Froude number) left to study ,which does not involve a variation in geometric parameters but includes dynamic parameters (velocity, wave celerity etc.). Hence, the next chapter of this dissertation studies the effect of varying the Froude's number on the flow structure and dynamics of 3D bend channel flows.

Chapter 6

The effect of Froude number variation on the flow structure and dynamics of open channel bends.

6.1 Preamble

There is a vast body of literature on general aspects of bend channel flows (Chapter 2). There has also been a few studies that vary geometric parameters in order to see their effect on flow structure (refer to the first section of chapter four of this thesis). However, existing research literature only addresses the issue of flow structure and dynamics from a geometric perspective. To the knowledge of this author, there has been no systematic study of the effect of varying Froude number (or other dynamic parameters like velocity or celerity) on the flow structure of open channel bends. It is for this reason that this chapter attempts this study. In order to accomplish this task, 6 large eddy simulations with non-dimensional curvature radii 8.2 and 0.75 were run at Froude numbers of 0.28, 0.5 and 0.8. The Froude number F*r* is defined as

$$Fr = \frac{V}{\sqrt{gy}} \ldots\ldots\ldots\ldots\ldots\ldots\ldots\ldots (6.1),$$

where V is the velocity,

g is the acceleration due to gravity,

y is the flow depth.

All six simulations had the same upstream and downstream geometries. Thus upstream of each bend there is a straight inlet with a length of 11 m, chosen to ensure that the fluid reached its fully developed state before encountering the bend. Also all the curves have a straight downstream outlet of 6.7 m. The same initial and boundary condition was imposed on all six simulations except at the inlet. Since the aim is to examine the effect of the Froude number (equation 6.1) on flow structure, various flow rates corresponding to the various Froude numbers to be studied were imposed on the appropriate channel

(see table 6.1 for details). Because the walls and the bed are assumed to be smooth the no-slip boundary condition was imposed. The outlet and the free surface have atmospheric boundary conditions imposed. The fluid in all six simulations were initialized at a flow depth of 0.052 meters and allowed to run up to steady state before measurements were taken. All simulation details are given in Table 6.1.

Table 6.1: Geometric and hydraulic parameters for all the simulations in this chapter.

	R/T_w	$Q(m^3/s)$	$U_{avg}(m/s)$	Re	Fr
Simulation 1	8.2	0.0052	0.2	10400	0.28
Simulation 2	8.2	0.0093	0.36	18570	0.5
Simulation 3	8.2	0.0149	0.57	29712	0.8
Simulation 4	0.75	0.0052	0.2	10400	0.28
Simulation 5	0.75	0.0093	0.36	18570	0.5
Simulation 6	0.75	0.0149	0.57	29712	0.8

Section 6.2 examines the effect of Froude number variation on the shear stress distribution. This naturally leads to Section 6.3 which examines the velocity distribution and how it changes with variation in Froude number. Section 6.4 examines how the free surface evolves with a change in Froude number. Finally, a critical examination of the vortex structure in section 6.5 is presented.

6.2 Shear Stress

Figure 6 shows the bed shear stresses for a mild channel ($\frac{R}{T_w} = 8.2$) for the three different Froude numbers from the 0^o plane to the 35^o plane in increments of 5^o. The maximum shear stress in the mild bend entrance region is located close to the inner bend (see figure 6.1 panel (a)). This happens in the mild bend regardless of the Froude number. As the flow moves further into the channel, the maximum shear stress shifts towards the outer bend (see Figures 6.1 (b),(c),(d)). This trend remains until the channel exit regardless of the Froude number. The wall shear stresses follow the same trend as the bed shear stresses with the maximum shear stress exerted on the inner wall at the entrance of the bed and on the outer wall as the flow moves deeper into the bend. This pattern also persists regardless of the Froude number.

In the tight bend ($\frac{R}{T_w} = 0.75$), the position of the maximum shear stress is exerted close to the inner bend and wall at the entrance to the bend (for reasons similar to those of the mild channel). However, unlike in the mild bend, as the flow moves further into the bend, the maximum shear stress never shifts towards the outer bend region throughout the channel length (see Figure 6.2). From new results in chapter 5 (see section 5.4 for details), it is now known that this is due to the extremely high magnitude of the radial pressure gradient because of the extreme curvature of the bend. This pattern is maintained for the whole of the channel length regardless of the Froude number. The only visible effect of a Froude number change on the shear stress pattern is an increase in the magnitude of the shear stress exerted at each point as the Froude number increases.

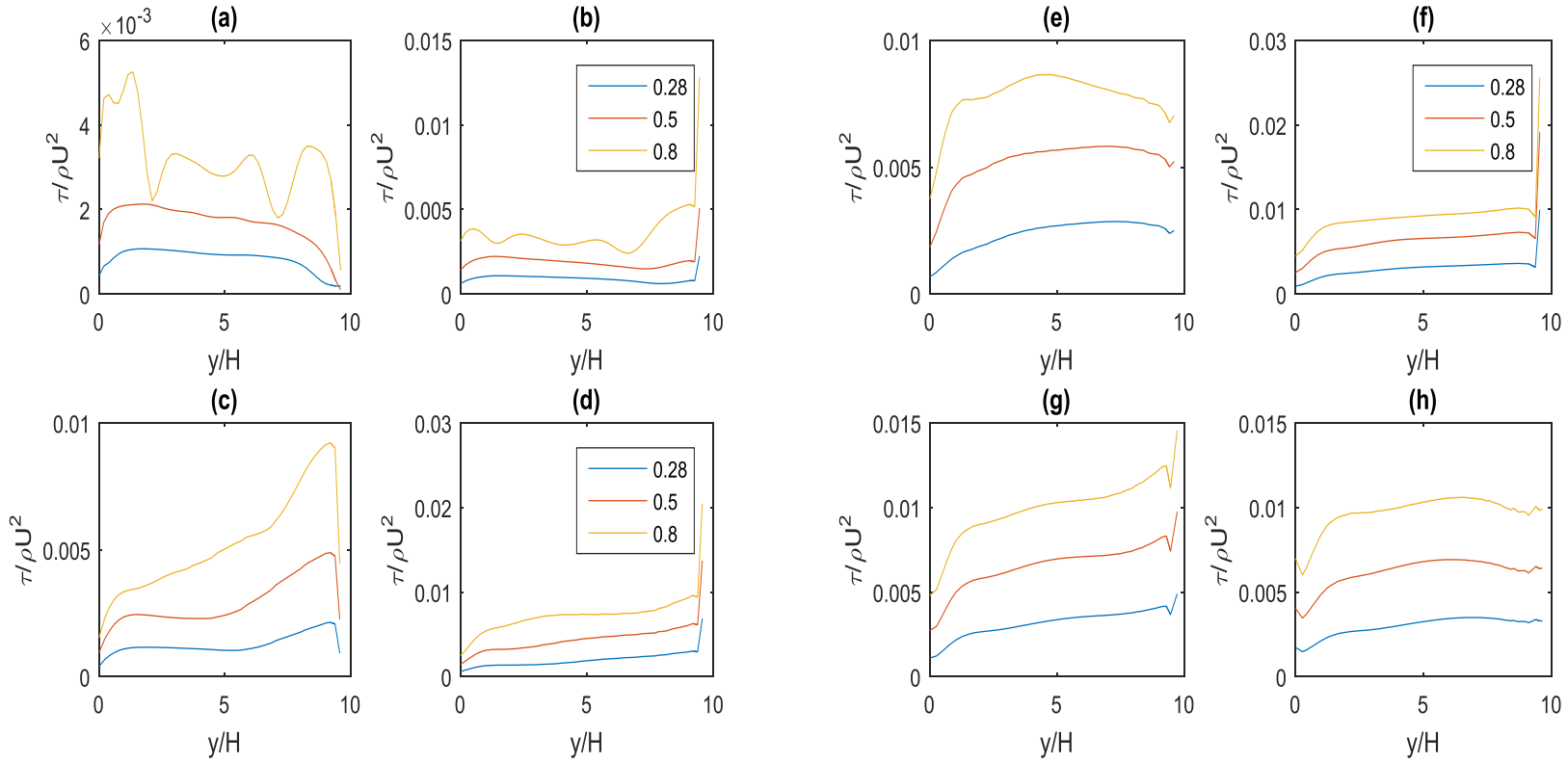

Figure 6.1: Bed shear stress plots for the mild channels $R/T_w = 8.2$ from 0^O plane to the 35^O plane, in increments of 5^O. Note the numbers in the legend denote the Froude numbers. Panel (a) shows the bed shear stress at the 0^O plane, panel (b) shows the bed shear stress at the 5^O plane, panels (c) at the 10^O plane while panel (d) at the 15^O plane. Panels (e), (f), (g), (h) show the bed shear stress at the 20, 25 ,30 ,and 35 degree planes.

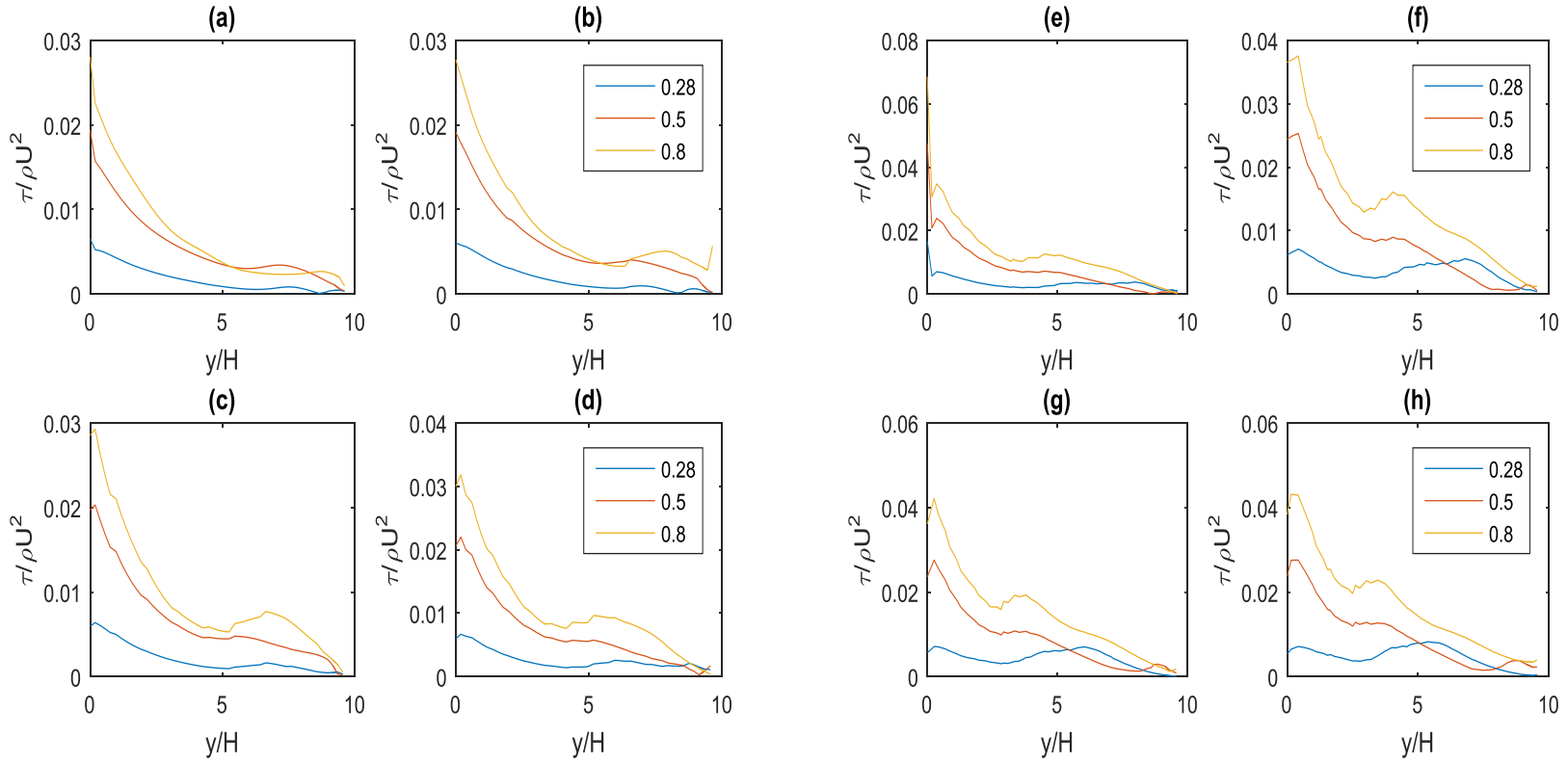

Figure 6.2: Bed shear stress plots for the tight channels $R/T_w = 0.75$ from 0^O plane to the 35^O plane, in increments of 5^O. Note the numbers in the legend denote the Froude numbers. Panel (a) shows the bed shear stress at the 0^O plane, panel (b) shows the bed shear stress at the 5^O plane, panels (c) at the 10^O plane while panel (d) at the 15^O plane. Panels (e), (f), (g), (h) show the bed shear stress at the 20, 25 ,30 ,and 35 degree planes.

6.3 Velocity Distribution

In the mild channel at the entrance the flow physics of the bend entrance pushes energetic fluids towards the inner wall (refer in chapter 4). This means at the entrance region the highest velocities are closer to the inner wall, since at the wall the velocity must vanish due to the no slip boundary condition the region of higher velocity gradient is set up close to the inner wall at the entrance region. However, as the fluid moves deeper into the bend the fluid's inertia is imparted more and more by the centrifugal acceleration such that the fluid in the bend is pushed towards the outer wall for most of the water column (see details in Chapter 4). These velocity patterns appear in the mild channel regardless of the Froude number (see Figures 6.3 to 6.5). The only visible effect of a change in Froude number is the increased magnitude of the velocities at different parts of the curve. However even with these increase in velocity magnitudes the pattern described for the mild channel is maintained.

In the tight channel the flow physics of the entrance region is similar to that of the mild channel. However, unlike in the mild channel, the streamlines of higher velocity stay closer to the inner wall for almost the entire length of the channel. Only close to the outlet of the tight channel do the higher velocity streamlines shift to the outer bend. This pattern is maintained regardless of the Froude number. Again the only discernable effect of the Froude number variation on the tight channel is the increase in the magnitude of the velocity at corresponding parts of the channel (see Figures 6.6 to 6.8). Hence, there is a positive correlation between an increase in the Froude number and an increase in the velocity magnitude while the above described pattern is maintained.

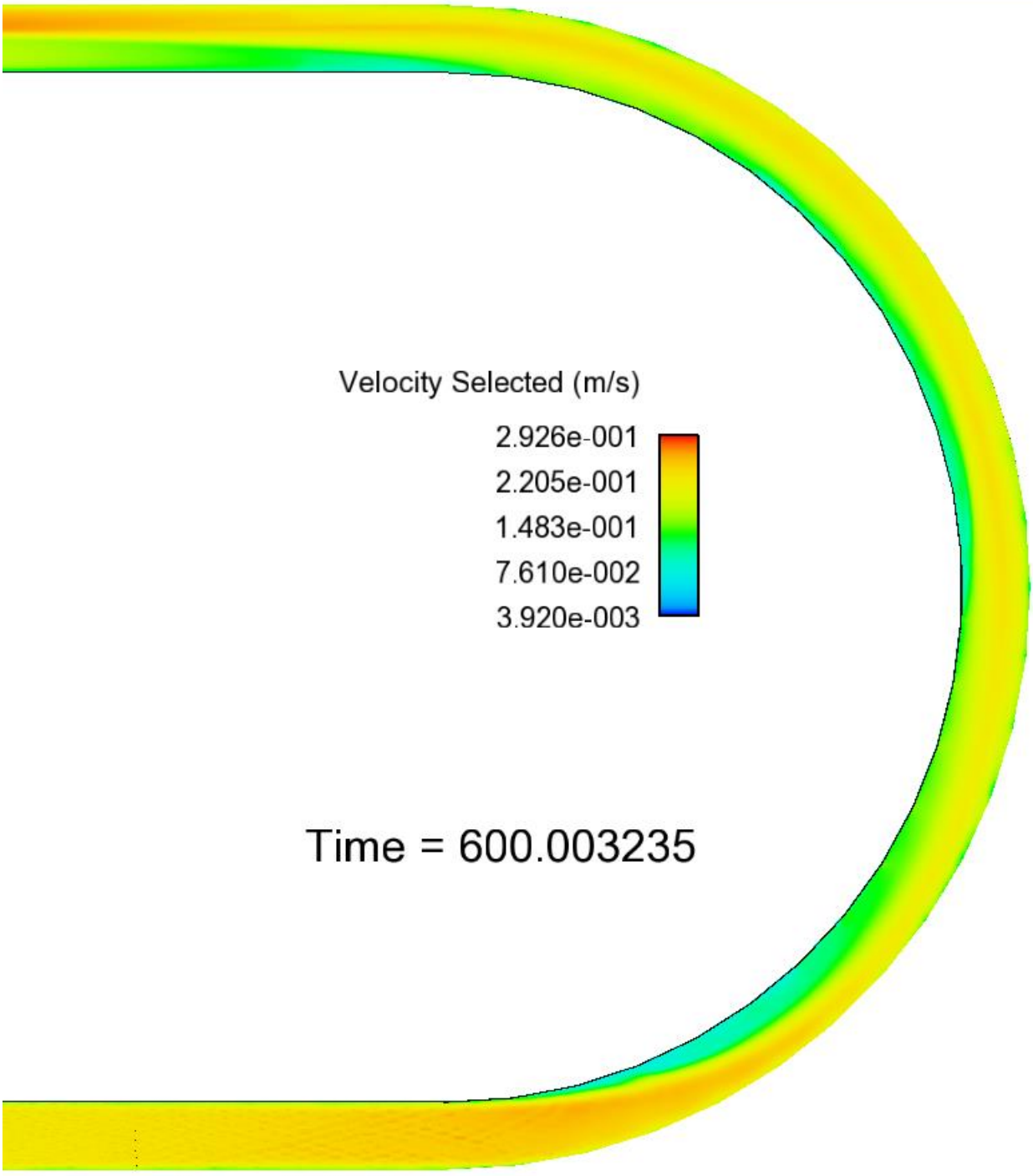

Figure 6.3: Velocity distribution at the surface for mild channel R/T_w = 8.2 at Froude number 0.28.

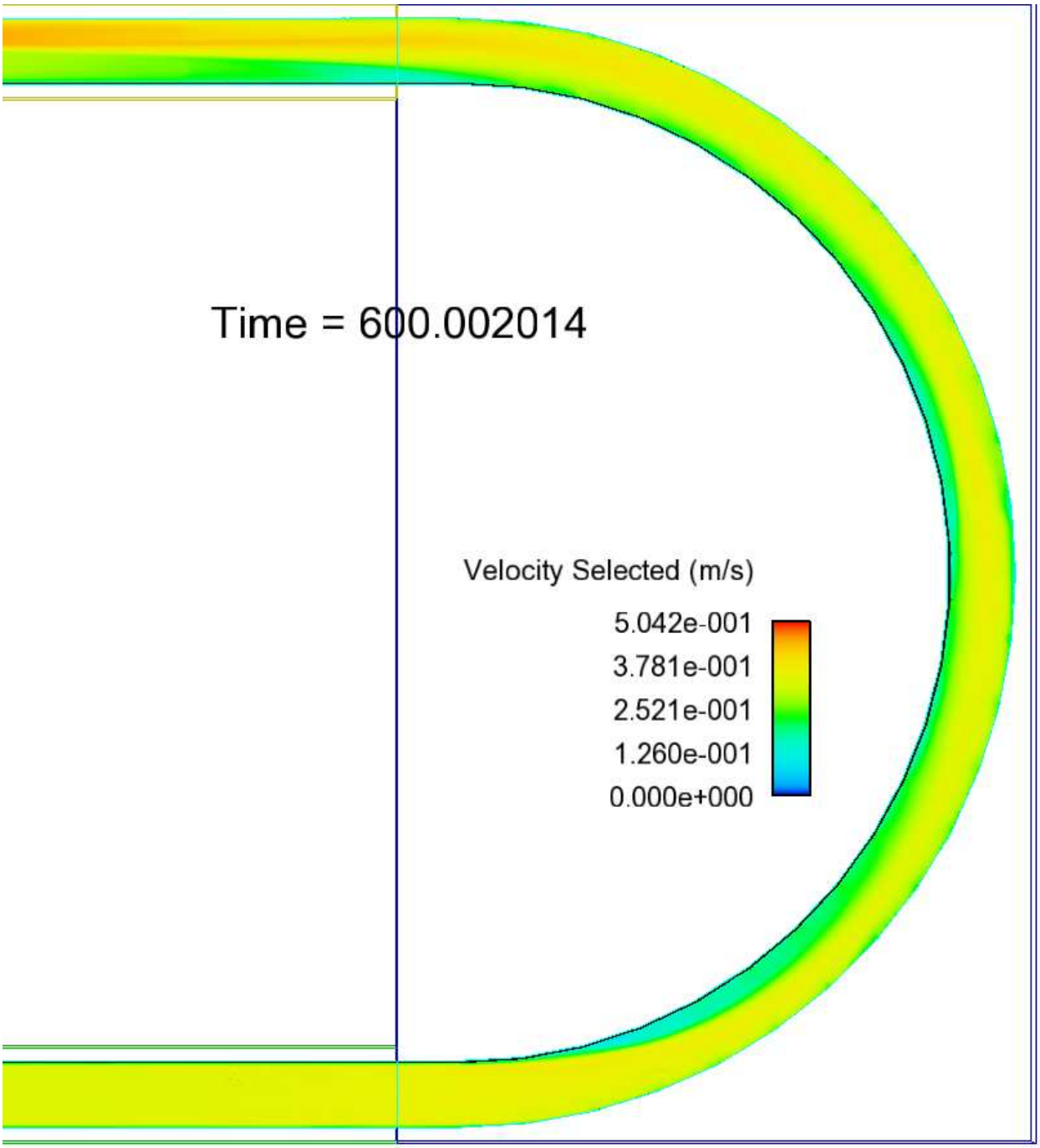

Figure 6.4: Velocity distribution at the surface for mild channel R/T_w = 8.2 at Froude number 0.5.

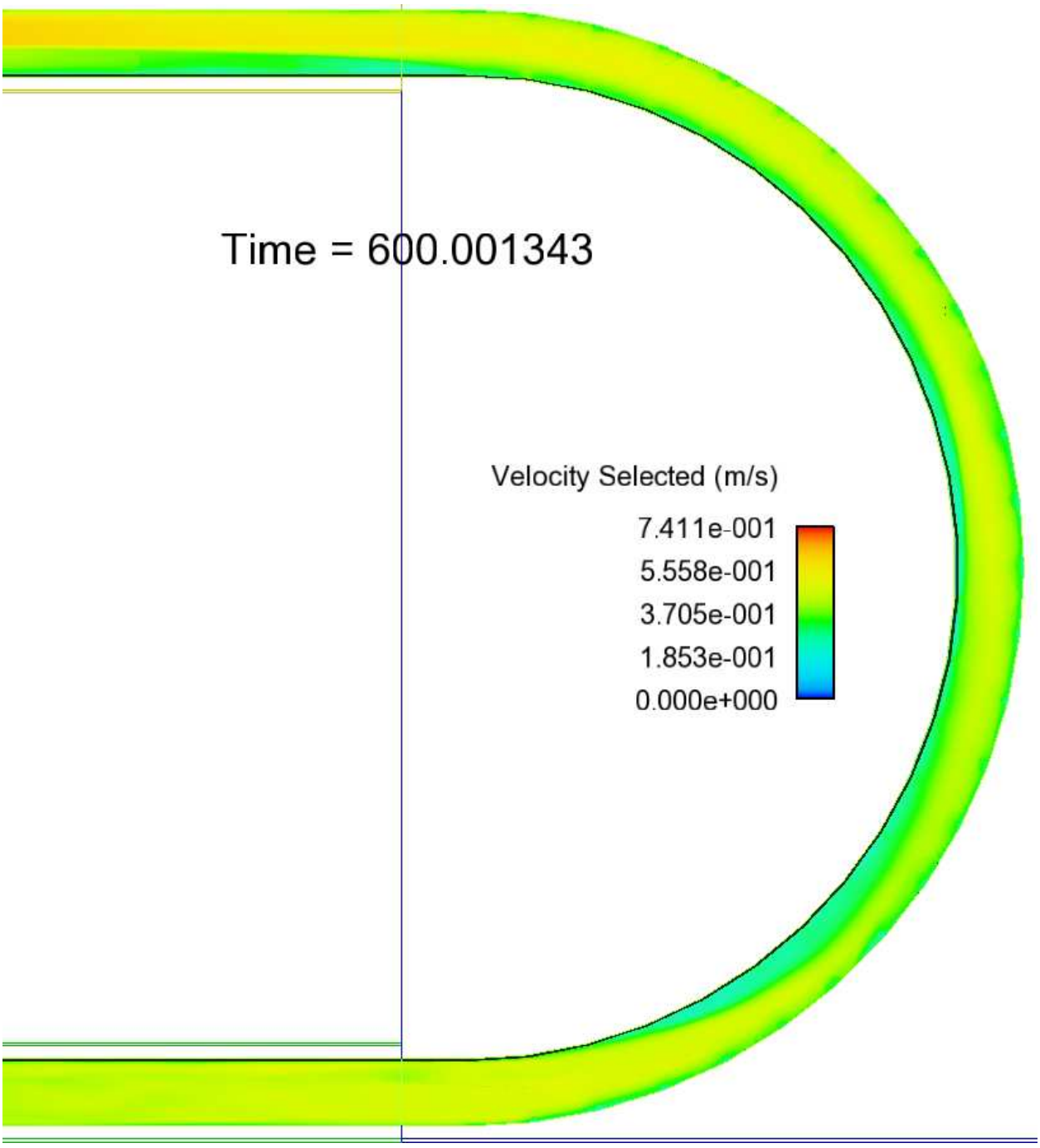

Figure 6.5: Velocity distribution at the surface for mild channel R/T_w = 8.2 at Froude number 0.8.

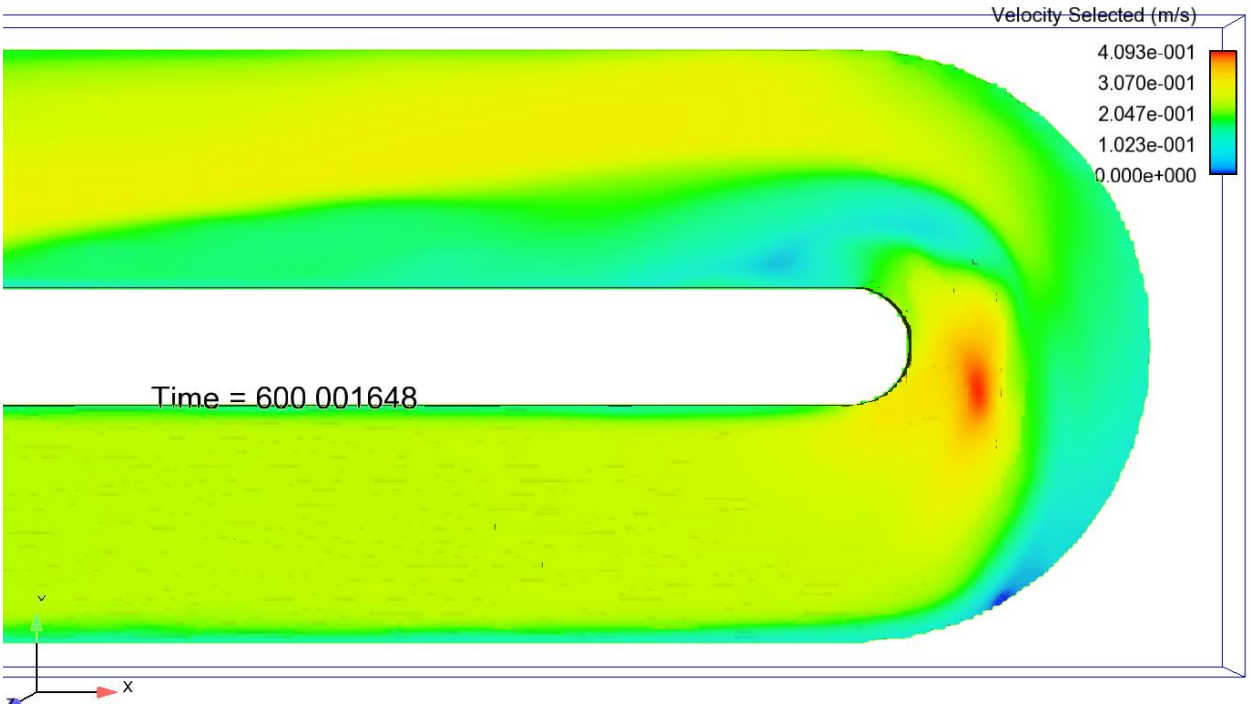

Figure 6.6: Velocity distribution at the surface for tight channel R/T_w = 0.75 at Froude number 0.28.

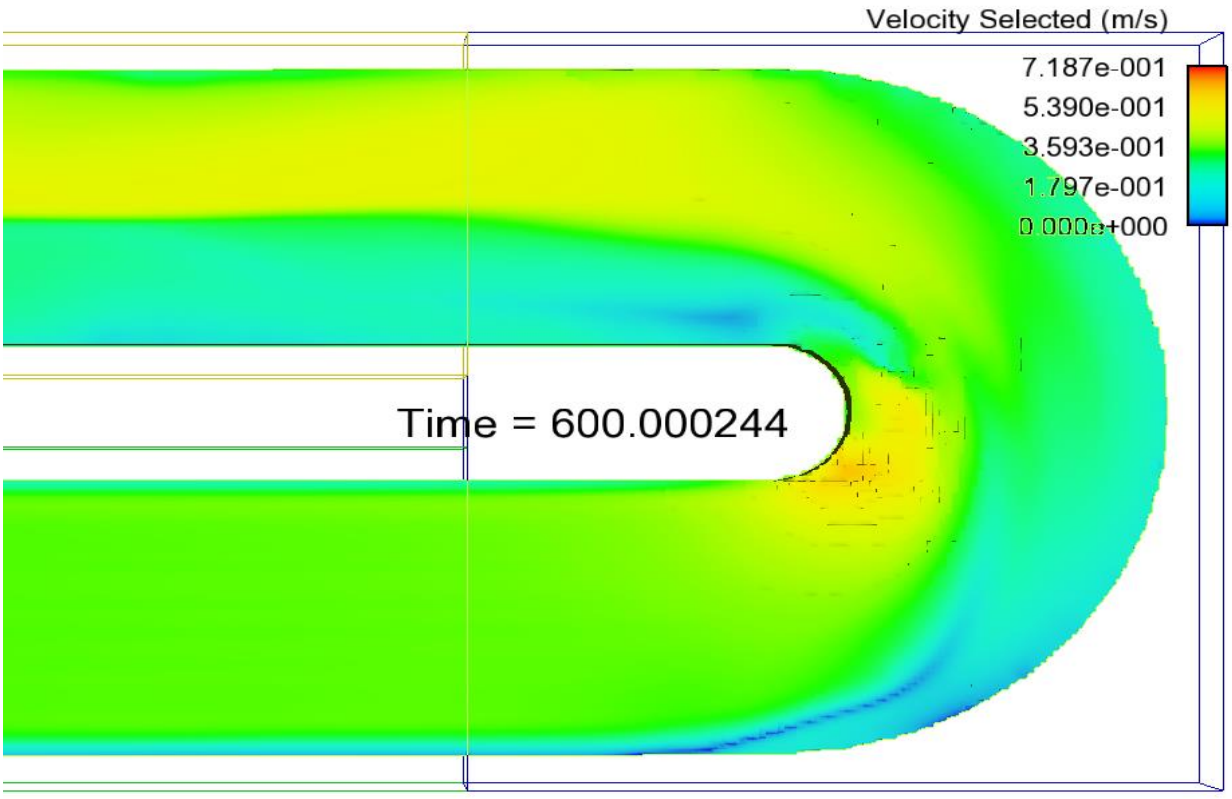

Figure 6.7: Velocity distribution at the surface for tight channel R/T_w = 0.75 at Froude number 0.5.

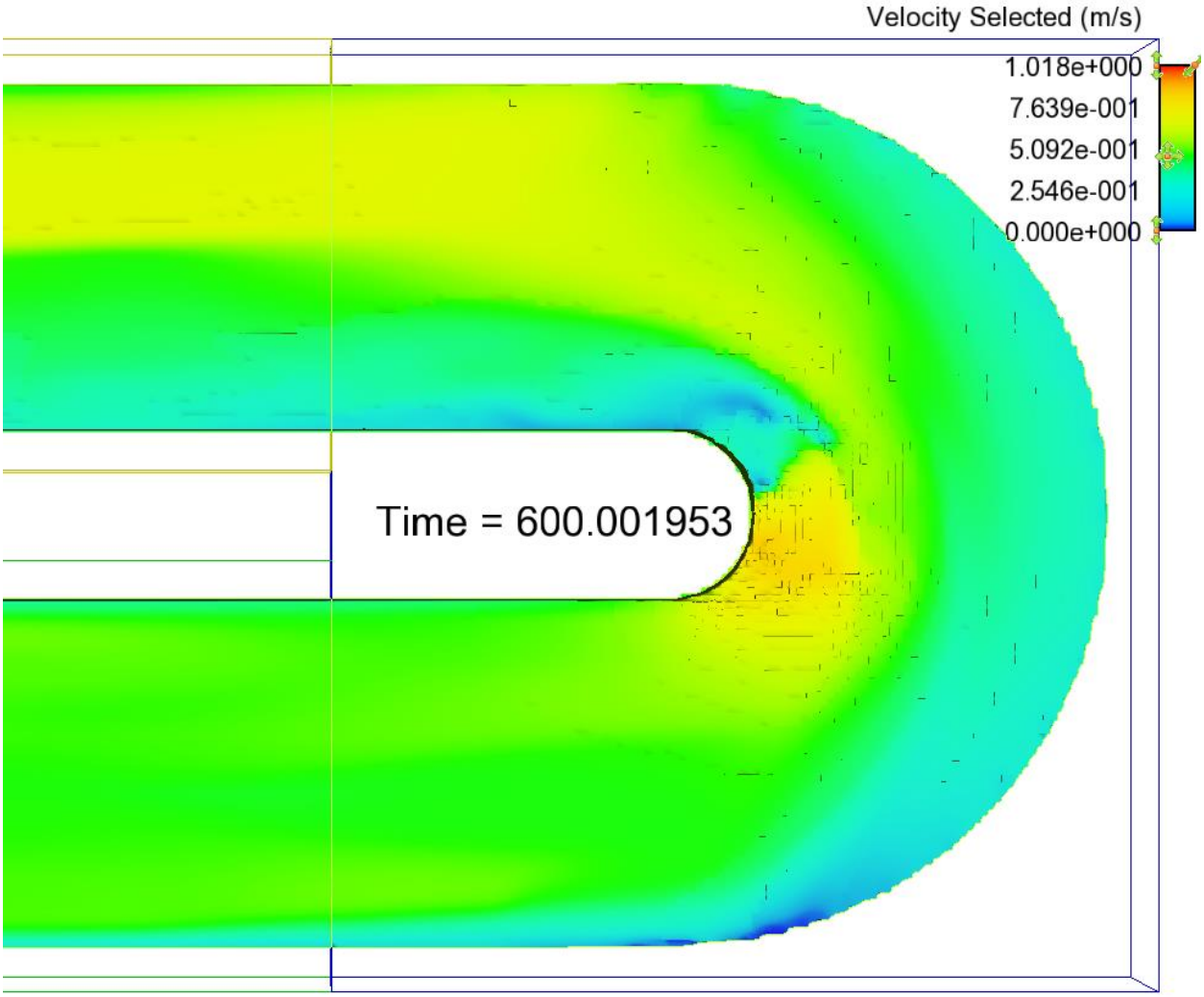

Figure 6.8: Velocity distribution at the surface for tight channel $R/T_w = 0.75$ at Froude number 0.8.

6.4 Free Surface Dynamics

Aside from the velocity structure, the tilting of the transverse free surface in the channel bend induces one of the major forces that is critical to shaping the dynamics of bend channel flows. Therefore, an examination of the evolution of the free surface with a variation in Froude number can provide more insight into the dynamics of bend flows.

Results from the simulations in this chapter show that there are two distinct free surface evolution patterns with variation in Froude number depending on whether the channel is mild or tight. In the mild channel when the fluid coming from a straight inlet encounters the bend, it experiences a centrifugal acceleration which pushes the fluid volume towards the outer wall. The accumulation of more volume closer to the outer wall causes a tilting of the free surface such that the transverse elevation of the free surface at the outer wall is greater than that at the inner wall inducing a transverse pressure gradient. Hence the pattern of the free surface is always that of a positive slope towards the outer bend. The only visible effect of the variation of Froude on the transverse free surface slope in the mild bend is an increase in the flow depth (see Figure 6.9). The free surface slope in the mild bend however remains constant as the Froude number increases. This behavior has some implications for the dynamics of bend flows one of which is that, as long as the curvature is mild, an increase in the Froude number does not result in an increase in the radial pressure gradient force.

In the tight channel however an increase in the Froude number results in something truly remarkable. As shown in Figure 6.10 as the Froude number increases not only does the flow depth increase, (and the pattern of positive free surface slope towards the outer bend is maintained), the free surface slope increases as well. The immediate implication of this observation in a tight channel is that just by increasing the Froude number of the flow, the radial pressure gradient force increases significantly. This is drastically different from the case of the mild channel where the radial pressure gradient force remains constant regardless of the Froude number. It appears that the combined effect of the tight curvature and increased inertial lead to a highly complex flow pattern.

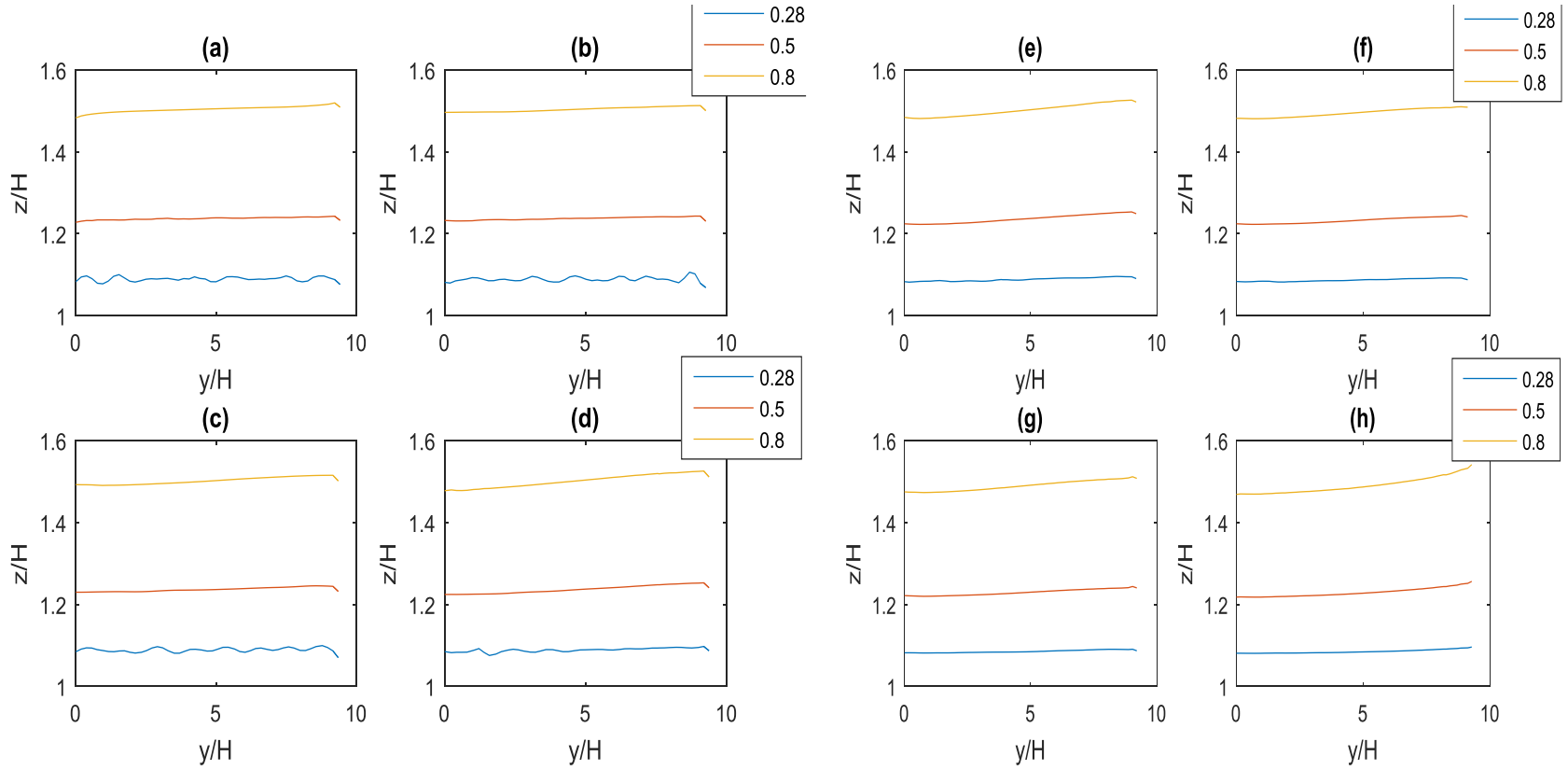

Figure 6.9: Free surface plots for the mild channels R/T_w = 8.2 from from 0^O plane to the 35^O plane, in increments of 5^O. Note the numbers in the legend denote the Froude numbers. Panel (a) shows free surface elevation at 0^O plane, panel (b) shows the free surface elevation at the 5^O plane, panels (c) at the 10^O plane while panel (d) at the 15^O plane. Panels (e), (f), (g), (h) show the free surface elevation at the 20, 25 ,30 ,and 35 degree planes. These plots are typical of what goes on in the whole channel.

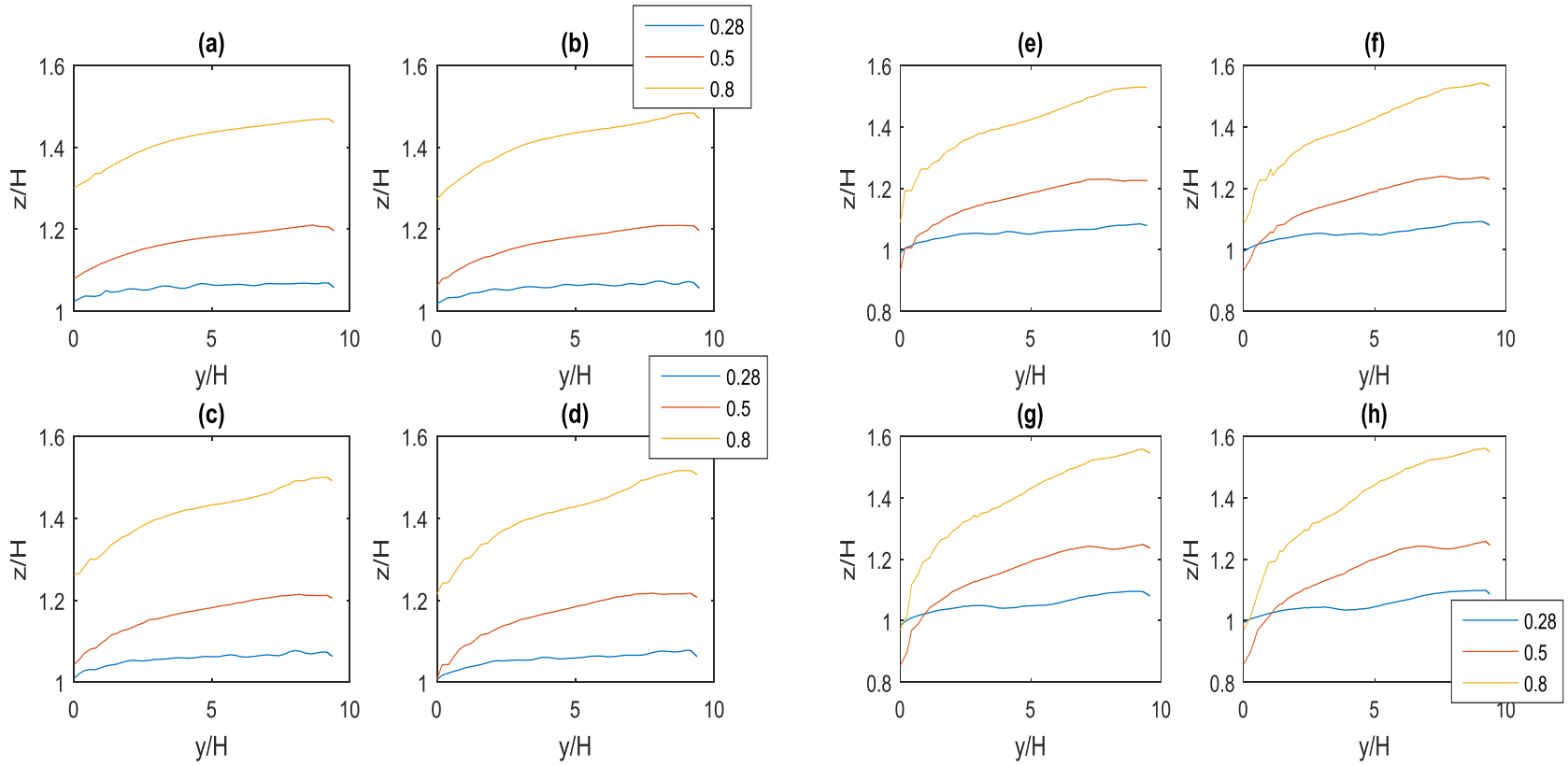

Figure 6.10: Free surface plots for the tight channels $R/T_w = 0.75$ from from 0^O plane to the 35^O plane, in increments of 5^O. Note the numbers in the legend denote the Froude numbers. Panel (a) shows free surface elevation at 0^O plane, panel (b) shows the free surface elevation at the 5^O plane, panels (c) at the 10^O plane while panel (d) at the 15^O plane. Panels (e), (f), (g), (h) show the free surface elevation at the 20, 25 ,30 ,and 35 degree planes. These plots are typical of what goes on in the whole channel.

6.5 Vorticity Distribution

The magnitude and distribution of vorticity contributes to the overall dynamics of bend channel flows in ways that have already been explained in previous chapters. However, it is worth investigating what the effect of the Froude number is on the vorticity structure.

At the channel entrance in the mild curve, the circulation structure is that of a single cell due to the interaction between the centrifugal acceleration and the radial pressure gradient (refer to Chapters 4 and 5). As the flow moves further into the bend, a second counter rotating cell close to the outer bank surface develops. This outer bank counter rotating cell has been attributed in literature to the complex interaction between the centrifugal acceleration and the Reynolds stresses. This pattern is maintained in the fully developed region of the bend till the channel exit regardless of the Froude number.

In the tight channel, the vortex structure begins with a single cell circulation due also to the interaction between the centrifugal acceleration and the radial pressure gradient. As the fluid moves deeper into the bend an outer bank counter rotating cell develops as described in the previous chapter. Finally, the main cell circulation in the tight channel breaks into two clockwise rotating cells because of the enormous magnitude of the vorticity. This gives the three cell circulation in the fully developed region of the tight bend regardless of the Froude number. The only discernable effect of a change in Froude number is the increase in vorticity magnitude as Froude number increases as can be seen from an analysis of the vorticity magnitude plots (see Figures 6.11 to 6.16).

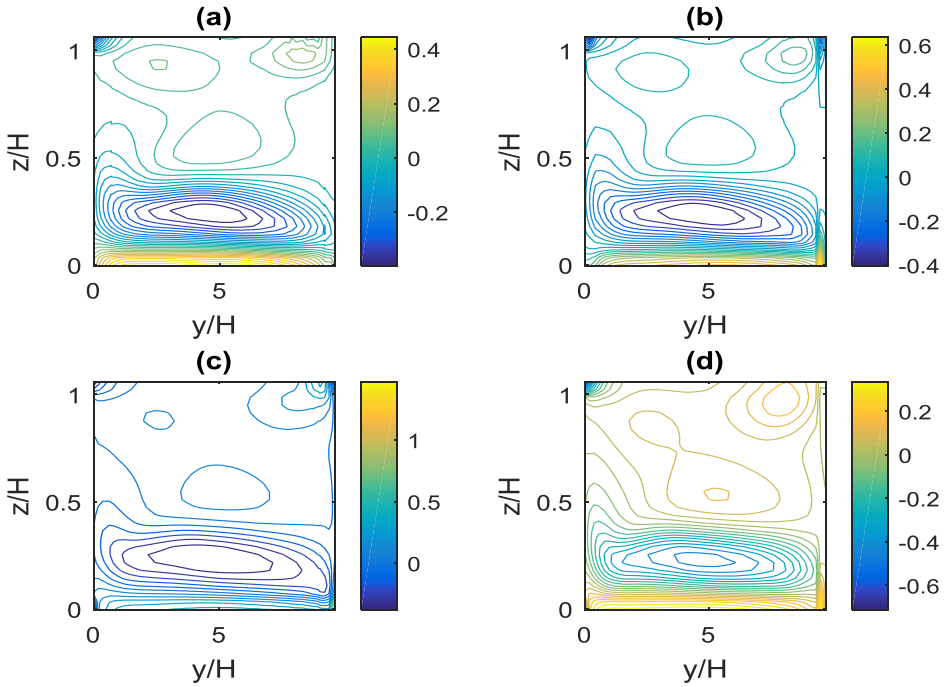

Figure 6.11: Vortex patterns at Froude number 0.28 for the mild channle $R/T_w = 8.2$. Panel (a) shows the 60^o plane, panel (b) shows the 65^o plane, panel (c) shows the 70^o plane and panel (d) shows the 75^o plane.

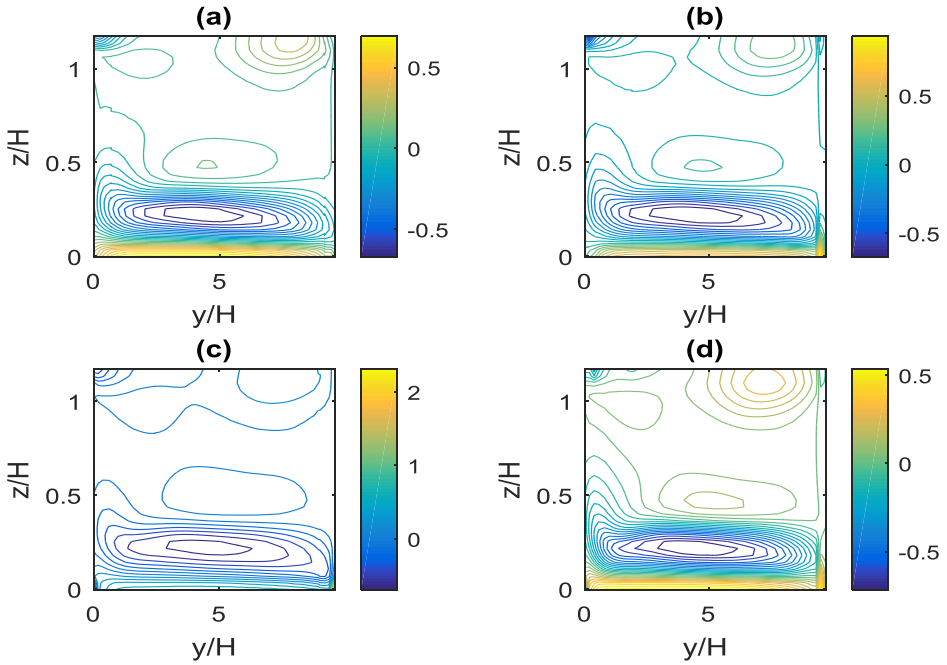

Figure 6.12: Vortex patterns at Froude number 0.5 for the mild channle $R/T_w = 8.2$ Panel (a) shows the 60^o plane, panel (b) shows the 65^o plane, panel (c) shows the 70^o plane and panel (d) shows the 75^o plane.

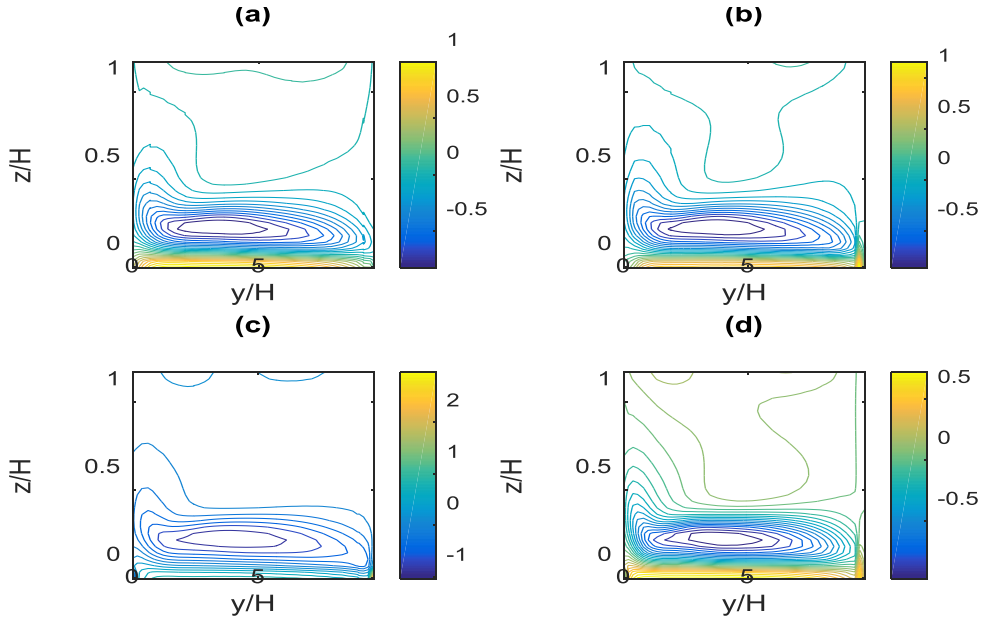

Figure 6.13: Vortex patterns at Froude number 0.8 for the mild channle $R/T_w = 8.2$. Panel (a) shows the 60^O plane, panel (b) shows the 65^O plane, panel (c) shows the 70^O plane and panel (d) shows the 75^O plane.

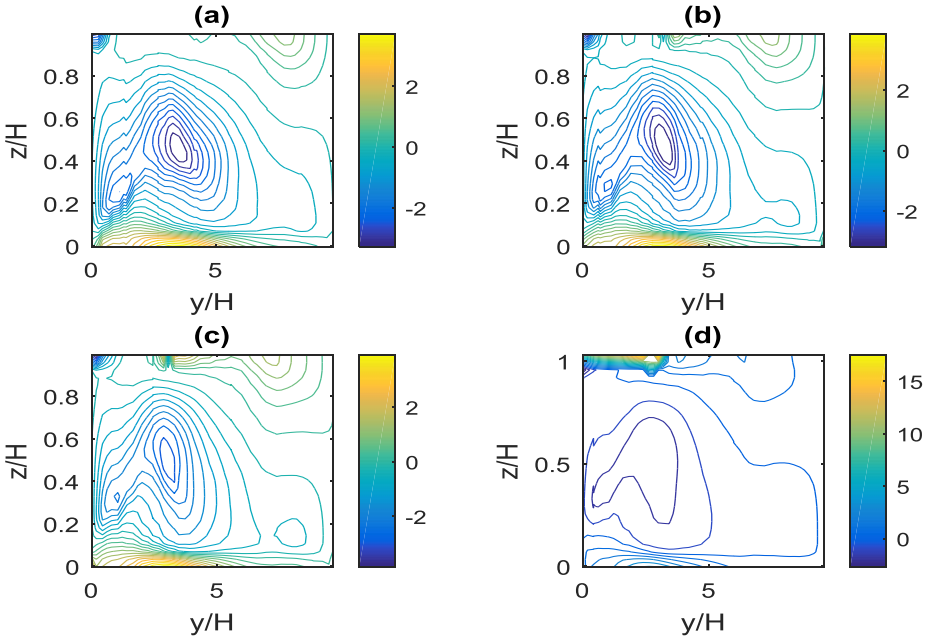

Figure 6.14: Vortex patterns at Froude number 0.28 for the mild channle $R/T_w = 0.75$. Panel (a) shows the 60^O plane, panel (b) shows the 65^O plane, panel (c) shows the 70^O plane and panel (d) shows the 75^O plane.

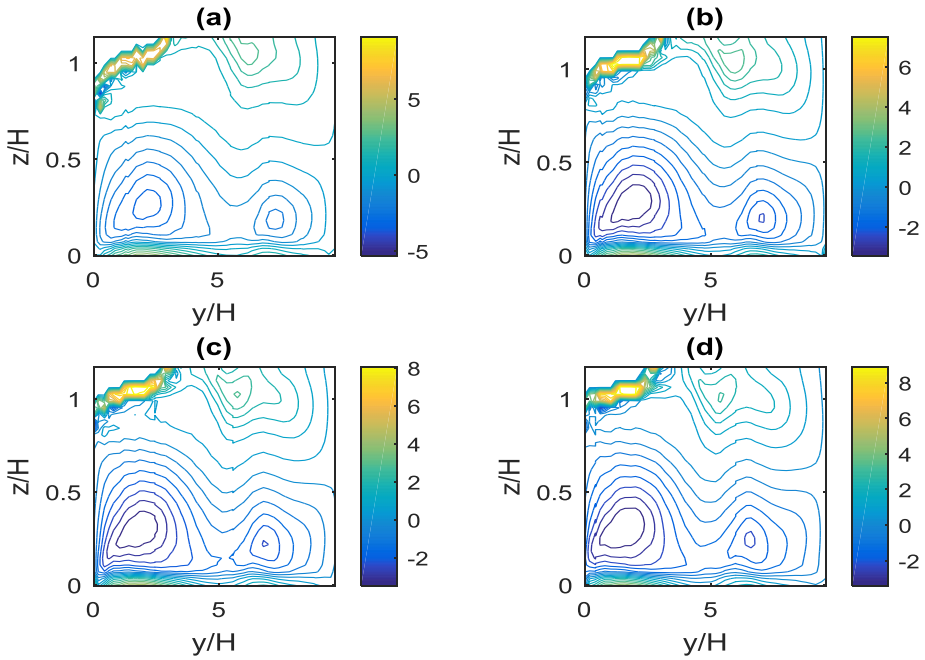

Figure 6.15: Vortex patterns at Froude number 0.5 for the mild channle $R/T_w = 0.75$. Panel (a) shows the 60^O plane, panel (b) shows the 65^O plane, panel (c) shows the 70^O plane and panel (d) shows the 75^O plane.

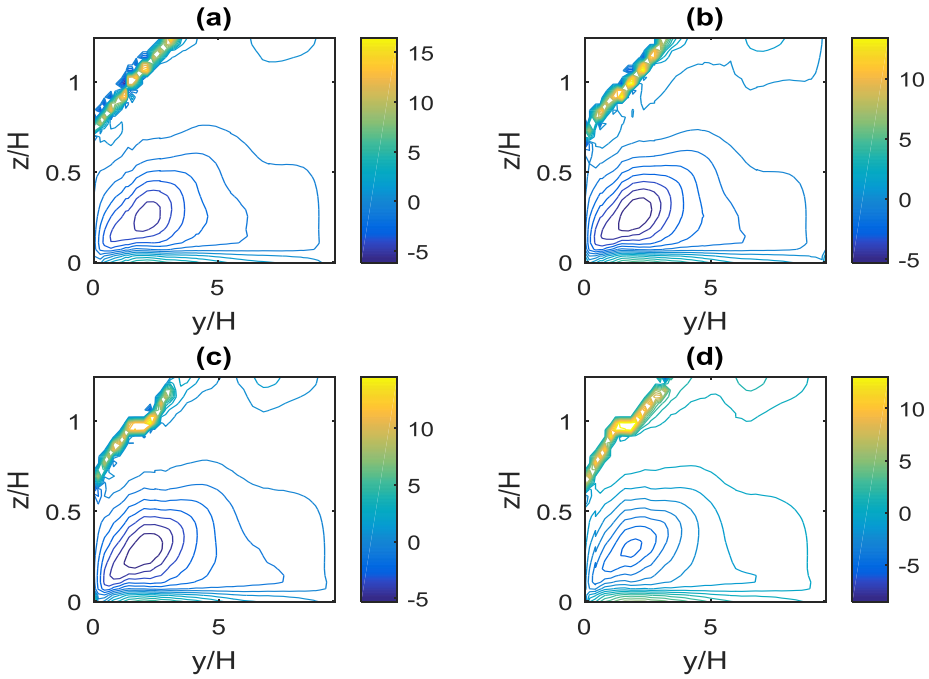

Figure 6.16: Vortex patterns at Froude number 0.5 for the mild channle $R/T_w = 0.75$. Panel (a) shows the 60^O plane, panel (b) shows the 65^O plane, panel (c) shows the 70^O plane and panel (d) shows the 75^O plane.

6.6 Summary

This chapter studied the effect of Froude number variation on the flow structure and dynamics of bend channel flows. To accomplish this task, 6 simulations with two non-dimensional curvature radii of $\frac{R}{T_w} = 8.2$ (mild) and $\frac{R}{T_w} = 0.75$ (tight) were chosen.

Results in this section show that the shear stress distribution for a mild channel is that of the maximum close to the inner bend at the entrance region. This maximum subsequently shifts to the outer bend as the flow moves deeper into the bend. The tight bend experiences the maximum shear close to the inner wall for the whole bend length. These results hold irrespective of the Froude number. The increase in Froude number results in an increase in the magnitudes of the shear stresses while maintaining these respective patterns. The mild channel initially has its streamlines of highest velocities close to the inner wall at the entrance region. These streamlines of higher velocity subsequently shift to the outer wall as the flow proceeds into the bend. In contrast to the mild channel, the tight channel has it higher velocity streamlines close to the inner bend for the entire channel length. The effect of the increase in the Froude number is to increase the velocity magnitude while maintaining the same pattern. The results from simulations in this chapter also show that the free surface experiences a similar evolution with a variation in Froude number. When flow coming from a straight inlet encounters a bend, it is subjected to a centrifugal acceleration which deflects much of the fluid volume towards the outer wall. This creates an accumulation of volume on the outer bend region and a depletion of volume from the inner bend region causing a free surface super elevation towards the outer wall. Results from the simulations in this chapter show clearly that the effect of increasing the Froude number on the free surface is to increase the flow depth in the mild channel while the free surface slope remains constant. In the tight bends however the effects of increasing the Froude number is an increase in both the flow depth and slope. Finally, this study shows that the vortex structure in the bend is as expected with the two cell circulation structure in the

fully developed region of the mild channel and the three cell circulation structure in the fully developed region of the tight channel. Again the effect of an increase in the Froude number is to increase the magnitude of the vorticity as can be seen from an analysis of the vorticity contours.

Many of these results have important implication for manmade bend channel design, natural river management and even river modelling. The next (closing) chapter summarizes all the findings from this research, their relevance to river dynamics and management, and suggests possible direction for future research.

Chapter 7

Conclusion

7.1 Summary of Investigation

This research was carried out to gain fundamental insights into the fluid dynamics of river flows. However, because of the difficulties that the complex geometries of natural rivers introduce and the complications the mechanics of sediment transport adds to fluid flows in rivers, simplifying assumptions had to be made. Hence in this research, as a first step, rivers were idealized as a single open channel bend with rigid boundaries and without sediment transport. This single channel bend was then studied using computational fluid dynamics simulations with the Volume of Fluid method to resolve the free surface and large eddy simulation technique to incorporate turbulence. Understanding the dynamics and three dimensional flow structure in open channel bends was carried out in three stages.

In chapter 4 the effect of a variation in curvature on the three dimensional flow structure and dynamics was examined. In that chapter, four 180 degree open channel bends with curvature ranging from mild $\frac{R}{T_w} = 8.2$ to tight $\frac{R}{T_w} = 0.75$ were studied in detail. In order to isolate cause and effect, identical upstream and downstream geometries were used for all channels. Hence in each channel the upstream straight inlet had a rectangular cross-section of 0.5 meter width, a length of 11m and the downstream outlet was 6.7 m long. All channel simulations were carried out with the same inlet boundary conditions; a volume flow rate of 0.0052 m^3/s, while all channel outlets and free surfaces were set at the atmospheric pressure boundary condition. All walls and beds were imposed with the no-slip boundary condition and an initial condition with the flow depth of 0.052 m was used. All simulations were also initialized as stationary and allowed to run up to steady state before measurements were taken.

In chapter 5, the effect of a variation in curvature length on the three dimensional flow structure and dynamics of open channel bend flows was studied. In that study, 12 large eddy simulations with two non-dimensional radii of curvature were run with the computational code already described in detail in Chapter 3. Channel lengths of $0^o, 30^o, 60^o, 90^o, 120^o, 150^o$ and 180^o respectively, were simulated with the same upstream and downstream conditions described in the previous paragraph. The same initial conditions previously described were also used with all simulation initialized as stationary and allowed to run up to steady state before measurements were taken.

Chapter 6 examined the effect of variation in dynamics factors on open channel bend mechanics by studying the effect of Froude number variation on the three dimensional flow structure and dynamics of an open channel bend. Six large eddy simulations of a 180 degrees channel at non dimensional curvature radii of 8.2 (mild) and 0.75 (tight) were performed. The same upstream and downstream geometries as detailed in the second paragraph of this section were used in the study. At the inlet to the various channels, various volume flow rates corresponding to the three Froude numbers of 0.28, 0.5 and 0.8 were imposed. Other boundary conditions used are similar to those previously described.

A summary of the key finding in this research is given in the next section.

7.2 Key Findings in this Research

Results from the first part of the research (chapter 4) show clearly that further into the channel bend, the shear stress distribution depends on the curvature ($\frac{R}{T_w}$) of the channel. Hence from an analysis of simulation data, the maximum shear stress is exerted on the inner bend region at the entrance to the curve regardless of the channel curvature. As the flow evolves further into the bend, this maximum shifts to the outer bend region depending on the curvature. Thus, in the mild channel, the maximum shear stress initially exerted on the inner bend at the entrance region shifts quickly to the outer bend at only a short

angular distance from the entrance. As the curvature decreases (gets tighter) the maximum shear stress stays on the inner bend for longer angular distances from the entrance such that in the tightest bend the maximum shear stress is never on the outer bend region or the outer wall. One main implication of this finding especially in natural and manmade curved channels is that the apparent bias towards reinforcing the outer bend and wall in curved channel design and bank protection works may not be effective in preventing channel failure. Even in mild channels where for the most part the maximum shear stress is exerted on the outer wall and bed, there is still the initial 0 to 20 degrees (depending on the radius of curvature) where the maximum shear stress is still exerted on the inner wall and bed and thus could cause the onset of failure.

The reason for the shear stress evolution described in the previous paragraph was found to be due to the velocity distribution and the changes it undergoes as curvature varies. In the mildest channel, the flow coming from the straight upstream inlet on the outer wall side experiences an adverse pressure gradient while fluid encountering the bend from the upstream straight inlet on the inner wall side experiences a favorable pressure gradient. Therefore, fluid momentum entering the bend is forced towards the inner wall such that the higher velocity gradients are located in the inner bend region. However, as the flow moves deeper into the channel the effect of the centrifugal acceleration takes hold and pushes the streamlines of higher velocity towards the outer bend. How much angular distance into the bend before the high velocity streamlines shift to the outer wall depends on the curvature of the channel. Thus, in the mild channel (with large curvature), the region of maximum velocity gradients shifts to the outer wall a short angular distance from the entrance while in the tightest channels (with extremely small curvatures) the region of maximum velocity gradients is never on the outer bend or wall.

While the vortical structure in mild channels has been extensively studied and some of the results in this dissertation serve to confirm their authenticity, new results from this research now help to put some of those old findings in the proper context. It is clear from results in this research that regardless of the

channel curvature, flow in the spatially developing regions of any curved channel is characterized by a single cell circulation. However, when the flow reaches its spatially invariant state, the circulation structure depends on the channel curvature. In the mild channel, the fully developed flow state is characterized by a two cell circulation structure with a main body clockwise rotation and a counter rotating outer cell (as seen in literature). Contrary to this, the tight channel has a three cell circulation structure with two clockwise circulation cells and one counter clockwise circulation cell. While this three cell circulation has been hinted at in literature, the reason for such a circulation structure was previously unknown. New results from this research now show that the tight channel initially develops the two cell circulation structure, but the main cell circulation splits into two clockwise circulation cells due to the enormous magnitude of the vorticity in the tight channel. This result has serious significance in river modeling since the hydraulics community usually makes extensive use of reduced order river models to plan river training works and even man made channel designs. These reduced order models work by reducing the (three) dimensions of the relevant equations of fluid motion and parameterizing what is lost in the reduction process. A critical loss is the circulation structure which is usually parameterized and added to the reduced order model. A good number of these reduced order models are based on a parameterization that assumes the two cell circulation structure. As results from this research has shown, these models cannot reproduce correctly critical flow structures in bends with tight curvatures and in the developing regions of open channel bends.

The study on effects of curvature length on the vortex structure also led to some new and interesting results. In the mild channel, results show that development length (the length of the channel for which the flow is spatially changing) depends on curvature length. As a concrete example, in the mild 180 degree channel, the flow development region spanned from the curve entrance at the 0 degrees planes to about the 85 degrees plane with the fully developed two cell circulation structure occurring coherently at about the 90 degree plane. A similar channel of the same curvature but of shorter length (i.e. 30 degrees)

reached the fully developed two cell structure at only the 20 degree plane. Even more remarkable is the evolution of vortex structure in the tight bend with curvature length. Results from simulations showed that for the shorter tight channels (the 30 and 60 degrees channel lengths) a single cell circulation exists for the entirety of the channel length. Only in the longer channels (90, 120, 150 and 180 degree lengths) did the outer wall counter rotating cell and the two main body clockwise rotating cells develop. Analysis of the vorticity plots show clearly that the shorter channel only develops a single cell circulation in the main body of the flow (and not the two clockwise main body cells) because the vorticity developed in these channels are low compared to their longer counterparts. These results also have serious implications for river systems modelling especially in the formulation of reduced order river models as explained in the previous paragraph.

The finding in Chapter 4 that the maximum shear stress for the tight bend stayed on the inner bend region for the entirety of the channel length was interesting. However, no physical explanation was presented in chapter 4 (or even in current literature). New results in chapter 5 now show that this shear stress distribution is caused by the value of the radial pressure gradient force exceeding the value of the centrifugal force for the full channel. This means that the radial pressure gradient force is forcing the streamlines of high velocity towards the inner wall region throughout the channel length because it far exceeds the centrifugal force magnitude whose direction is opposite. This sets up the region of higher velocity gradients and thus shear stress on the inner wall in the tight channel for the entirety of its length. Another finding is that of a new type of flow regime in the tightest bend. This flow regime characterized by extreme shear instability in the bend and a break down to periodic motions in the straight outlet was first discovered in Chapter 4.

In Chapter 6, it was shown that for a mild channel, increasing the Froude number only increased the flow depth but did not increase the free surface slope. This essentially means in a mild channel an increase in the inertia of the fluid does not change the magnitude of the radial pressure gradient force. However,

when the bend is very tight new results show that the radial pressure gradient forces increases as the Froude number increases. This shows that a variation in inertial forces changes both the centrifugal and the radial pressure forces.

All these key findings significantly improve insight into the physics of open channel bend flows. However, there are still questions that remain unanswered which future researchers may attempt to work on. The next section highlights these questions.

7.3 Suggestions for Further Research

This research set out to provide new fundamental insights into bend channel flow physics to better understand the fluid mechanics of natural river systems. While new results from this work provides valuable insight not yet found in current literature, more questions have come up in the course of this research work that still remain to be answered.

For instance, it would be interesting to study the effect of bottom and wall roughness on the fluid dynamics of open channel bends. This would better mimic the flows of natural rivers with an immovable bed as can be found in various parts of nature. In the simulation studies conducted in Chapters 4 and 5, wall roughness was excluded to make the problem less complex and to provide a basis for comparison should any future researcher attempt to carry out such a study. Insights into the effect of roughness on bend channel dynamics would also improve parameterization of this aspect of river flows so that river models can better capture the physics of flow.

Another interesting question would be the flow structure and dynamics in a river meander. Even though results from idealizing rivers as a single channel bend has provided valuable insights, more can be learnt from a detailed study of a single river meander first and then a couple of meanders joined to mimic the geometry of a natural river. Again results from this research can serve as a good spring board for such a study as a meander is simply two or more curves joined in the appropriate way.

All natural rivers at some point in their existence transport sediment either in suspension or as bed load. Since sediment modifies the flow structure in ways that are still being understood, it would be interesting to study the flow physics of fluid with sediment transport moving through a river bend. Even more interesting would be such a study including the effects of an erodible bed just like the case in most natural rivers.

References

Bagnold, R. A. 1960. Some aspects of the shape of river meanders. US Geological Survey Professional Paper 282-E, US Geological Survey, Washington, DC.

Bathurst, J. C., Thorne, C. R. & Hey, R. D. 1977. Direct measurement of secondary currents in river bends. Nature 269, 504-506.

Blanckaert, K. & Graf, W. H. 2001. Mean flow and turbulence in open-channel bend. Journal of hydraulic Engineering ASCE 127, 835–847

Blanckaert, K. & Graf, W. H. 2004. Momentum transport in sharp open-channel bends. Journal of Hydraulic Engineering ASCE.

Blanckaert, K. & de Vriend, H. J. 2004. Non-linear modeling of mean flow redistribution in curved open channels. Water Resources Research.

Blanckaert, K. 2009. Saturation of curvature induced secondary flow, energy losses and turbulence in sharp open channel bends, laboratory experiments, analysis and modeling. Journal of Geophysical Research 114.

Blanckaert K. 2015. Flow separation at convex banks in open channels. Journal of Fluid Mechanics 779,432–467.

Booij, R. 2003. Measurements and large eddy simulations of the flows in some curved flumes. Journal of Turbulence 4, 1–17

Demuren, A. O., and Rodi, W. 1986. Calculation of flow and pollutant dispersion in meandering channels. Journal of Fluid Mechanics, Cambridge, U.K., 172, 63–92.

DeSerres, B., A. G. Roy, P.M. Biron, and Best, J. L. 1999. Three dimensional structure of flow at a confluence of river channels with discordant beds. Geomorphology, 26, 313 - 335.

Dietrich, W. E., and Smith, J. D. 1983. Influence of the point bar on flow through curved channels. Water Resources Research, 19(5), 1173– 1192.

De Vriend, H. J. 1981. Flow measurements in a curved rectangular channel. II: Rough bottom. Rep. No. 5-81, Lab. Fluid Mech., Dept. of Civ. Engrg., Delft University of Technology, the Netherlands.

DeVriend, H, J. 1977. A mathematical model of steady flow in curved shallow channel. Journal of hydraulic research, 15(1), 37-54.

Engelund, F. 1974. Flow and bed topography in channel bends. Journal of the hydraulic division, ASCE, vol. 100, No. HY 11.

Ferguson, R. I., Parsons, D. R., Lane, S. N. & Hardy, R. J. 2003. Flow in meander bends with recirculation at the inner bank. Water Resources Research, 39 (11), 1322–1333.

Frothingham, K.M. and Rhoads, B.L. 2003. Three dimensional flow structure and channel change in an asymmetrical compound meander loop, Embarras River, Illinois. Earth Surface Processes and Landforms, 28(6), 625-644.

Hirt, C. W. and Sicilian, J. M. 1985. A porosity technique for the definition of obstacles in rectangular cell meshes. International Conference on Numerical Ship Hydrodynamics, Washington D.C.

Hirt, C.W. and Nichols, B. D. 1981. Volume of fluid (VOF) method for the dynamics of free boundaries. Journal of Computational Physics, 39(1):201–225, 1981.

Holmén V. Methods for vortex identification. PhD Thesis, Lund University, Sweden, 2012.

Ippen, A.T., Drinker, P.A., Jobin, W.R and Shemdin, O.H. 1962a. Stream Dynamics and Boundary Shear Distributions for Curved Trapezoidal Channels" *Report No 47.* Massachusetts Institute of Technology January, 1962.

Jin, Y. C., and Steffler, P. M. 1993. Predicting flow in curved open channels by depth-averaged method. Journal of hydraulic engineering, ASCE, 119(1), 109–124.

Kashyap, S., G. Constantinescu, C. D. Rennie, G. Post, and R. Townsend. 2012. Influence of channel aspect ratio and curvature on flow, secondary circulation and bed shear stress in a rectangular bend, Journal of hydraulic engineering, 138, 294.

Koken, M and Constantinescu, G. 2009. An investigation of the dynamics of coherent structures in a turbulent channel flow with a vertical sidewall obstruction. Physics of fluids **21**, 085104 (2009).

Lane, S.N., Biron P.M., Bradbrook K.F., Butler J.B., Chandler J.H., Crowell M.D., McLelland S.J., Richards K.S., Roy A.G. 1998. Three-dimensional measurement of river channel flow processes using acoustic Doppler velocimetry. Earth Surface Processes and Landforms 23: 1247–1267.

Leschziner, M. A. and W. Rodi. 1979. Calculation of strongly curved open channel flow, Journal of the hydraulic division ASCE. 105, 1297-1314 (1979).

Rodi, W. 1980. Turbulence models and their application in hydraulics: a state of the art review. International Association for Hydraulic Research (IAHR), Delft, the Netherlands, 1980.

McLelland, S. J., P. J. Ashworth, and J. L. Best. 1996. The origin and downstream development of coherent flow structures at channel junctions, in Coherent flow structures in open channels edited by P. J. Ashworth, S. J. Bennett, J. L. Best and S. J. McLelland, 459 – 490, John Wiley, New York, 1996.

Nanson, R. A. 2010. Flow fields in tightly curving meander bends of low width-depth ratio. Earth Surf. Process. Landf. 35 (2), 119–135.

Nelson, J. M., and J. D. Smith 1989. Evolution and stability of erodible channel beds, in River Meandering, Water Resour. Monogr. Ser., vol. 12, edited by S. Ikeda and G. Parker, pp. 321-378, AGU, Washington, D.C.

Odgaard, A. J., and Bergs, M. A. 1988. ‘‘Flow processes in a curved alluvial channel.’’ Water Resources Research, 24, 1, 45–56.

Odgaard, A. J. 1986. ‘‘Meander flow model. I: Development.’’ J. Hydr. Engrg., ASCE, 112(12), 1117–1136.

Ottevanger, W., Blanckaert, K., and Uijttewaal, W. 2011. A parameter study on bank shear stresses in curved open channel flow by means of large-eddy simulation. Proc., 7th IAHR Symp. on River, Coastal and Estuarine Morphodynamics, International Association for Hydro-Environment Engineering and Research, Madrid, Spain, 1917–1927.

Pope, S. B. 2000 Turbulent flows. Cambridge University Press.

Ramamurthy A, Han S, Biron P. 2013. Three-Dimensional simulation parameters for 90° open channel bend flows. Journal of Computing in Civil Engineering 27(3):282- 291.

Rozovskii, I. L. 1957. Flow of water in bends of open channels, Academy of Sciences of the Ukrainian SSR, Kiev, 1957; Israel Program for Scientific Translations, Jerusalem, 1961.

Saad Y., Schultz M.H. 1986. GMRES: A generalized minimal residual algorithm for solving non-symmetric linear systems SIAM J. Sci. Stat. Comput., pp. 856-869

Schnauder, I. & Sukhodolov, A. N. 2012. Flow in a tightly curving meander bend: effects of seasonal changes in aquatic macrophyte cover. Earth Surf. Process. Landf. 37 (11), 1142–1157.

Simpson, R. L. 1989. Turbulent boundary-layer separation. Annu. Rev. Fluid Mech. 21, 205–234.

Simpson, R. L. 1996. Aspects of turbulent boundary-layer separation. Prog. Aerosp. Sci. 32, 457–521.

Sin, K.S. 2016. Three dimensional computational modelling of meandering channel flow. PhD thesis Colorado State University.

Stoesser, T., C. Braun, M. Garcia-Villalba, and W. Rodi. 2008. Turbulence structures in flow over two-dimensional dunes, J. Hydraul. Eng., 134(1), 42–55.

Sukhodolov, A. N., and B. L. Rhoads. 2001. Field investigation of three-dimensional flow structure at stream confluences: 2. Turbulence, Water Resour. Res., 37, 2411 – 2424, 2001.

Sukhodolov, A. N. 2012. Structure of turbulent flow in a meander bend of a lowland river. Water Resour. Res. 48, W01516.

Thorne, C. R., L. W. Zevenbergen, J. C. Pitlick, S. Rais, J. B. Bradley, and P. Y. Julien. 1985. Direct measurements of secondary currents in a meandering sand-bed river, Nature, 315, 746-747, 1985.

Van Balen, W., W. S. J. Uijttewaal, and Blanckaert, K. 2009. Large-eddy simulation of a mildly curved open channel flow, J. Fluid Mech., 630, 413–442.

Whiting, P. J., and W. E. Dietrich. 1993a. Experimental studies of bed topography and flow patterns in large amplitude meanders, 1, Observations, Water Resour. Res., 29, 3605 – 3622, 1993a.

Whiting, P. J., and W. E. Dietrich. 1993b. Experimental constraints on bar migration through bends: Implications for meander wavelength selection, Water Resour. Res., 29, 1091 – 1102, 1993b.

Yeh, K. C., and Kennedy, J. F. 1993. ‘‘Moment model of non-uniform channel-bend flow. I: Fixed beds.’’ J. Hydr. Engrg., ASCE, 119(7), 776–795.